Schweizerische Eidgenossenschaft
Confédération suisse
Confederazione Svizzera
Confederaziun svizra

Federal Department of the Environment,
Transport, Energy and Communications DETEC

Swiss Federal Office of Energy
Energy Research and Cleantech

Interim report from 6 October 2024

ADCAP

Demonstrator for carbon capture from flue gas and exhaust gas streams using solid adsorbents

Source: Demonstrator Pilot Plant Unit, EPFL

Publisher:
Swiss Federal Office of Energy SFOE
Energy Research and Cleantech
CH-3003 Berne
www.energy-research.ch

Co o-financing:
Canton of Valais
Place St-Théodule 15, 1951 Sion
https://www.vs.ch

Subsidy recipients:
EPFL Valais-Wallis c/o EPFL
Bâtiment CE 3.316, Station 1
1015 Lausanne

HES-SO Valais Wallis. School of Engineering
Rue de l'Industrie 23
1950 Sion

Casale SA
Via G. Pocobelli 6
6900 Lugano

GAZNAT SA
Av. Général-Guisan 28
1800 Vevey

Autors:
Wendy Lee Queen, EPFL, wendy.queen@epfl.ch
Sanjay Venkatachalam, EPFL, sanjay.venkatachalam@epfl.ch
Pratap Narayan Soni. EPFL, pratap.soni@epfl.ch
Anne Belin, EPFL, anne.belin@epfl.ch

SFOE project coordinators:
Men Wirz, Men.Wirz@bfe.admin.ch

SFOE contract number: SI/502432-01

Summary

Over the past few decades, CO_2 emissions have become a major societal concern due to the adverse effects that rising atmospheric greenhouse gas concentrations are having on the environment; such effects make the implementation of large-scale CO_2 capture efforts pertinent; however, this implementation has been hampered by the high economic and energy costs of the capture process. The most mature capture technology are liquid amine-based scrubbers. Although they perform well, the CO_2 capture with liquid alkanolamines requires an energy cost ranging from 2.5 to 3.5 MJ / kg CO_2;[1] values that are still far from the target, 1 MJ / kg CO_2, where capture processes are considered to be more viable. Given their lower heat capacities, solid adsorbents are being explored as alternatives to liquid amines. Thus, it is the goal of this project to demonstrate the use of various solid adsorbents in a kg scale capture process and elucidate the best adsorbent/process combination that gives rise to the lowest economic and energy cost. We estimate that using solid adsorbents, one can decrease the energy consumption < 1MJ/kg CO_2, while keeping CO_2 productivity > 200 kg $CO_2/m^3/h$.[2] Reaching such targets can lead to considerable decreases in the size (fixed cost) and energy consumption (variable cost) of the carbon capture plant. Thus, within the context of this project it is our goal to optimize performance of targeted adsorbents, construct a pilot plant to capture CO_2 from gas mixtures that have compositions and temperatures matching those of power plants and other exhaust gas streams, and implement those adsorbents into the pilot plant. Several different types of solid CO_2 adsorbents, such as zeolites, silicas, and MOFs (either with or without amine impregnation) will be implemented in the pilot plant, and from the pilot plant, various key performance indicators, like productivity, % purity, and % recovery with varying material and process parameters, will be monitored. This data output, combined with process design engineering and technoeconomic analyses, will be used to optimize the materials and process combination, allowing us to obtain a CO_2 capture process that has the lowest economic and energy cost possible.

In the first year, significant progress was made. Firstly, we have worked to optimize our solid adsorbents, tested their cyclability >250 cycles, began successfully scaling up selected MOFs to 250 grams and shaping those materials into larger structures using several different approaches. Notably, for the MOF synthesis, the washing step was refined, leading to a substantial cost reduction by a factor of 4.5 in the synthesis. Importantly, the pilot plant has been factory tested and is close to final. We expect it to be installed at the end of this year once the building where the pilot plant will be installed is finalized. Finally, from the process design side, a comprehensive TSA (Temperature Swing Adsorption) process model has been developed in collaboration with Professor François Maréchal. The model was validated with experimental data from the literature.

During the second year, significant progress was achieved in both material development and process optimization. The construction of the pilot plant building was completed, and the gas analyzer was successfully installed. The installation of the pilot system was carried out in November 2024. On the materials front, substantial efforts were made to increase production. We successfully scaled up the production of a MOF to 1 kg and worked on protocols for structuring the material into pellets using a tableting machine, achieving promising results. Additionally, we synthesized an amine-impregnated MOF that exhibited excellent stability and cyclability in multiple tests. For KIT-6 silica, production was ramped up to 500 grams, after which the material was grafted with amines and protocols for structuring the material into pellets were developed. These materials demonstrated significant potential for applications in CO_2 separation processes. Lastly, we investigated N-doped carbons, which displayed high CO_2 capacities at 0.15 bar and 40°C and CO_2/N_2 selectivity, indicating much promise for post-combustion carbon capture. By using cheaper monomeric building blocks for the carbon, we were able to reduce production costs while enhancing its performance. In the area of process modelling, we built on last year's work by validating the TSA model for NaUSY zeolites. In the second year, we also successfully developed models for both the TCSA (Temperature-Concentration Swing Adsorption) and TVSA (Temperature-Vacuum Swing Adsorption) processes. These new models incorporate a vacuum step for regenerating the adsorption bed and were simulated using Zeolite 13X as the adsorption material. Additionally, a comprehensive life cycle assessment (LCA) was conducted to evaluate the environmental impact and sustainability of these processes. While the techno-economic assessment (TEA) remains a critical component

of our project, it is planned. The TEA will be conducted once the demonstrator has been fully commissioned and the model validated.

Zusammenfassung

In den letzten Jahrzehnten sind die CO_2-Emissionen aufgrund der negativen Auswirkungen der steigenden Treibhausgaskonzentrationen in der Atmosphäre auf die Umwelt zu einem wichtigen gesellschaftlichen Anliegen geworden; diese Auswirkungen machen die Durchführung groß angelegter CO2-Abscheidungsmaßnahmen sinnvoll. Die ausgereifteste Abscheidungstechnologie sind Wäscher auf der Basis von flüssigem Amin. Obwohl sie gut funktionieren, erfordert die CO_2-Abscheidung mit flüssigen Alkanolaminen Energiekosten von 2.5 bis 3.5 MJ/kg CO_2;[1] Werte, die noch weit von dem Zielwert von 1 MJ/kg CO_2 entfernt sind, bei dem Abscheidungsverfahren als rentabler gelten. Aufgrund ihrer geringeren Wärmekapazitäten werden feste Adsorbentien als Alternative zu flüssigen Aminen erforscht. Ziel dieses Projekts ist es daher, den Einsatz verschiedener fester Adsorbentien in einem Abscheidungsprozess im Kilogramm-Maßstab zu demonstrieren und die beste Kombination aus Adsorbent und Prozess zu ermitteln, die die geringsten wirtschaftlichen und energetischen Kosten verursacht. Wir schätzen, dass durch den Einsatz fester Adsorbentien der Energieverbrauch < 1 MJ/kg CO2 gesenkt werden kann, während die CO_2-Produktivität > 200 kg $CO_2/m^3/h$ bleibt.[2] Das Erreichen solcher Ziele kann zu einer erheblichen Verringerung der Größe (Fixkosten) und des Energieverbrauchs (variable Kosten) der Kohlenstoffabscheidungsanlage führen. Im Rahmen dieses Projekts ist es daher unser Ziel, die Leistung bestimmter Adsorbentien zu optimieren, eine Pilotanlage zur Abscheidung von CO_2 aus Gasgemischen zu bauen, deren Zusammensetzung und Temperaturen denen von Kraftwerken und anderen Abgasströmen entsprechen, und diese Adsorbentien in der Pilotanlage einzusetzen. In der Pilotanlage werden verschiedene Arten von festen CO_2-Adsorbentien wie Siliziumdioxid, metallorganische Gerüste (MOFs) und Zeolithe (mit oder ohne Aminimprägnierung) eingesetzt, und in der Pilotanlage werden verschiedene wichtige Leistungsindikatoren wie Produktivität, prozentuale Reinheit und prozentuale Rückgewinnung bei unterschiedlichen Material- und Prozessparametern überwacht. Diese Daten werden in Verbindung mit verfahrenstechnischen und technisch-wirtschaftlichen Analysen zur Optimierung der Material- und Verfahrenskombination verwendet, um ein CO_2-Abscheidungsverfahren mit den geringstmöglichen wirtschaftlichen und energetischen Kosten zu erhalten.

Im ersten Jahr wurden bereits bedeutende Fortschritte erzielt. Erstens haben wir an der Optimierung unserer festen Adsorbentien gearbeitet, ihre Zyklierbarkeit mit mehr als 250 Zyklen getestet und begonnen, ausgewählte MOFs erfolgreich auf 250 Gramm zu vergrößern und diese Materialien mit verschiedenen Ansätzen zu größeren Strukturen zu formen. Bei der MOF-Synthese wurde insbesondere der Waschschritt verfeinert, was zu einer erheblichen Kostensenkung um den Faktor 4.5 bei der Synthese führte. Wichtig ist, dass die Pilotanlage im Werk getestet wurde und kurz vor der Fertigstellung steht. Wir gehen davon aus, dass sie Ende dieses Jahres installiert werden kann, sobald das Gebäude, in dem die Pilotanlage installiert wird, fertiggestellt ist. Was schließlich die Prozessgestaltung betrifft, so wurde in Zusammenarbeit mit Professor François Maréchal ein umfassendes TSA-Prozessmodell (Temperaturwechseladsorption) entwickelt. Das Modell wurde bereits mit experimentellen Daten aus der Literatur validiert und wird in Zukunft zusammen mit den experimentellen Daten aus der Pilotanlage verwendet werden, um die optimalen Prozessbedingungen (Prozess/Materialkombination) für den Abscheidungsprozess zu ermitteln.

In diesem Jahr wurden sowohl bei der Materialentwicklung als auch bei der Prozessoptimierung erhebliche Fortschritte erzielt. Der Bau des Gebäudes für die Pilotanlage ist abgeschlossen, und der Gasanalysator wurde erfolgreich installiert. Es ist geplant, die Pilotanlage bis Mitte November zu in-stallieren. Auf der Materialseite haben wir erhebliche Anstrengungen unternommen, um die Produktion zu steigern. Wir haben die Produktion von MOF erfolgreich auf 1 kg hochgefahren und das Material mit einer Pelletiermaschine zu Pellets strukturiert, wobei wir vielversprechende Ergebnisse erzielt ha-ben. Außerdem haben wir ein aminimprägniertes MOF synthetisiert, das in mehreren Tests eine ausge-zeichnete Stabilität und Zyklierbarkeit bewiesen hat. Für KIT-6-Kieselerde haben wir die Produktion auf 500

Gramm hochgefahren, das Material mit Aminen gepfropft und erfolgreich Pellets hergestellt. Die daraus resultierenden Pellets erwiesen sich als stabil und bieten einen weiteren vielversprechenden Weg für weitere Tests und Anwendungen. Wir untersuchten auch N-dotierte Kohlenstoffe, die hohe Kapazitäten und Selektivitäten für die Gas-abscheidung aufwiesen. Durch den Einsatz billigerer Monomere konnten wir die Produktionskosten senken und gleichzeitig die Leistung verbessern. Im Bereich der Prozessmodellierung haben wir auf der Arbeit des letzten Jahres aufgebaut, in der das TSA-Modell für NaUSY-Zeolithe validiert wurde. In diesem Jahr haben wir erfolg-reich Modelle sowohl für den TCSA- (Temperature Concentration Swing Adsorption) als auch für den TVSA-Prozess (Temperature-Vacuum Swing Adsorption) entwickelt. Diese neuen Modelle beinhalten einen Vakuumschritt zur Regeneration des Adsorptionsbetts und wurden mit Zeolith 13X als Adsorpti-onsmaterial simuliert. Außerdem wurde eine umfassende Ökobilanz durchgeführt, um die Umweltaus-wirkungen und die Nachhaltigkeit dieser Verfahren zu bewerten. Die technisch-wirtschaftliche Bewer-tung (TEA) bleibt zwar ein wichtiger Teil unseres Projekts, ist aber für die Zukunft geplant. Die TEA wird durchgeführt, sobald der Demonstrator in Betrieb genommen und das Modell vollständig validiert worden ist.

Résumé

Au cours des dernières décennies, les émissions de CO_2 sont devenues une préoccupation sociétale majeure en raison des effets néfastes de l'augmentation des concentrations atmosphériques de gaz à effet de serre sur l'environnement. De tels effets rendent pertinente la mise en œuvre à grande échelle d'efforts de captage du CO_2 ; cependant, cette mise en œuvre a été entravée par les coûts économiques et énergétiques élevés du processus de capture. La technologie de capture la plus mature est celle des épurateurs liquides à base d'amines. Bien que performant, le captage du CO_2 avec des alcanolamines liquides possède un coût énergétique allant de 2.5 à 3.5 MJ/kg CO_2; [1] des valeurs encore loin de l'objectif d'1 MJ/kg CO_2, où les procédés de captage sont jugés plus viables. Compte tenu de leurs capacités thermiques inférieures, les adsorbants solides sont étudiés comme alternative aux amines liquides. Ainsi, l'objectif de ce projet est de démontrer l'utilisation de divers adsorbants solides dans un processus de capture à l'échelle du kg et d'élucider la meilleure combinaison adsorbant/processus qui donne lieu au coût économique et énergétique le plus bas. Nous estimons qu'en utilisant des adsorbants solides, nous pouvons diminuer la consommation d'énergie à moins d'1 MJ/kg CO_2, tout en maintenant la productivité de capture du CO_2 supérieure à 200 kg $CO_2/m^3/h$. [2] Atteindre de tels objectifs peut conduire à des diminutions considérables de la taille (coût fixe) et de la consommation d'énergie (coût variable) de l'usine de captage du carbone. Ainsi, dans le contexte de ce projet, notre objectif est d'optimiser les performances des adsorbants ciblés, de construire une usine pilote pour capturer le CO_2 à partir de mélanges gazeux dont les compositions et les températures correspondent à celles des centrales électriques et des flux de gaz d'échappement types, puis de mettre en œuvre ces adsorbants dans l'usine pilote. Plusieurs classes différentes d'adsorbants solides, tels que les silices, les structures métallo-organiques (MOF) et les zéolites (avec ou sans imprégnation d'amines) seront mis en œuvre dans l'usine pilote, et à partir de l'usine pilote, divers indicateurs de performance clés, comme la productivité, le pourcentage de pureté et le pourcentage de récupération avec différents paramètres de matériaux et de processus seront surveillés. Ces données, combinées à l'ingénierie de conception des procédés et aux analyses technico-économiques, seront utilisées pour optimiser la combinaison de matériaux et de procédés, nous permettant d'obtenir un procédé de captage du CO_2 ayant le coût économique et énergétique le plus bas possible.

Dès la première année, des progrès significatifs ont été réalisés. Premièrement, nous avons travaillé pour optimiser nos adsorbants solides, testé leur cyclabilité > 250 cycles, commencé avec succès à augmenter l'échelle de production des MOF sélectionnés jusqu'à 250 grammes et à façonner ces matériaux en structures plus grandes en utilisant plusieurs approches différentes. Notamment, pour la synthèse des MOF, l'étape de lavage a été affinée, conduisant à une réduction substantielle des coûts d'un facteur 4,5 dans la synthèse. Il est important de noter que l'usine pilote a été testée en usine et est proche de la version définitive. Nous prévoyons qu'elle soit installée à la fin de cette année, une fois que le bâtiment où elle sera installée sera finalisé. Enfin, du côté de la conception du procédé, un modèle

de procédé TSA (Temperature Swing Adsorption) complet a été développé en collaboration avec le Professeur François Maréchal. Le modèle a déjà été validé avec des données expérimentales de la littérature et sera utilisé dans le futur, avec les données expérimentales obtenues de l'usine pilote, nous permettant d'élucider les conditions de procédé optimales (combinaison procédé/matériaux) pour le procédé de capture.

Cette année a été marquée par des avancées substantielles tant dans le développement des matériaux que dans l'optimisation des processus. La construction du bâtiment destiné à accueillir l'usine pilote est terminée et l'analyseur de gaz a été installé avec succès. L'installation de l'usine pilote est prévue pour la mi-novembre. En ce qui concerne les matériaux, les efforts de mise à l'échelle ont été importants. Nous avons réus-si à augmenter la production de MOF à 1 kg et à structurer le matériau en granulés à l'aide d'une ma-chine à granuler, ce qui a donné des résultats prometteurs. En outre, nous avons synthétisé un MOF imprégné d'amines, qui a démontré une excellente stabilité et cyclabilité à travers de multiples tests. Pour la silice KIT-6, nous avons augmenté la production à 500 grammes, greffé le matériau avec des amines et créé avec succès des granulés. Ces matériaux ont montré un grand potentiel d'application dans les processus de séparation. Les pastilles obtenues se sont avérées stables, offrant une autre voie pro-metteuse pour des essais et une mise en œuvre ultérieurs. Nous avons également étudié les charbons dopés à l'azote, qui présentent des capacités et des sélectivités élevées pour la capture de CO_2. Grâce à l'utilisation de monomères moins chers, nous avons pu réduire le coût de production tout en améliorant les performances. En ce qui concerne la modélisation des processus, nous nous sommes appuyés sur les travaux de l'année dernière, qui ont permis de valider le modèle TSA pour les zéolithes NaUSY. Cette année, nous avons développé avec succès des modèles pour les procédés TCSA (Temperature Concentra-tion Swing Adsorption) et TVSA (Temperature-Vacuum Swing Adsorption). Ces nouveaux modèles intègrent une étape de vide pour la régénération du lit d'adsorbant et ont été simulés en utilisant la zéolithe 13X comme matériau adsorbant. En outre, une évaluation complète du cycle de vie (ACV) a été réalisée pour évaluer l'impact environnemental et la durabilité de ces procédés. Bien que l'évalua-tion technico-économique (TEA) reste une partie importante de notre projet, elle est prévue pour l'avenir. Elle sera réalisée une fois que le démonstrateur aura été mis en service et que le modèle aura été entièrement validé.

Contents

List of abbreviations

BET - Brunauer–Emmett–Teller

DSC - Differential Scanning Calorimetry

FAT - Factory Acceptance Test

gPROMS - general PROcess Modelling System

KIT - Karlsruhe Institute of Technology

KPI - Key Performance Indicator

MFC - Mass Flow Controller

MOF - Metal-organic framework

PEI - Polyethyleneimine

PID - Process and Integral Development

PLC - Programmable Logic Controller

PSA - Pressure swing adsorption

PSE - Process Systems Engineering

SBA - Santa Barbara Amorphous

TGA - Thermogravimetric Analysis

TSA - Temperature swing adsorption

TVSA - Temperature vacuum swing adsorption

VPSA - Vacuum pressure swing adsorption

VSA - Vacuum swing adsorption

MIL - Matériaux de l’Institut Lavoisier

TEPA – Tetraethylenepentamine

TAEA – Tris(2-aminoethyl)amine

BDE – 1,3-Butadiendiepoxide

TMPTE – Trimethylolpropane triglyciyl ether

1 Introduction

1.1 Context and motivation

The last twenty years have witnessed significant climatic changes, with ten of those years being the hottest on record.[1] This has resulted in various environmental challenges such as melting arctic glaciers[2], rising ocean levels[3], and extreme weather patterns[4]. Since the 1970s, there has been a 70% increase in global anthropogenic CO_2 emissions, primarily due to the combustion of carbon-based fossil fuels. These fuels account for 70 to 80% of global energy. Large point sources, like coal-fired power plants, contribute to over 40% of global CO_2 emissions.[5]

Carbon dioxide (CO_2) capture is a critical process in mitigating the effects of climate change. Albeit that liquid-amine scrubbers are the most mature technology for CO_2 capture,[6] their implementation on a large scale is hindered by the high energy requirement for regeneration, which consumes about 30% of the total energy output of the power plant.[7] Additionally, liquid amines have several drawbacks, such as being corrosive, volatile, and instability over time, which negatively impacts their performance. The most mature method of CO_2 capture involves the use of liquid alkanolamines, which require an energy cost ranging from 2.5 to 3.5 MJ/kg CO_2. This energy consumption is considerably higher than the target of 1 MJ/kg CO_2, which is considered viable for capture processes.

Considering the limitations of liquid amines, solid adsorbents emerge as a promising alternative owed to their lower heat capacities, which could significantly reduce the parasitic energy cost of the capture process. These adsorbents have the potential to significantly reduce energy consumption to as low as 500 kJ/kg CO_2,[8] making them a focal point of current research and development in the field of CO_2 capture. Moreover, amine-functionalized materials, where amines are incorporated into the pores of solid adsorbent materials, like silicas and metal-organic frameworks (MOFs), have shown significant potential for CO_2 capture with high CO_2 selectivity and capacity. While these materials present promising attributes, they also come with inherent challenges that have also posed barriers to their real-world implementation. A predominant challenge is the amine degradation and loss during the CO_2 capture and release, which challenges the material's efficiency over the long-term. In the context of this project, we aim optimize both the materials performance and the capture process.

Given this, our group is developing solid adsorbents for CO_2 capture applications and assessing their performance in the targeted separation. Due to the lower heat capacity of solids, when compared to aqueous liquid amines, they can offer significantly lower regeneration energies. For materials design, we incorporate amines directly into the pores of materials, such as silicas and metal-organic frameworks. One example of a silica material, SBA-15, is shown in Figure 1. While this material offers a reasonable adsorption in the low-pressure regime, 1.5 mmol/gram of CO_2, when we test the CO_2 desorption (at and above 120 ºC) we find that many of the primary amines degrade forming linear and cyclic ureas, which kill the materials performance with adsorption/desorption cycling, Figure 1a and b. As such, we have developed methods to chemically modify the primary amines to inhibit such transformations in SBA-15, Figure 1c. Through this simple modification, which decreases the percentage of primary amines from 41% to 19%, we find much improved cyclability with a consistent CO_2 capacity of ~1.2 mmol per gram at 120 ºC.

Moreover, we hypothesized that using porous materials with larger pore volumes might help increase the materials capacity as they can incorporate more amines. Thus, we took a larger pore silica, referred to as KIT-6, which has an internal surface area of 550 m^2 per gram and a pore volume of ~1.3 cm^3 per gram, a value that is 40% higher than SBA-15. Next, we infused the material with the modified polyethylene imine giving rise to a cyclable capacity of ~1.5 mmol of CO_2 per gram, Figure 2.

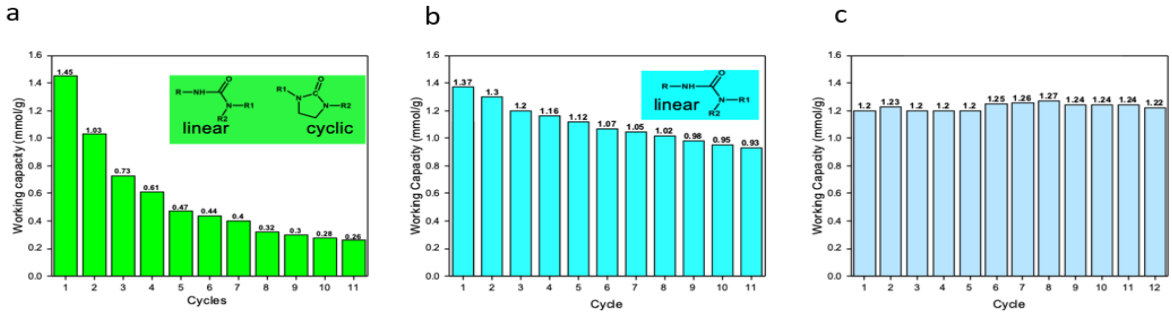

Figure 1. The CO_2 adsorption capacity drops with adsorption desorption cycling, diminishing the materials desorption capacity, when desorption is carried out at (a) 150ºC and (b) 120ºC due to the formation of linear and cyclic ureas. However, when we modify the amines we see that we can stabilize the materials allowing them to desorb CO_2 over many cycles without the formation of any urea species (c) when the desorption is carried out at 120ºC.

The main purpose of the project is to demonstrate a capture process, on the kilogram scale, that offers a low energy cost, e.g., < 1 MJ/kg CO_2. To achieve this, both the materials and separation process must be optimized. For instance, to counteract the challenges with amine degradation and loss during the adsorption/desorption cycling process, we have embarked on chemical modification (similar to the silicas as described above) of the adsorbents with the aim of enhancing their stability and CO_2 adsorption capacity. We are also loading chemically modified amines into the pores of various porous templates, including MOFs and silicas. It is known that the chemical composition and pore structure of the template can alter amine degradation and loss and so we are aiming to optimize their performance metrics (capacity and selectivity). Notably, we are simultaneously developing strategies to study their long-term separation performance (cyclability) in our laboratory using thermogravimetric analyzers.

We have specifically developed amine functionalized solid sorbents with 2 different supports:

1. Silica / amine composite: By infusing KIT-6, a silica material with a larger pore volume, with chemically modified amines (Polyethylenimine, PEI), we have achieved a cyclable capacity of approximately 1.5 mmol of CO_2 per gram (Figure 2).

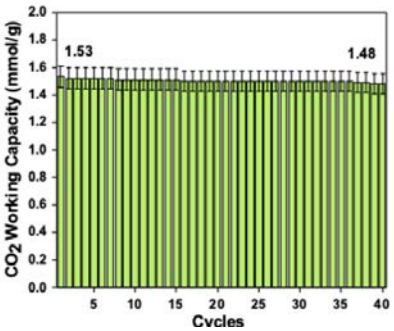

Figure 2. The CO_2 adsorption capacity of KIT-6/PEI is around 1.5 mmol per gram with a desorption temperature of 120ºC. Adsorption was carried out at 40ºC, a temperature that is relevant to post-combustion flue gas.

2. MOF/amine composites: Utilizing the structural attributes of MOFs, known for their expansive surface areas and pore volumes, we have impregnated amines inside selected MOF pores, using several different strategies. The best performing composite not only boasts a high adsorption capacity, surpassing >2 mmol CO_2 per gram of adsorbent in the low-pressure regime relevant to post-combustion carbon capture, but also demonstrates superior CO_2/N_2 selectivity (>250) and long-term cyclability (Figure 3).

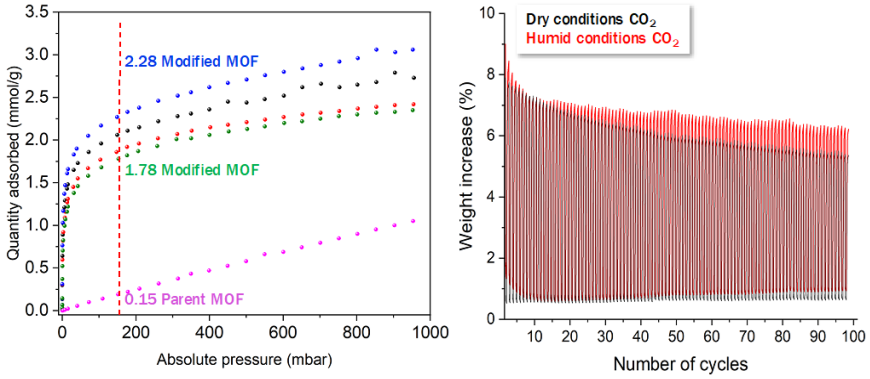

Figure 3. (left) The CO_2 adsorption capacity of a MOF modified with amines. The modified materials offer capacities > 2 mmol per gram. (right) Moreover, the materials made offer stable adsorption (40 °C) desorption (120 °C). We have already tested several materials over 250 cycles. They show minimal change in their performance in humid gas mixtures containing CO_2 (15%) and N_2 (85%) after such cycling. We note the cyclability is improved in wet conditions over dry ones.

While we are also continuing with adsorbent design and optimization, the primary aim is now is to scale up these chemically modified adsorbents, shape the fine powders into larger aggregates, and implement them in a pilot unit dedicated to CO_2 capture. This transition is pivotal to validate the laboratory findings under real-world conditions and to explore the broader applicability of these adsorbents in mitigating CO_2 emissions.

1.2 Project objectives

The goal of the project is to develop and demonstrate the effectiveness of energy-efficient CO_2 capture using amine-decorated solid adsorbents developed in our laboratory. The project aims to:

1. Scale-up and evaluate the production of two novel solid adsorbents (amine incorporated KIT 6 and a MOF/amine composite).

2. Collaboratively structure these adsorbents on a kilogram scale through extrusion, microdroplet, or tableting processes.

3. Execute a continuous CO_2 separation process using the demonstrator over extended periods of time (with continuous adsorption/desorption cycling).

4. Assess CO_2 capture capabilities in both simulated environments and actual gas emissions.

5. Benchmark the efficiency and cost-effectiveness of our carbon capture against different processes (PSA, VSA, TVSA or combinations thereof) and commercial materials (Zeolite 13X (alternatively known as NaX) is the benchmark material), specifically examining different variables such as temperature, pressure, and vacuum swings.

7. Analyze the optimal material/process conditions through process design and simulation.

8. Conduct technoeconomic analysis on the proposed separation process and compare against others.

9. Achieve the target of separating ~1 kg of CO_2 daily from gas mixtures.

10. If time is permitting, we may incorporate other adsorbents into the demonstrator and process modeling for further comparison; these could include, for instance, nitrogen-doped carbons, and other MOF-based physisorbents, like Mg-MOF-74, CALF-20, and Al-fumarate.

11. Finally, integrate the developed adsorbent material/optimal technology identified into a designated district demonstrator.

At its core, the project seeks to answer whether solid adsorbents can compete, in terms of energy efficiency and cost-effectiveness, with conventional liquid amine CO_2 scrubbers and identify the most critical parameters that influence the energy and cost effectiveness as needed for the implementation of carbon capture on large scales.

2 Approach, method, results and discussion

2.1 Description of facility, procedures, and methodology

2.1.1. WP 1 Design of the CO_2 separation demonstrator:

The pilot plant was designed based on the needs for post-combustion flue gas capture and is meant to help us meet our objectives outlined above. Notably, the unit is versatile allowing us to simulate flue gas and other exhaust gas mixtures or can be used for real industrial gas mixtures. For the unit design, we have had regular communication with the company over the past year to evaluate progress in the unit construction and to discuss optimization of the unit design and its performance. The detailed specifications (Figure 4) were communicated to the company PID Eng & Tech, whom was responsible for assembling the customized pilot plant. We notably have spent much time during the unit construction and optimization, making modifications as needed to meet our needs. In addition, once the pilot plant was almost finalized, two EPFL team members traveled to the company's facility in Spain to perform a factory acceptance test (FAT). Figure 5 shows the actual pilot plant and Figure 6 shows the user interface that is employed to control the unit's function. We note the unit, once programmed, can operate continuously without human intervention for extended periods of time and is equipped with a number of safety controls so that it shuts down automatically should there be a system failure. This FAT served to double check the parts that were included in the unit as well as testing the basic operation conditions using a commercial adsorbent, namely zeolite NaX (zeolite 13X). Afterwards, we made a few minor modifications to the pilot plant to access the full potential of the unit. These final modifications were meant to enable several types of adsorption/desorption separation types such as temperature swing adsorption (TSA), vacuum swing adsorption (VSA), pressure swing adsorption (PSA), or combinations thereof.

The specifications of the pilot plant are described below:

- 3 adsorption beds of 1.2 m length and 2.54 cm diameter. Two of them have the ability to work in parallel (adsorption and desorption mode continuously) while the third can operate independently and is aimed at coupling it after an upstream membrane separation step of Professor Kumar Agrawal.
- The unit has 6 mass flow controllers (MFC) that will allow for preparing synthetic gas mixtures containing CO_2, N_2, O_2 and traces of contaminants as well as inert gases such as Ar and N_2 to perform the activation of the adsorbents in situ. Notably the unit can also be utilized with acid gas impurities, like SO_x and NO_x. Flow rates can range from 0.2 to 10 L/min.
- Industrial flue gas mixture cylinders can also be readily connected to the separation unit and flown through the system with the mentioned MFCs.
- Humidity will be measured and adjusted prior to the inlet of the adsorption beds via a control loop with a humidity generator. The gas lines will be heated throughout the unit to avoid water condensation in cold spots.
- The pressure of the gas will be monitored and adjusted before and after the beds using pressure control valves, accounting for pressure drops across the packed adsorbent as well as our expected process pressure in case of PSA tests (1 bar to 39 bar max).
- Vacuum levels will also be controlled in VSA processes. We will be able to fine tune the vacuum level inside the bed accurately down to 30-50 mbar in the desorption step by using the same pressure control valves.

- The beds are surrounded by heating (electrical) and cooling (water/cooling liquid) jackets. This will allow for controlled TSA processes. The adsorbent temperature will be continuously monitored with 5 thermocouples throughout the bed. This will allow us to assess the heat released during the exothermic gas adsorption step, while also to control the heating and cooling rates for both the adsorption and desorption steps.
- A set of 4 rotary valves will allow for the control of the direction of the gas flow in the bed, being either top-down or bottom-up, which will let us have more control in the design of adsorption/desorption processes.
- The current compressor can compress gas from 1 bar to 6 bar as a first compression step. To compress CO_2 up to 50 bar (maximum pressure below supercritical point at room temperature) we will have to couple our compression system with a more powerful compressor. For that, we plan to share the compressor with another demonstrator unit, which is in the same building and could reach the expected high pressure to prove the CO_2 storage in 50 L gas cylinders. We have also considered buying a compressors; however, the cost exceeds our budget.
- 2 vacuum pumps are included to control the vacuum levels of the 2 beds in parallel and of the independent 3rd bed in case of in situ activation or VSA processes.
- Downstream of the beds we included a water condensation trap to avoid damaging the compression and vacuum systems.
- All the outlet lines from the 3 beds can be directed to the mass spectrometer analyzer, to the compressor, or to vent by using the automated valves installed in the unit.
- An HPR-20 R&D gas analysis system was purchased independently from Hiden (UK) and will be connected to the outlet of the demonstrator (Figure 7). This will allow us to determine the gas composition in real time, including the mentioned gases (CO_2, N_2, O_2, Ar), corrosive gases (NO_x and SO_x in trace amounts) and water present in the stream. The outlet gas concentrations will provide insights on relevant key performance indicators (KPIs) such as purity, recovery, and productivity. These parameters, together with the energy employed in the desorption step will be critical to identify the most adequate CO_2 capture process.
- All these features will be controlled from a computer by the user-friendly Programmable Logic Controller (PLC) designed by the PID Tech&Eng company (Figure 6).

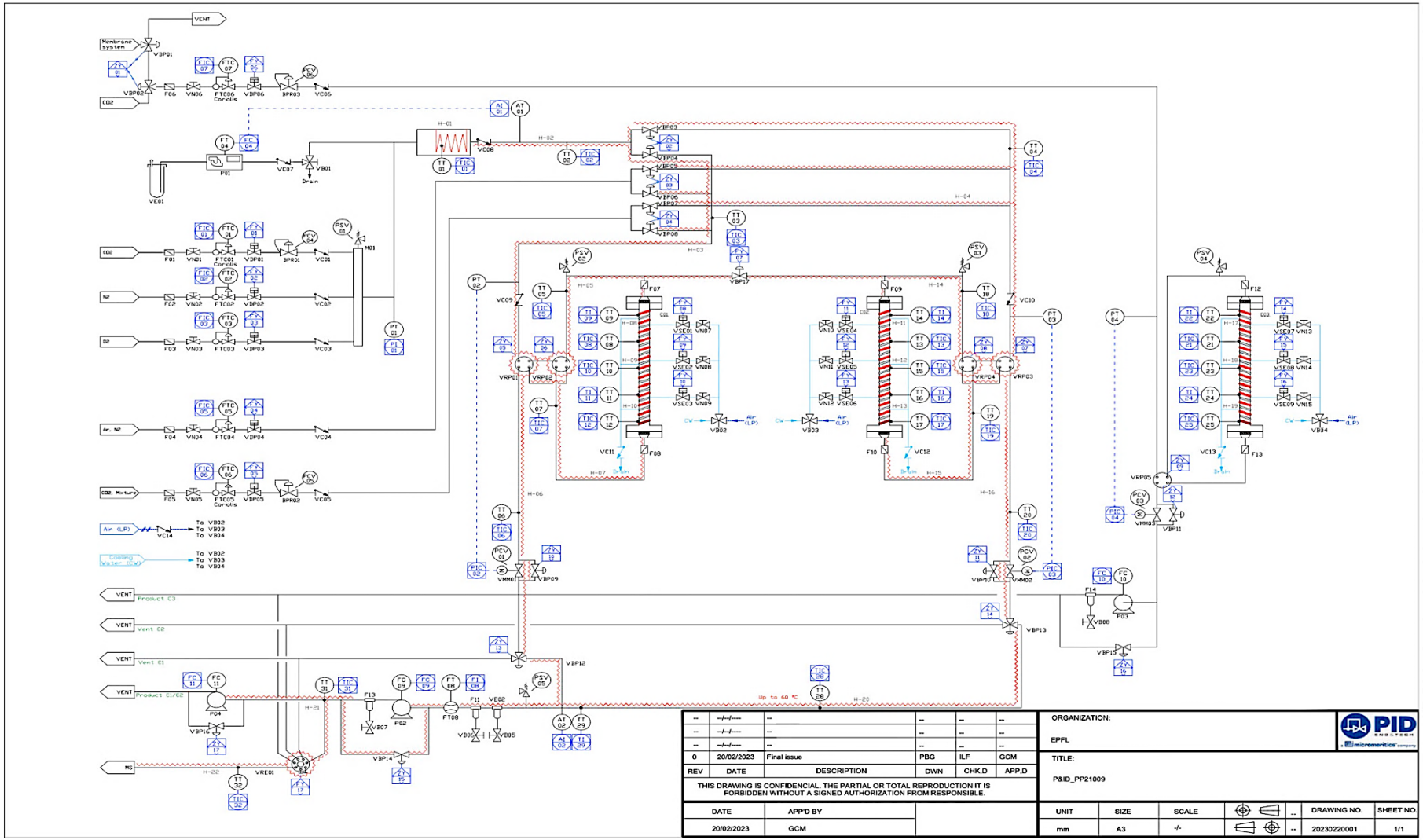

Figure 4. Process and instrumentation diagram of the CO_2 demonstration unit.

Figure 5. Picture of the pilot plant during the FAT at the PID Eng&Tech facility.

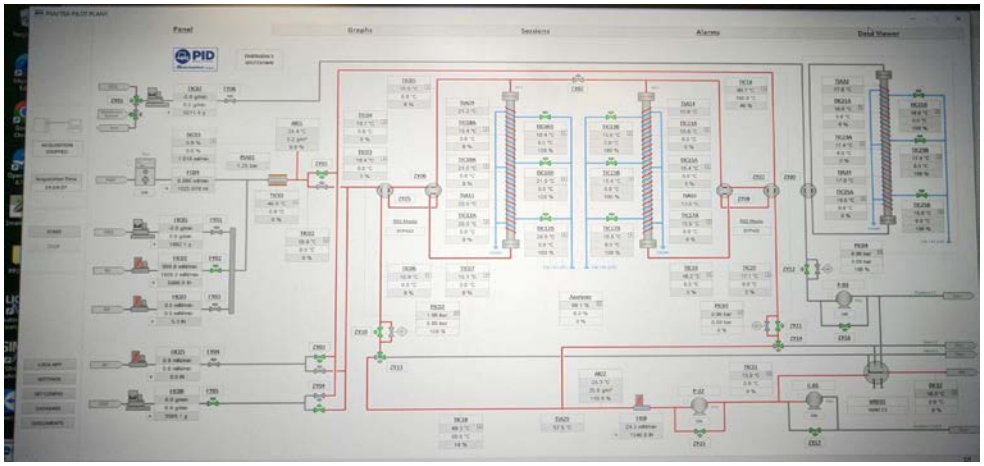

Figure 6. Programmable Logic Controller (PLC) image that will control the pilot plant from a PC.

Figure 7. Image of the HPR-20 R&D gas analyzer from Hiden.

2.1.2. WP 2 Design, scale-up, and structuring of adsorbents for carbon capture:

Over the past year, we have worked on the MOF scale. The protocols we use are described in Section 3. For scale-up we are using a 1L autoclave, where the MOF building blocks are mixed along with their solvents. The materials are sealed in the autoclave and heated (up to 200 ^{o}C) over extended periods of time. To get to larger scales, we aim to purchase a 10L reactor in the near future. Once materials are made, they are washed (to remove residual ligand from the MOF pores) and subsequently activated (via heat and vacuum typically) to remove solvent from the pores. The materials are additionally subjected to PXRD to test crystallinity and N_2 adsorption measurements (at 77 K) are carried out to assess surface areas and pore volumes. This allows us to ensure material quality with scaling.

We have also begun shaping the scaled-up MOF and commercially available zeolite powders. For this, each powder is placed in a dye and then the powder is pressed into a tablet using a press (Figure 8a). All samples are first pressed by hand using a manual press (with and/or without the addition of various binders) which offers pressure ranges from 0.125~15 ton force. For making binder-free tablet, 0.1 g of Zeolite or MOF powder were employed and pressure was applied for ~2 min (Figure 8b). After filling a certain volume (for example 5 mL) of the material, the sample weight was obtained using a balance and the density was calculated by dividing the weight by the volume. Crush strength measurements were performed on a ProLine materials testing device (ZwickRoell). For this, tablets were tested three times per sample, and the average crush strength was assessed. Notably, for this, the tablets are put under pressure (laid flat) and the pressure at which the tablet breaks was recorded. Last, mechanical friability tests were performed on a digital rotator (IKA Loopster digital) with 2 mL SafeSeal microtube (PP). The speed was set at 50 rpm and the weight loss was measured after 500 cycles (Figure 8c). Notably various parameters including the BET (BET = Brunauer–Emmett–Teller) surface area (SA), pore volume, PXRD patterns, gravimetric and volumetric CO_2 adsorption capacity (40 ^{o}C and 0.15 bar) are assessed before and after tableting. Further, once the correct parameters for the tablets are elucidated, they can be transferred into an automated tableting DT25 Desktop tableting press, which (Figure 8d) allows us to make tablets under continuous flow.

The specifications for the high throughput tableting press (Figure 8d) include the following:

- Makes 3 to 25 mm diameter tablest with ease;

- Produces up to 1,500 tablets per hour;
- Hopper holds up to 5 kg of sample;
- Is equipped with a transparent turret shield that provides operator safety (from fine powder inhalation) and prevents cross-contamination of powder between batches;
- Up to 100 kN pressure can be achieved for strong, properly finished pharmaceutical grade tablets;
- Tunable pressure;
- Safety shut-off button for emergencies.

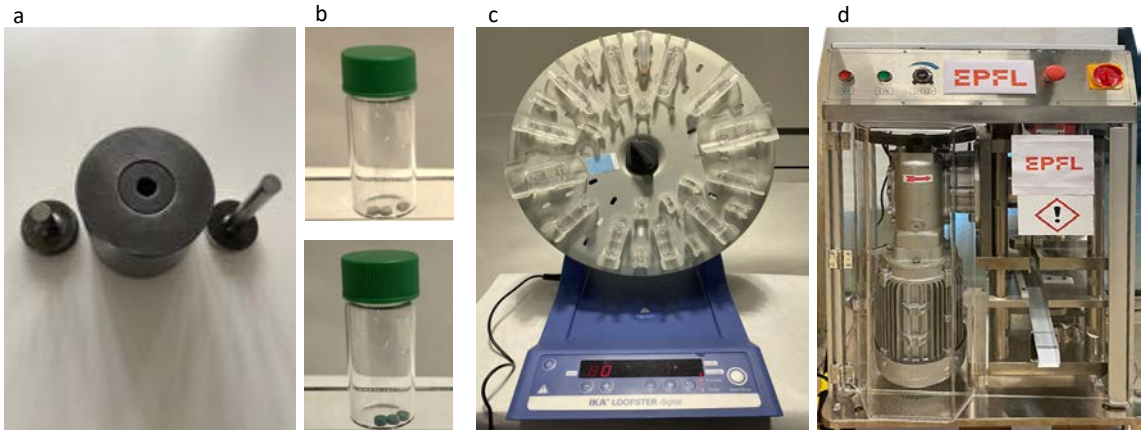

Figure 8. Image of the process flow for tableting from a a) single punch press allowing variable pressures to be tested, b) tablet formation, and c) testing the friability of tablets using a rotary wheel, to d) the automated, high throughput tableting press that can operate under continuous flow, with up to 1,500 tablets per hour produced.

In addition, an instrument was also purchased to better assess the friability of the obtained pellets/beads/extrudates in a standardized manner (Figure 9). We will screen the adsorbents by placing them onto the wheel and spin it around at least 500 times. After that, we will weigh the adsorbents that are still in one piece and compare that to the mass of the pellets taken before the test.

Figure 9. Picture of the attrition instrument that will be used in the future to assess the robustness of the structured adsorbents.

In addition to this, several new adsorbents were designed and tested in the lab. Notably, after making adsorbents, surface areas, pore volumes, PXRD patterns, low pressure (0-1.1 bar, 40-80 ^{o}C) CO_2 adsorption properties, and breakthrough analysis are tested. For the best performing materials, cyclability studies are also carried out. For the latter, we have purchased a TGA/DSC (thermogravimetric analyzer/differential scanning calorimeter) combo instrument from Linseis (Germany) (Figure 10). This new instrument, to be dedicated to such studies, will also allow us to measure the enthalpy of adsorption and regeneration energies associated with CO_2 adsorption inside the materials along with running continuous cycles under relevant gas mixtures, with and without humidity (Figure 10). It will also allow us to do accelerated aging studies of the adsorbents (having higher O_2 content in the gas stream) and assess the enthalpy of adsorption and regeneration energies of various adsorbents in CO_2 gas mixtures. We have recently sent one researcher to perform the FAT of this device on July, 2023 in Germany. Notably, much time was spent trying to do consistent cycling studies on our existing TGAs as well. Significant problems were encountered related to declining CO_2 concentrations and variability of temperatures and humidity levels. Such variability can make it difficult to assess materials performance decline with cycling, and so we believe a temperature and humidity-controlled chamber may be required in the future.

The specifications of the new TGA/DSC combo include the following:

- Simultaneous measurement of weight differences and heat of adsorption under relevant post combustion gas mixtures (CO_2, N_2, O_2) with controllable humid levels.
- Cycling testing for long term stability of the adsorbents.
- Potential TSA and VSA operation modes.
- Liquid N2 dewar to faster cool down the furnace.
- 4 MFCs will allow for mixing gases under dry or humid conditions or flowing premixed gas compositions from cylinders.
- Two different thermocouple systems that allow for long range temperature measurements from -150 ^{o}C to 1000 ^{o}C.
- Two different humidity generators:
    - 1 bubbler for room temperature saturation with water vapor which allows for working under VSA conditions thanks to the presence of a check valve that would avoid the water from the bubbler to reach the furnace under vacuum conditions (Figure 10b).
    - 1 commercial humidity generator with a heated transfer line that will allow for precisely tuning the humidity in the gas streams at controlled temperatures. This system will be useful under TSA cycling, since the lack of check valve will create issues under vacuum when attempting VSA cycling (Figure 10c).
- Upon upgrading the measuring system, we could be able to extract heat capacities (more stable balance pans, metallic ring to retain heat dissipation, reference sapphire sample).

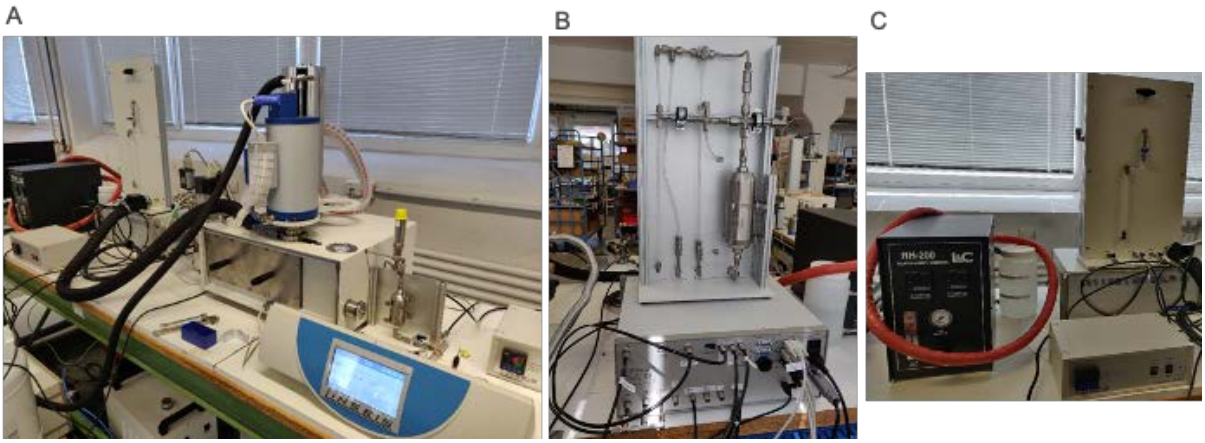

Figure 10. a) Image of the TGA/DSC combo instrument that will allow measuring in situ both the weight difference and heat adsorption/release during realistic CO_2 adsorption cycles. b) Water bubbler to saturate gas mixtures with water vapor at room temperature that allows for working under TSA and VSA conditions. c) Controllable humidity generator that allows for setting precise humidity levels in the gas stream and is able to work under TSA conditions.

2.1.3. WP 3 Techno-economic studies to investigate the viability of the CO_2 capture process:

As materials are being scaled up and structured, the next logical step is their implementation in the pilot plant to monitor separation performance. Notably, numerous material properties and process design parameters influence the CO_2 capture performance. Some examples of material properties and process parameters include specific heat, mass transfer coefficient, heat transfer coefficient, desorption temperature and vacuum pressure. However, manually tuning these variables, through a trial-and-error approach, is both time-consuming and resource-intensive.

Process modelling

To tackle this challenge, we have implemented a process modeling approach for CO_2 capture processes in collaboration with Industrial Process and Energy Systems Engineering (IPESE) headed by Professor Francois Maréchal. The process modelling opens many possibilities, enabling us to explore and identify the optimal values of material and process variables necessary to achieve the desired process performance. To facilitate this modeling, we employ gPROMS, a modeling tool developed by Siemens Process Systems Enterprise.[9] This tool serves as a platform for constructing a comprehensive process model. Our primary aim is to establish a robust feedback loop that seamlessly connects process design with material properties. This simulation approach provides deep insight into the sensitivity of each material property/parameter on the final process performance. These properties include, not only the adsorption capacity but also factors like kinetics, selectivity of CO_2 over other gases in the flue gas mixture, and the desorption temperature at which CO_2 is efficiently released in the TSA process. Overall, this feedback enables us to prioritize and optimize critical aspects of the process for maximum efficiency and effectiveness.

To start, Temperature Swing Adsorption (TSA) process was modelled, which is a promising adsorbent regeneration process for CO_2 capture and involves swinging the temperature between a lower adsorption temperature, where CO_2 is captured, to a higher desorption temperature, where CO_2 is released. Using gproms, we have developed a model that simulates complex interactions between the adsorbents and the associated process parameters to make accurate performance prediction.

The developed model provides key performance indicators, which are as follows:

1. CO_2 Purity (%): Indicates the percentage of CO_2 in the captured product stream.

2. CO_2 Recovery (%): Reflects the percentage of CO_2 successfully separated and captured.

3. Productivity (kg CO_2/kg adsorbent per hour): Measures the efficiency of CO_2 capture per unit of adsorbent and time.

Afterwards, the energy consumption can be computed and compared to that of the state-of-the-art MEA based absorption process, which is discussed in the next chapter of this report.

Extension to TCSA and TVSA configurations

Notably, after building the foundational model, based on TSA, the next step is to extend the modeling framework to encompass other adsorption configurations. For instance, some of the configurations could include steam-assisted temperature swing adsorption (S-TSA), temperature vacuum swing adsorption (TVSA), steam-assisted temperature vacuum swing adsorption (S-TVSA). These configurations have been reported to provide improved performances offering a broader landscape of possibilities for CO_2 capture technologies.[10] However, there are trade-offs between energy consumption and productivity in each of the process, which has to be critically understood.

Optimization objectives

The primary objective of this extension is to identify an optimal process configuration that meets the performance criteria as defined by US DOE targets which includes CO_2 recovery of 90% and purity of 95% with minimum energy consumption. Desorption temperature, steam flow rate, vacuum pressure, cycle time constituting adsorption, desorption, heating, cooling, and purge time are some of the many critical parameters that will be assessed in the analysis for estimating the optimal performance. Furthermore, with the current demonstrator, we aim for the productivity 2-4 kg of CO_2 capture per day.

2.1.4. Techno-Economic Analysis (TEA) of optimal configuration

Upon identifying the most promising configuration through process modelling and optimization, a comprehensive TEA will be conducted. This analysis will help in assessing the economic feasibility of the optimal configuration by computing key performance criteria such as annualized capital expenditure, annualized operational costs, and finally estimating the specific cost of the CO_2 capture (CHF/kg-CO_2 captured).

TEA methodology

System boundary of the analysis

The scope of the analysis will be to perform a techno-economic analysis of a CO_2 capture at a pilot scale producing ~1 kg of CO_2 per day. Components within the system boundary for this preliminary phase include the cost of adsorption vessels, feed gas blowers/compressors, heat exchangers, control valves, simulated feed gas mixtures, and coolants for Temperature Swing Adsorption (TSA) and additionally, vacuum pumps in the case of Temperature Vacuum Swing Adsorption (TVSA).

Cost analysis

The economic framework takes input (material and energy flows) from the process model to calculate both capital and operational costs. Capital expenses encompass the costs of equipment and adsorbent material along with the miscellaneous components, while operational expenses are determined by cost of utilities (electricity, cooling water), adsorbent regeneration, and maintenance costs. Necessary data, regarding costs, will be acquired using the following approaches:

- *Vendor cost data*: For specific equipment and materials, the cost data will be obtained from the vendor.

- *Literature and published data*: The purchase cost of the sized equipment (vacuum pump, compressors, heat exchangers, contactor vessels etc.,) would be calculated with the empirical equations available from the scientific literature including Seider et al[11], Couper et al[12],and Turton et al.[13]

The cost analysis will be based on the Total Annualized Cost (TAC) per unit mass of CO_2 capture defined as:

TAC = $AIC + AOC$

where AIC and AOC are the Annualized Investment Costs and Annual Operating Costs, respectively.

The AIC is computed as the sum of the initial plant purchase cost, whose capital investment is subject to annualization and of the further maintenance cost, as follows:

AIC = $AMC + TPC * CRF$

with TPC being the Total Plant Cost, AMC being the Annual Maintenance Cost and CRF is the Capital Recovery Factor (CRF), which relates the discount rate *(i)* and the number of annuities received (*n* = plant lifetime) and is commonly defined as[15]

CRF = $\frac{i(i+1)^n}{(1+i)^n-1}$

The procedure and the empirical equations presented by Hasan et al.[14,16] will be adopted to calculate the cost parameters for the large-scale capture unit. The way in which the cost terms will be estimated are given in Table 1.

Table 1: Some of the cost terms and equations for their estimations (adapted from[16])

Cost term	Formula	Details
Total Plant Cost (TPC)	TPC = Σ (TIC+IDC+BOPC) IDC = 0.32*TIC BOPC = 0.2*TIC	TIC: Total installed costs IDC: Indirect costs BOPC: Balance of plant costs EPC: Equipment purchase costs EIC: Equipment installation costs
Total Installed Costs (TIC)	TIC = Σ (EPC+ EIC)	
Annualized Maintenance Cost (AMC)	5% of TPC	

Total installed costs (TIC) will include equipment purchased cost, installation costs, instrumentation and control costs, painting, insulation, electrical and piping costs, buildings, service facilities costs, spare part taxes, and insurance and freight charges. Indirect costs (IDC) will include engineering and supervision, construction expenses and contingencies. Balance of plant costs (BOPC) would account for auxiliary buildings, service facilities and yard improvements. TIC will be estimated as the function of equipment installation cost (EIC) and equipment purchase cost (EPC). EIC will be estimated by calculating the equipment installation cost proportionally to its purchase cost as proposed by Garrett.[17] Finally, operating expenses will include all costs related to the utilities required for process operation (mainly the energy supplies) which is largely driven by electricity and the use of hot gases and/or steam as a purge.

Cost data will be updated for the current year (i.e., CHF_{2023}) using the Chemical Engineering Plant Cost Index (CEPCI). Relevant assumptions will be made in case of data being not available and those will be clearly stated in the final report.

Overall, from the TEA, one can expect the **sensitivity analysis** of how different **process variables affect the key performance indicators over the cost variables.** Furthermore, the **estimated unit cost of CO_2 capture** for the in-house developed **MOF composite and silica-amine composite** along with the **commercial Zeolite 13X** will be computed.

If resources and time permits, we will consider implementing other physisorbent materials. Some examples of such materials could be Mg MOF 74, Al-fumarate, Al-formate, or CALF-20. It would be interesting to implement them in the demonstrator and perform a TEA. Being physisorbents, these materials are interesting as they may provide reduced energy consumption when implemented in the process due to easier CO_2 desorption. Furthermore, we will undertake a comprehensive life cycle assessment to gauge the environmental implications of these materials from production to disposal. Additionally, we are considering a future extension of our study to include a TEA focused in capturing 1 ton of CO_2 per day (for an industrial scale). This expansion would entail an analysis of equipment sizing and cost estimations accordingly.

By adhering to this methodology, we aim to provide a well-rounded, accurate, and insightful TEA that will provide economic feasibility and viability of the CO_2 capture pilot plant.

2.2 Activities and results (first year)

2.2.1. WP 1 Design of the CO_2 separation demonstrator:

During the first year, the design of the CO_2 capture demonstrator was finalized. It was constructed in the facilities of PID Eng&Tech (Micromeritics, Spain), and the specifications are described above. During the funding period, the FAT was carried over 3 days at their facility in Spain and was approved from our side. Only minor modifications were requested including: i) fine tuning the vacuum levels to allow VSA processes, ii) the installation of a pressure sensor after the adsorbent beds, which will provide us with information about the pressure drop across the packed bed, and iii) the installation of a larger water trap before the compression and vacuum systems. These needs were determined during the FAT, when preliminary tests were carried out for CO_2 capture using zeolite 13X (NaX), which consisted of overnight cycles of adsorption/desorption under humid CO_2 while applying a temperature swing between 40 and 150 ^oC.

The pilot plant was delivered to EPFL Valais on the 21st of March 2023; despite this, the installation was not possible. Importantly, the demonstrator is partly funded by the Canton of Valais, which is providing the funding necessary for a new building that will house the pilot plant. In addition to the building, there are needs for other infrastructure like gas lines, containers for gas cylinders, extraction systems, etc. Given this the project has required strategic planning and safety evaluations. The complexity of the project and other issues have delayed the construction. Although we considered using the pilot plant in our laboratory, there were other cost issues related to the need to install new gas lines and also safety issues as the high gas flow rates in the pilot plant would likely put stress on the buildings extraction systems. Given this, we have postponed the installation of the pilot plant until the building is finalized.

2.2.2. WP 2 Design, scale-up, and structuring of adsorbents for carbon capture:

For CO_2 capture materials to be placed inside the demonstrator unit, we have proposed the use of various adsorbents including a MOF containing amines, an amine infused silica (KIT-6), and a commercial Faujasite zeolite, like zeolite13X (NaX), which will be used as the benchmark adsorbent throughout

the project and to commission the pilot plant. Given that the zeolite is commercially available, we have started focusing on the MOF synthesis and scale-up, which will be used as a support for an amines.

Based on reported synthesis of the MOF synthetic procedures, the production cost on a laboratory scale is 200 CHF/100 g (considering only the cost of raw materials). However, it should be noted that 90% of this stems from the extensive washing steps, which requires the use of expensive organic solvents. As such, reducing the volume of solvent and washing steps while keeping similar porosity has been one of our main motivations during the first part of this project, aiming at making such materials in a more scalable and less resource intensive manner. Thus, a protocol for the MOF scale-up was developed, which is described below.

Cr-MOF synthesis:

Cr-MOF was synthesized using a protocol that is similar to one previously reported. For this, a 1 L autoclave is charged with 52.8 g $Cr(NO_3)_3.9H_2O$, 18 g terephthalic acid (BDC), 660 mL DI water and 8.56 mL HNO_3 (65 %), and the mixture is stirred for 30 mins to homogeneous the solution. The autoclave is then kept in a preheated oven at 200 ^oC for 16 h and cooled to RT in 4 h. The reaction yields ~18 grams of green MOF powder.

Cr-MOF washing protocol:

After vacuum filtration, to remove the as-prepared MOF, the material must be extensively washed before subsequent modification with the amines. The need for washing stems from residual starting materials that are trapped inside the MOF pores, namely ligands. In the reported protocol,[18] for producing the MOF in 1 L scale with high crystallinity and surface area of 3400 m^2/g, about 3 L of DMF and 3L of ethanol is used. Hence, the total cost in producing MOF is 66.25 CHF per L of reaction. Remarkably, about 60 CHF/L reaction comes solely from the use of DMF solvent. Here, to reduce the cost, we optimized the amount of DMF used in the washing protocol. Such optimization is achieved by careful characterization of each washing step and analyzing aliquots of the washed solvent in ^1H-NMR to detect the concentration of MOF ligand removed in each washing step. We used four different washing protocols with DMF, to achieve the optimum material with the lowest amount required of DMF solvent.

Protocol 1 : The 1 L reaction product is separated in four flasks with a volume of 250 mL each. The as-synthesized MOF is centrifuged to remove the mother liquor and dispersed in 50 mL of DMF and stirred at RT for 4 h, 12 h and 6 h with fresh solvent (50 mL each). Then the material is washed with ethanol at RT for 6 h, 12 h and 6 h with fresh solvent (50 mL each) and subsequently air dried for 2-3 days.

Protocol 2 : The 1 L reaction product is separated in four flasks with a volume of 250 mL each. The as-synthesized MOF is centrifuged to remove the mother liquor and dispersed in 50 mL of DMF and stirred at RT for 24 h and 24 h with fresh solvent (50 mL each). Then the material is washed with ethanol at RT for 6 h, 12 h and 6 h with fresh solvent (50 mL each) and subsequently air dried for 2-3 days.

Protocol 3 : The 1 L reaction product is separated in four flasks with a volume of 250 mL each. The as-synthesized MOF is centrifuged to remove the mother liquor and dispersed in 50 mL of DMF and stirred at RT for 72 h with fresh solvent. Then the material is washed with ethanol at RT for 6 h, 12 h and 6 h with fresh solvent (50 mL each) and subsequently air dried for 2-3 days.

Protocol 4 : The 1 L reaction product is separated in four flasks with a volume of 250 mL each. The as-synthesized MOF is centrifuged to remove the mother liquor and dispersed in 100 mL of DMF and stirred at RT for 72 h with fresh solvent. Then the material is washed with ethanol at RT for 6 h, 12 h and 6 h with fresh solvent (50 mL each) and subsequently air dried for 2-3 days.

NMR analysis:

In all cases, the supernatant after centrifugation was vacuum dried at 80 ^oC and analyzed via ^1H NMR in dmso-d6, with 2.5 µL CH_2Br_2 as internal standard. For instance, the MOF washed with 50 mL DMF for three times is presented in Figure 11. Here, we ignore the wash 1 (W1) since the supernatant was greenish in color, which formed complexes with some unreacted Cr to form some complex under the drying conditions. Hence the ^1H NMR could not be quantified. Whereas, in W2 and W3, clearly the

proton signals are sharp and there is a huge drop in BDC ligand conc at 8.2 ppm from W2 to W3. This implies, with only two washing steps we could efficiently remove all the unreacted ligands from the MOF pores.

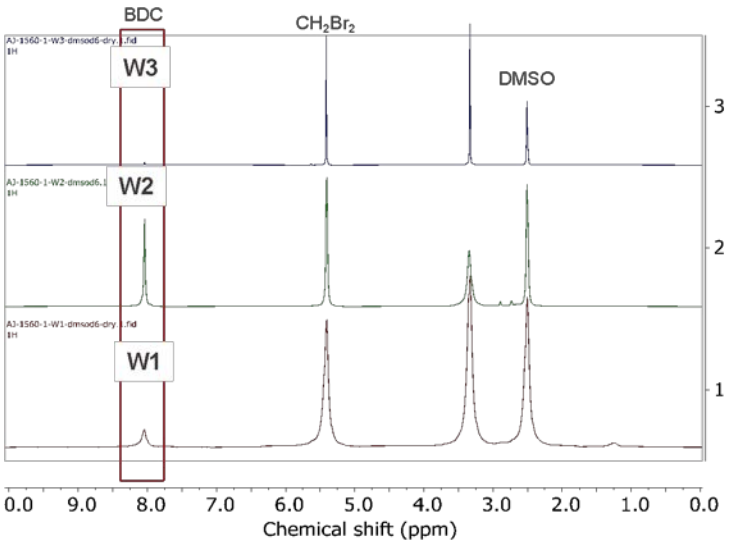

Figure 11: ^{1}H NMR of aliquot of washed solvent, dried in vacuum oven and dissolved back in DMSO-d_6 solvent with 2.5 µL of CH_2Br_2 as internal standard. W1, W2 and W3 is wash 1, wash 2 and wash 3 respectively.

PXRD analysis:

We also carried out PXRD analysis to assess the phase purity and crystallinity of the as-synthesized MOF using four different washing protocols. For protocol 1, 2 and 4, the material is found to be phase pure, and for protocol 3, diffraction data indicates the presence of unreacted BDC ligands (Figure 12). Hence, we discarded this protocol. This work indicates that washing with 1x100 mL of DMF (protocol 4) is enough to provide a phase pure XRD pattern (by removing unreacted ligand).

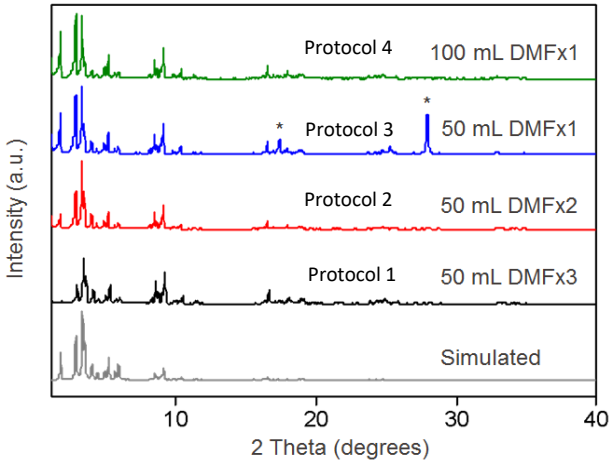

Figure 12: PXRD of MOF after three different washing protocols. Simulated Cr-MOF (grey), for 1 L synthesis, 150 mL L DMF (50 mL three times, protocol 1) (black),100 mL DMF (50 mL two times, protocol

2) (red), 50 mL DMF (blue, protocol 3), 100 mL L DMF (olive, protocol 4). *unreacted ligand entrapped within the MOF pores.

Surface area measurement:

Next, N_2 adsorption measurements at 77 K were employed to assess the porosity of the phase pure MOFs obtained from protocols 1, 2 and 4. The samples are activated at 150^{0}C under vacuum for 12 h prior to the adsorption measurements. Here we compare the N_2 isotherms of MOFs obtained after protocols 1, 2, and 4 (250 mL scale MOF synthesis) to the MOF extensively washed using 0.2 L DMF for 6 times in Figure 13. The surface area of MOF obtained from the extensive washing is 3300 m^2/g, very close to the reported procedure of 3400 m^2/g.[18] Surface area for the MOFs obtained from the optimized washing is 3000 m^2/g for protocol 1 and 2800 m^2/g for protocol 2 and 4, slightly lower than reported surface areas.

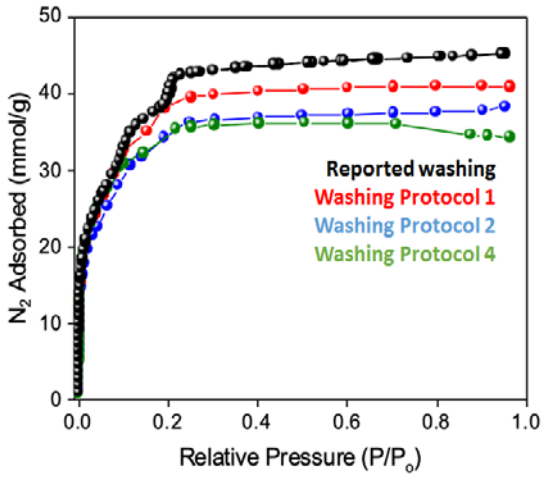

Figure 13: N_2 adsorption at 77 K for Cr-MOF obtained from protocol 1 (red), protocol 2 (blue) and protocol 4 (olive) is compared to Cr-MOF obtained from extensive washing of 0.2 L DMF x 6 times in 1 L scale synthesis (black).

With the goal to conclude if these MOFs obtained after optimizing the washing procedure were suitable for the subsequent amine impregnation step, we next performed the post-synthetic amine modification and further characterized them.

Ref.	Cr salt	BDC	H_2O	HNO_3	Wash DMF	Wash EtOH	Yield (%)	BET (m^2/g)	Cost (CHF/L)
Ref. [10]	192 g (0.48 mol)	81.3 g (0.48 mol)	2.4 L	0.49 mol	4.5 L x 2 times	4.5 L x 2 times	68 %	3400	66.25
Test 1 Rep	52.8 g (0.132 mol)	18.0 g (0.108 mol)	660 mL	8.56 mL (1.132 mmol)	200 mL x 6 times	200 mL x 4 times	47 %	3300	36.5
Protocol 1	52.8 g (0.132 mol)	18.0 g (0.108 mol)	660 mL	8.56 mL (1.132 mmol)	200 mL x 3 times	200 mL x 3 times	47 %	~3000	18.5

Protocol 2	52.8 g (0.132 mol)	18.0 g (0.108 mol)	660 mL	8.56 mL (1.132 mmol)	200 mL x 2 times	200 mL x 3 times	47 %	~2800	14.5
Protocol 3	52.8 g (0.132 mol)	18.0 g (0.108 mol)	660 mL	8.56 mL (1.132 mmol)	200 mL x 1 times	200 mL x 3 times	The sample has unreacted BDC ligand		10.5
Protocol 4	52.8 g (0.132 mol)	18.0 g (0.108 mol)	660 mL	8.56 mL (1.132 mmol)	400 mL x 1 times	200 mL x 3 times	47 %	~2800	14.5

Table 2: Protocols used for the washing steps and the cost associated with each.

Synthesis of MOF-amine composites and their CO_2 uptake:

For the amine-impregnation, we used a protocol previously developed in our laboratory. For this process, phase pure MOF obtained from protocol 1 and 2 (with surface area of 3000 m^2/g and 2800 m^2/g, respectively) were employed. The purpose of this study was to understand if the new washing protocols impact the CO_2 adsorption performance of the materials after amine impregnation in the pores. Given this, CO_2 adsorption measurements (at 313 K) were carried out on the composites and compared to the one previously developed (Figure 14). Interestingly, the material with a surface area of 3000 m^2/g (Protocol 1) gives the same CO_2 adsorption isotherm after impregnation compared to the one with the extensively washed MOF, which has a surface area of 3300 m^2/g. The MOF obtained with a surface area of 2800 m^2/g (Protocol 2) gives a slightly lower CO_2 uptake capacity. Hence, here we confirmed that protocol 1, where the MOF is washed using three steps and 50 mL DMF wash (Protocol 1) gives appropriate surface area of 3000 m^2/g and reproducible amine impregnation with CO_2 uptake of ~2.0 mmol/g at 0.15 bar and 313 K.

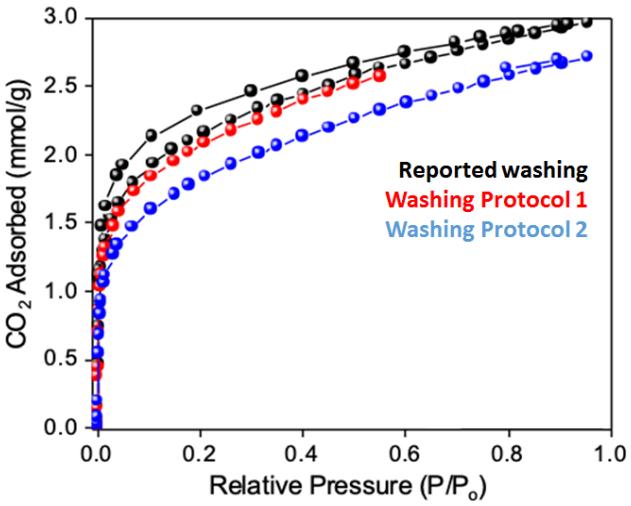

Figure 14: CO_2 adsorption at 313 K after amine impregnation using the original synthesis (black) and then protocol 1 (red) and protocol 2 (blue).

After optimization of the washing step, we aimed to begin scaling the Cr-MOF. To obtain the optimal material with reproducible CO_2 uptake, the amount of DMF used for a 1 L scale reaction is 600 mL, a value that is 4 times lower than the one reported.[18] Therefore, for the overall synthesis and washing of

the MOF, Cr-BDC, the total cost required is now ~18.5 CHF/L, reducing the cost by a factor of 3.6 times from the original 66.25 CHF/L and 2 times from the material previously synthesized in our laboratory. From each 1 L batch reaction, we obtain about 18 g of MOF and we have repeated the reaction several times to obtain 250 g of the desired Cr-MOF by the end of year one (Figure 15).

Figure 15: Approximately 250 g of Cr-MOF, made in 13 batches.

Given these results, with the purchase of a 5 or 10L stirred reactor, we will be able to reach a synthesis up to a 90-180 grams scale per batch.

Grafting amines inside a Cr-MOF using a new method:

Last, for our continued effort in materials design, we assessed a new strategy for amine impregnation inside the Cr-MOF of interest, which is done by grafting the amines to the MOF wall. Notably, it was hypothesized that this may better inhibit amine leaching as the amine is immobilized in the pore via covalent grafting, which is a common issue when incorporating alkylamines in a porous support.[19]

We find that, the grafting strategies lead to significant enhancements in the CO_2 adsorption properties (Figure 16), much higher breakthrough times (Figure 17), and extensive cyclability (Figure 18) (tested >400 times for the best materials). The covalent grafting study was published in *Advanced Functional Materials* (See Section 8: Publications).

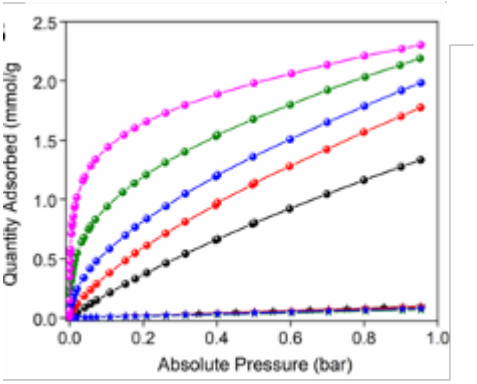

Figure 16. CO_2 adsorption isotherms at 313K for the grafting of amines onto the ligand of a Cr-MOF. (a) Different amines were grafted (blue, black, red and green circles) inside the Cr-MOF and then compared to the bare Cr-MOF (magenta). N_2 adsorption of the same materials in squares. N_2 adsorption of the same materials in stars.

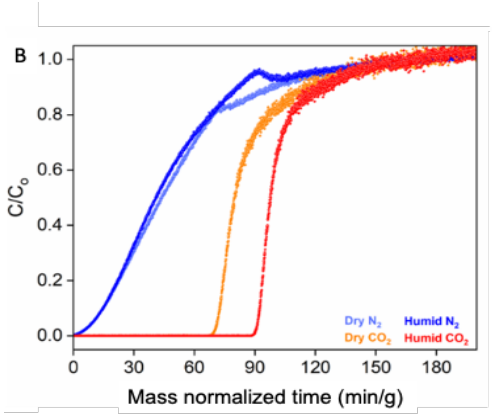

Figure 17. Breakthrough plots at 40 ºC and a 15% CO_2 85 % N_2 gas composition for the best-performing material having amines grafted on the ligand of Cr-MOF. Dry tests (N_2 in light blue and CO_2 in orange) and humid including 80% RH in the gas mixture after 2h pre-saturating with humid He (N_2 in dark blue and CO_2 in orange).

CO_2 adsorption/desorption cycling studies of amine-impregnated Cr-MOF:

With the aim to understand the long-term performance of the adsorbents developed in our laboratory, we tested them via TGA to simulate a TSA process. To achieve that, we flow gas mixtures (15% CO_2 and 85 % N_2) during the adsorption step at 40 ºC and pure CO_2 streams during the desorption step at 120 ºC. It should be noted that both adsorption and desorption steps are carried out under humid conditions (80 % RH) using a water bubbler. The latest results obtained with the grafted amine approach is shown in Figure 18. One of the main conclusions of these tests are the flat baselines observed confirms the lack of amine leaching during the cycling process, which would lead to a decrease in the baseline over time, and also the stability towards urea formation in the amine groups in the Cr-MOF, which would be seen as an increase in the baseline over time. However, one of the main issues that we are facing during these tests is the varying temperature in the laboratory during these last months, which clearly contributes to varying humidity levels in the gas stream during the water bubbling step, which is finally reflected as periodic fluctuations on the topline in both plots (Figure 18).

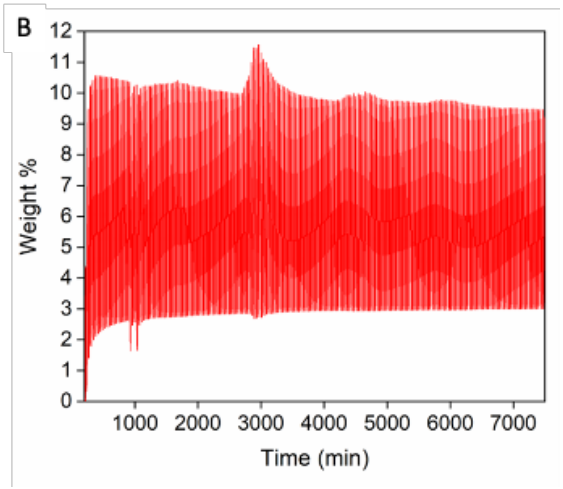

Figure 18. TGA cycling data of amine grafted on the ligand of Cr-MOF. Adsorption at 40 ºC of humid 15% CO_2 85 % N_2 gas stream and desorption at 120 ºC under humid 100 % CO_2. The weight increase is attributed to the adsorption of CO_2 and water.

To confirm this, we have restarted the TGA cycling under the same conditions for 200 more cycles, confirming that the topline is still at the same weight percentage (9-9.5%) while also the temperature in the room was confirmed to match the fluctuations observed in the cycling experiment (Figure 19). Given these fluctuations, we are exploring the addition of a temperature and humidity-controlled box, that may eliminate the issues associated with the fluctuations with the room. Despite these issues, we have demonstrated cycling the adsorbents over 400 times to date, without a decline in the baseline.

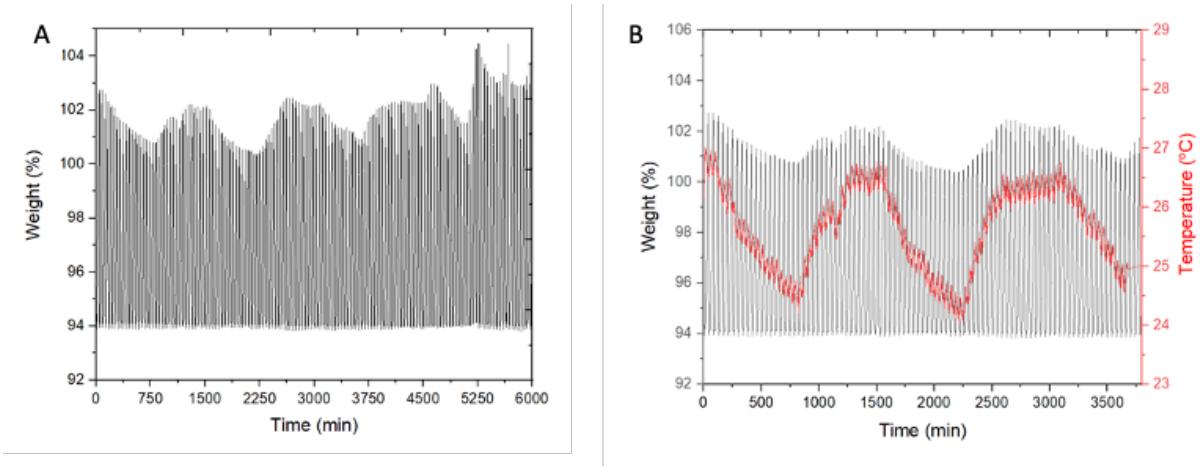

Figure 19. (A) Continuation of the cycling experiment for an amine impregnated MOF and (B) plot of the temperature next to the TGA instrument proving the direct relationship between the fluctuations and the humidity generated in the bubbler.

Shaping the zeolite 13X (NaX):

Even though the adsorbents exhibit nice performance for post-combustion CO_2 capture, we should take into account that powders cannot be used in large scale pilot plants for several reasons; there is difficulty handling large amounts of adsorbents in powder form and they pose a potential health risk if such fine powders are inhaled. Moreover, fine powders can create large pressure drops across the adsorption beds when gases are flowed at high flow rates.

Table 3. BET surface area and pore volume of Zeolite 13X (NaX) before after pressing into tablets.

	BET surface area (m^2 g^{-1})	pore volume (cm^3 g^{-1})
No binder		
Powder	501	0.2480
Tablet (25 MPa)	502	0.2485
Tablet (50 MPa)	499	0.2414
Tablet (75 MPa)	479	0.2309
Tablet (100 MPa)	472	0.2175
Tablet (200 MPa)	436	0.2120
Tablet (300 MPa)	409	0.1885
Tablet (400 MPa)	311	0.1523

Given this, the next important step is to have such adsorbents structured in the shape of pellets, beads, or extrudates, while trying to retain as much as possible their original performance. With the aim to explore the best structuring methods, we are collaborating with Prof. Mathieu Soutrenon from HES-SO Valais, an expert in structuring. To start, we have worked to structure materials into pellets. First, we started with tableting of the as-prepared Cr-MOF powder and the commercial Zeolite 13X (purchased from abcr GmbH). For Zeolite 13X (NaX), pressures ranging from 25 to 400 MPa were employed on the powder forming white tablets (Table 3). Next, N_2 adsorption isotherms (Figure 20a) revealed the surface area drops from 501 m^2/g (powder) to 311 m^2/g when the pressure is increased from 25 to 400 MPa and the pore volume decreases from 0.24 cm^3/g to 0.15 cm^3/g (Table 3). PXRD suggested that the crystal structure of the Zeolite 13X is well maintained during the structuring process albeit there is a decrease in intensity and peak broadening observed above 300 MPa (Figure 20b)

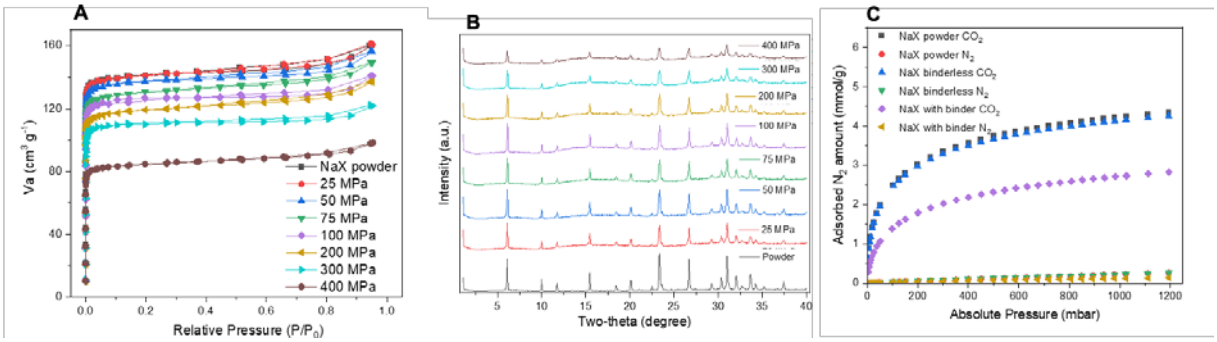

Figure 20. a) N_2 adsorption isotherms taken at 77K and used to calculate surface areas and pore volumes, b) PXRD patterns after tableting, and c) CO_2 and N_2 adsorption isotherms taken at 40°C. The red dotted line corresponds to ~0.15 bar, the partial pressure of CO_2 in post-combustion flue gas.

Notably, as observed from CO_2 adsorption isotherms at 313 K (Figure 20c**)**, the capacity of binderless tablets (2.78 mmol/g) at 0.15 bar is well-maintained. Unfortunately, when doing the friability tests, the binderless NaX tablet was found to be too fragile. Thus, the NaX powder was then mixed with various additives and then pressed into tablets to better bind the zeolite powder together. The additives also served as a plasticizing/lubricating agents, which enhances the rheological behavior in the press. After screening various possible additives, we were able to identify several binders that lead to robust NaX tablets, which was assessed via friability and crush strength tests (Table 6).

For the binder-based NaX tablet, the CO_2 adsorption capacity at 0.15 bar and 40°C is 2.79 mmol/g and 1.50 mmol/g for the parent powder and tablet (a 46% capacity drop), respectively. Despite this, the CO_2/N_2 selectivity of the tablet (80) is well-maintained when compared to the powder (82). Unfortunately, the cellulose-based binder was not further explored because after activation the materials show a very large decrease in surface area (Table 4). It was hypothesized that this decrease stems from the decomposition of the binder, which may lead to partial blocking of the zeolite pores. Notably, the zeolite requires a high activation temperature (~320°C)[21] to remove adsorbed water from the pores. Looking at the TGA results, obtained from the cellulose-based binders, there is decomposition at low temperatures of 250~300 °C. Notably, at the activation temperature, there is an oily by-product observed, which could possibly diffuse into the zeolite pores. In contrast, the second selected binder (betonite) was quite stable until heating to 400~500 °C according to the TGA curve; therefore, the N_2 and CO_2 adsorption performance of the zeolite in the tablet is not decreased as much by the betonite after activation.

Table 4. BET SA and pore volumes obtained from powder and tablets

Material	BET surface area ($m^2\ g^{-1}$)	pore volume ($cm^3\ g^{-1}$)
NaX powder	501	0.2480
NaX tablet (no binder)	498	0.2458
NaX tablet with betonite	406	0.2222
NaX-Methyl cellulose	190	0.1196
NaX-Ethyl cellulose	---	----
NaX-(Hydroxypropyl)methylcellulose	177	0.1392

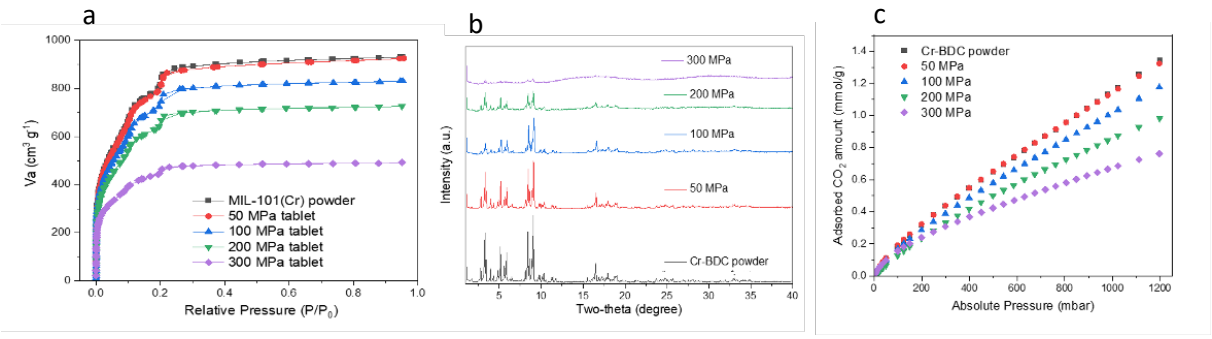

Figure 21. a) N_2 adsorption isotherms at 77 K for the Cr-MOF powder and after pressing at different pressures, b) PXRD patterns for the same samples (center) and c) CO_2 adsorption isotherms at 313 K for the same samples (right).

The protocol used for the bentonite-based NaX tablet includes:

The zeolite NaX powder was purchased from abcr GmbH and then shaped using a tableting approach. For this, 0.1 g of NaX powder was mixed with binder via grinding for around 5 minutes. Then 0.15 g of powder was added to a die having a diameter of 8 mm and then pressed using a commercial device D-6100, purchased from ORIEL GMBH, and held there for around 2 minutes. The resulting tablet had the following dimensions, 1.9 mm height by 8 mm diameter

Table 5. BET SA and pore volumes obtained from Cr-MOF powder and tablets.

Material (Pressure)	BET SA ($m^2\ g^{-1}$)	pore volume ($cm^3\ g^{-1}$)
Cr-BDC powder	3278	1.4409
Tablet (50 MPa)	3251	1.4310
Tablet (100 MPa)	2943	1.2849
Tablet (200 MPa)	2570	1.1242
Tablet (300 MPa)	1723	0.7608

Shaping the Cr-MOF:

Next, we set out to also structure the Cr-MOF via tableting using various pressures ranging from 50 to 300 MPa. Notably, the BET surface area drops significantly at higher pressure, particularly at 200 MPa where there is over a 20% reduction (Table 5, Figure 21a), possibly indicating a loss in the MOF integrity. Despite this, the PXRD pattern still indicates that the material is crystalline at 200 MPa albeit there is a slight decrease in peak intensity (Figure 21b). However, a full loss in the structural integrity is noted at 300 MPa as indicated by the disappearance of the peaks associated with crystalline Cr-MOF structure. This indicates that the material is becoming amorphous, and there is an even more significant decrease in the surface area. While the CO_2 adsorption (at 40°C) capacity at 0.15 bar is not significantly affected by the pressure, we also note that the CO_2 uptake of this MOF is already very low, likely making it more difficult to compare the loss (Figure21c)**.** Fortunately, the Cr-MOF tablets formed at 100 MPa, which still offer a high surface area, were found to be robust via friability and offer reasonable strength when the tablets during crush tests (Table 6). Given this, it is the sample that we decided to move forward with in our studies.

The protocol used for the binderless Cr-MOF and Cr-MOF-NH_2 tablet includes:

0.1 g of Cr-MOF powder was added to a die having a diameter of 8 mm and then pressed at 100 MPa using a commercial device D-6100, purchased from ORIEL GMBH, and held there for around 2 minutes. The resulting tablet had the following dimensions 3.7 mm height by 8 mm diameter.

Shaping the Cr-MOF-amine composite:

After shaping the Cr-MOF, we set out to shape the Cr-MOF amine composite into pellets, employing a binder-free pressing technique. The pellets, which were 8 mm in diameter, were produced under two different pressures including 60 MPa and 90 MPa. Interestingly, we observed a drop in CO_2 adsorption capacity after applying pressures of 60 and 90 MPa from the original 2.2 mmol/g to 1.5 mmol/g at 0.15 bar and 40°C (Figure 22). While this reduction could be attributed to a partial collapse of the MOF during tableting, we note that the parent Cr-MOF treated at 50 MPa and 100 MPa shown above (Figure 21a, Table 6) reveals a minimal change in the surface area after compression, respectively. This implies that the MOF is mechanically robust in this pressure regime, 0-100 MPa. Given this, the drop in the CO_2 adsorption performance is more likely to stem from lower access to primary amines in the MOF pores, which could decrease the CO_2 adsorption capacity.

Table 6. Shows various properties, including crush strength, friability test, and density of adsorbent tablets, and the pressure used for tablet preparation.

Material	Pressure during tableting (Mpa)	Strength no binder (Mpa)	Strength with binder (Mpa)	Selected Tableting method	Stability test (5000 cycles)	powder density (g/cm^3)	Tablet density (g/cm^3)	Increase (times)
NaX	100	6.8	34.4	With binder	96.2	0.540	1.492	2.76
Cr-MOF	100	18.8	-------	Binder-free	94.9	0.179	0.530	2.96
Cr-MOF-NH_2	100	33.5	-------	Binder-free	97.6	0.153	0.750	4.90
Al-formate	100	-------	26.3	With binder	95.3	0.444	1.492	3.36
CALF-20	100	-------	19.2	With binder	92.8	0.446	1.492	3.35
SIFSIX-3-Ni	100	-------	42.4	With binder	97.6	0.379	1.456	3.84
Mg-dobdc	100	18.0	-------	Binder-free	95.8	0.413	1.326	3.21

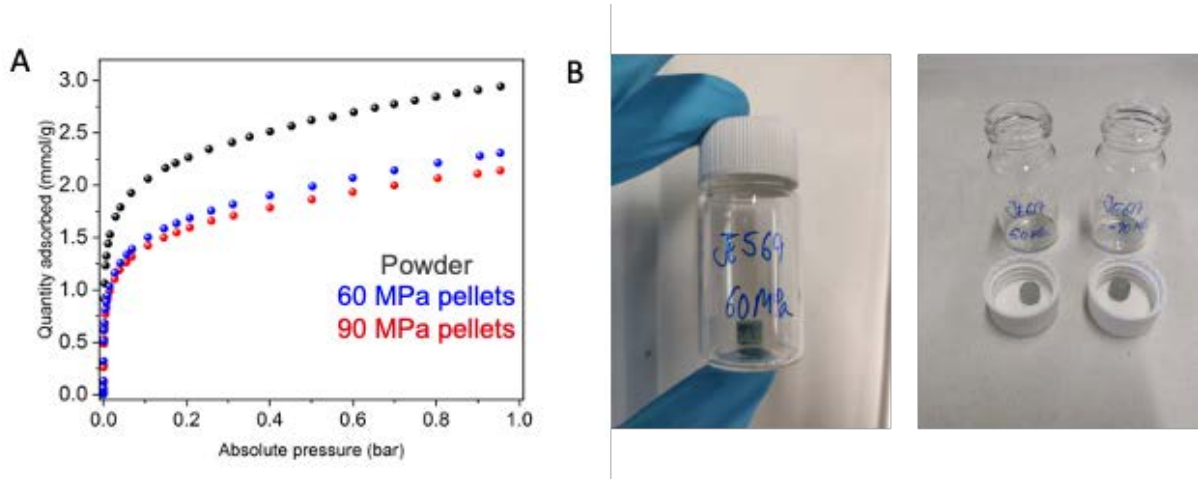

Figure 22. a) CO_2 isotherms at 313 K for the structured MOF composites. Different pressures were applied, 60 MPa (blue) and 90 Mpa (red) compared to powder (black). b) Pictures of the final 8 mm diameter pellets.

To date, we have developed a strategy to structure both the NaX, Cr-MOF, and Cr-MOF-amine composite; however further tests in adsorption cycling experiments are needed to see how robust the tablets are, particularly in the presence of humidity and over extended periods of time with extensive cycling. Further, we note that the density of the NaX (0.54 g/cm^3) and the Cr-MOF (0.179 g/cm^3) are increased by approximately a factor of 3 during tablet formation to 1.49 g/cm^3 and 0.53 g/cm^3, respectively (Table 7). Very dense structures could inhibit accessibility of the CO_2 to the inside the tablet leading to low performance under continuous flow. So, assessing such materials in flow in the future is important.

Shaping other MOFs:

To explore the general applicability of the tableting method, the structuring process was extended to a group of structurally diverse MOFs/zeolites, that are of interest for CO_2 capture applications. Notably, we have mentioned our interest in incorporating other materials into this study should time be permitting. So, we have included several other materials, particularly several MOF physisorbents, such as Mg-dobdc, SIFSIX-3, CALF-20, and Al-formate. Table 7 shows a comparison between the properties of NaX and Cr-MOF tablets with these CO_2 adsorbents. The table includes the selected tableting approach (with or without binder), the pressure at which the best performing tablets were formed, and also results from crush tests, friability, and density measurements for each material. Further, Table 7 shows comparisons of the gravimetric and volumetric CO_2 adsorption capacity (40^{o}C and 0.15 bar) of the best performing tablet for each adsorbent, and this value is compared against those of the parent powder. Notably, in all cases, for the tested MOFs and zeolites, the gravimetric capacity decreases, an observation that could stem from loss of material integrity or the added mass of dense binders. On the contrary, the volumetric capacity increases by factors ranging from 1.78 to 4.24, depending on the identity of the starting material. This is important as high volumetric capacities could permit smaller adsorbent bed volumes, a factor that could also help reduce the energy consumption of the separation process.

Synthetic protocol of CALF-20:

6.60 g of zinc oxalate, 5.00 g of 1,2,4-triazole and 66.0 mL of methanol were added into a 125 mL Teflon autoclave. The autoclave was heated in a convection oven at 180 °C for 48 hours. The product was washed with 40.0 mL of methanol by soaking for 1 hour. 7.30 g of air-dried white powder was collected. The MOF was activated under dynamic vacuum at 100 °C for 12 hours.

Table 7. Shows gravimetric and volumetric CO_2 adsorption capacity at 0.15 bar and 40°C for various tableted adsorbents.

Materials	Tableting method	Powder gravimetric capacity (mmol/g)	Tablet gravimetric capacity (mmol/g)	Decrease	Powder volumetric capacity (mmol/cm^3)	Tablet volumetric capacity (mmol/cm^3)	Increase (times)
NaX	With binder	2.70	1.63	39%	1.02	2.08	2.04
Cr-MOF	Binder-free	0.23	0.22	4%	0.041	0.117	2.85
Cr-MOF-NH_2	Binder-free	0.32	0.277	13%	0.049	0.208	4.24
Al-formate	With binder	0.90	0.62	31.2%	0.448	0.925	2.06
CALF-20	With binder	2.20	1.4	36.4%	0.981	2.09	2.13
SIFSIX-3-Ni	With binder	1.75	1.15	34.3%	0.663	1.674	2.52
Mg-dobdc	Binder-free	3.87	2.14	45%	1.598	2.838	1.78

Protocol of CALF-20 Tablet:

0.1 g of CALF-20 powder was mixed with the selected binder via grinding for around 5 minutes. Then 0.15 g of powder was added to a die having a diameter of 8 mm and then pressed using a commercial device D-6100, purchased from ORIEL GMBH, and held there for around 2 minutes. The resulting tablet had the following dimensions 2 mm height by 8 mm diameter.

Synthetic protocol of Al-formate:

Formic acid (100 ml) and aluminum hydroxide (1.2 g, 0.015 mol) were refluxed in a 250-ml three-neck round-bottom flask at 100°C (373 K) for 48 hours. After completing the reaction, excess formic acid was extracted by centrifugation, and the white solid was rinsed with a copious amount of ethanol for 1 hour and separated using vacuum filtration. The MOF was activated under dynamic vacuum at 150 °C for 12 hours.

Protocol of Al-formate Tablet:

0.1 g of Al-formate powder was mixed with the selected binder via grinding for around 5 minutes. Then 0.15 g of powder was added to a die having a diameter of 8 mm and then pressed using a commercial device D-6100, purchased from ORIEL GMBH, and held there for around 2 minutes. The resulting tablet had the following dimensions 2 mm height by 8 mm diameter.

Synthetic protocol of SIFSIX-3-Ni ($Ni(pyr)_2(SiF_6)$):

SIFISIX-3-Ni was synthesized by slurrying 870 mg (3 mmol) of $Ni(NO_3)_2$, 534 mg (3 mmol) of $(NH_4)_2SiF_6$ and 480 mg (6 mmol) of pyrazine in 4 mL of water for 2 days. The resulting suspension was filtered under vacuum and dried in air. This precursor was soaked in 20 mL methanol for 1 day and then washed twice with two portions (ca. 10 mL) of methanol on a Buchner filter with vacuum filtration. The MOF was activated under dynamic vacuum at 140 °C for 24 hours.

Protocol of SIFSIX-3-Ni Tablet:

0.1 g of SIFSIX-3-Ni powder was mixed with the selected binders via grinding for around 5 minutes. Then 0.15 g of powder was added to a die having a diameter of 8 mm and then pressed using a

commercial device D-6100, purchased from ORIEL GMBH, and held there for around 2 minutes. The resulting tablet had the following dimensions 2.1 mm height by 8 mm diameter.

Synthetic protocol of Mg-dobdc:

Typically, in a solution of 30 mL dimethylformamide, 2 mL ethanol, and 2 mL water were dissolved 0.299 g 2,5-dihydroxyterephthalic acid and 1.244 g $Mg(NO_3)_2 \cdot 6H_2O$ with sonication. The resulting stock solution was decanted into five 10 mL PTFE microwave reaction tubes. The reaction solution was then rapidly heated to 125 ^oC in 25 min (1200 W power) and was held at this temperature for 4 h. After cooling to room temperature, the solid products were collected by centrifugation and washed three times with methanol (shaking with 50 mL methanol for 1 hour) and dry for further use. The MOF was activated under dynamic vacuum at 150 ^oC for 12 hours.

Protocol of Mg-dobdc Tablet:

0.1 g of Mg-dobdc powder was added to a die having a diameter of 8 mm and then pressed using a commercial device D-6100, purchased from ORIEL GMBH, and held there for around 2 minutes. The resulting tablet had the following dimensions 2 mm height by 8 mm diameter.

Automated tableting of NaX:

Last, NaX-bentonite tablets were tested in process flow for their scale up production. For this, 8 mm and 3 mm NaX tablets were successfully produced using procedures that are similar to the ones outlined above, which were prepared individually and by hand. The porosity, crystallinity, and gas separation performance were confirmed by N_2 adsorption measurements (at 77 K), PXRD measurements, and CO_2 and N_2 adsorption isotherms (at 40^{o}C). We demonstrated that the NaX tablets could indeed be produced via continuous flow pelletization and that the resulting tablets are quite similar in terms of performance as the tablets manually pressed NaX tablets. For example, the CO_2 and N_2 adsorption isotherms of the tablets produced in the continuous process (Figure 23) are similar to those of the tablets produced by hand (Figure 20). Notably, the CO_2/N_2 selectivity, 78.3, is also quite similar to that of the parent NaX powder, 80.

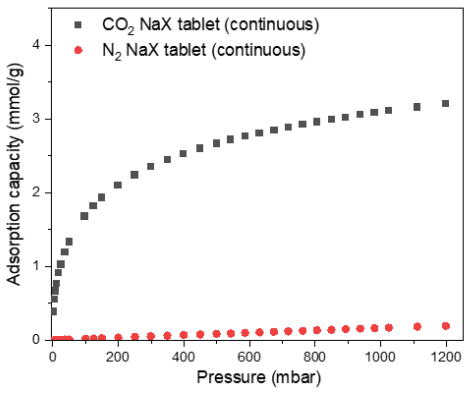

Figure 23. Shows gravimetric CO_2 and N_2 adsorption capacity at 40^{o}C for NaX tablets produced using the automated machine. These can be compared to Figure 20C.

Design of N-doped carbons:

Given that carbon materials can have a higher thermal conductivity and stability, relative to MOFs, these materials could be highly interesting for CO_2 capture. Unfortunately, most carbons suffer from low CO_2 adsorption capacities. Moreover, their internal surface is not easily functionalized due to their highly hydrophobic properties and inert nature. So, as a second area of interest we have designed carbon-based materials. We hypothesized that by pyrolyzing coordination polymers, we could create carbons with a high nitrogen content, boosting CO_2 adsorption performance due to stronger interactions with the heteroatom. Given this, we have demonstrated that a carbon, derived from a coordination polymer based on cobalt and 3,8-dibromo-1,10-phenanthroline (2Br-phen), which was produced at 600 ^oC for 2 hours results in highly porous carbon having a high N-content (12.2 %) and a CO_2 adsorption capacity at 40 ^oC and 0.15 bar of 1.1 mmol/g, which is twice that of existing commercial carbons, Norit (0.54

mmol/g) and Filtasorb-400 (0.47 mmol/g). We note this high-capacity stems from a high density of micropores (>70%), which we believe is owed to the small pores of the parent coordination polymer. This, combined with the high N-content, boosts the binding energy of CO_2 inside the carbon pores. Notably, in addition to the heightened CO_2 adsorption capacity, we have shown that the material performs well in separating CO_2 from N_2, even after being pretreated under highly humid conditions for 2 hours via breakthrough experiments. Importantly, the cyclability of this carbon adsorbent was fully retained for 100 cycles as seen in Figure 24. Moreover, the cobalt can be recycled and reused to remake the coordination polymer post pyrolysis. This work was recently published in *Advanced Functional Materials* (See Section 8: Publications). This may be a material that can be additionally incorporated into the unit in the future, should time be permitting at the end of the project.

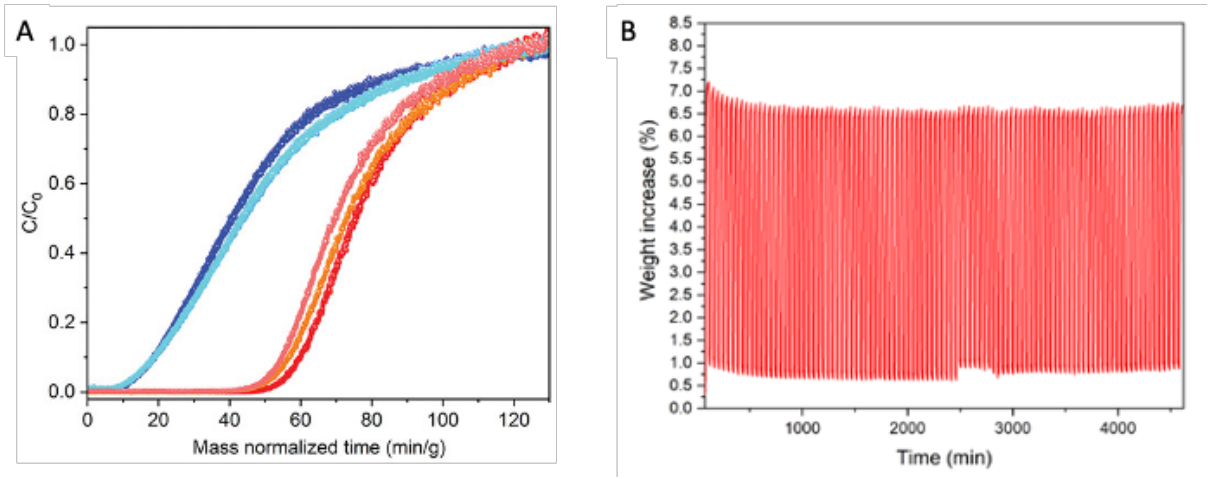

Figure 24. (a) Breakthrough plot using a 15% CO_2 and 85 % N_2 gas mixture at 40 °C under dry (N_2 in cyan and CO_2 in red), humid 80% RH gas mixture (N_2 in blue and CO_2 in orange) and pre-saturating the bed with humid He prior to the start of the experiment (N_2 in light blue and CO_2 in pink). (b) 100 cycles of CO_2 adsorption/desorption using TGA (adsorption at 313 K for 30 min, desorption at 393 K for 15 min using dry CO_2).

2.2.3. WP 3 Techno-economic studies to investigate the viability of CO_2 capture process:

Process modeling

Model development and validation of a temperature swing adsorption (TSA) process:

TSA is a key process in CO_2 capture, leveraging temperature changes to govern the adsorption and desorption phases. In this method, CO_2 is adsorbed onto specific adsorbents between 40-60 °C (the temperature of flue gas from power plants). The subsequent regeneration of the sorbent/desorption of CO_2 is achieved by elevating the system's temperature, usually between 80–200°C, contingent on the adsorbent in use. This temperature swing ensures a consistent and efficient cycle of CO_2 capture and release. Regeneration of the sorbent is predominantly achieved by indirect heating of the adsorption bed. Various methodologies, such as heating jackets, electric heating tapes, encircling coils, or concentric tubes circulating hot/cold fluids, are employed. This phase is paramount, accounting for a staggering 40-98% of the total energy requisites of the process.[23]

The developed TSA process is delineated into three different steps (Figure 25):

1. Adsorption of CO_2 at a designated temperature (T_{ads})

2. CO_2 desorption facilitated by indirect heating, elevating the temperature (T_{des})

3. Subsequent cooling of the bed

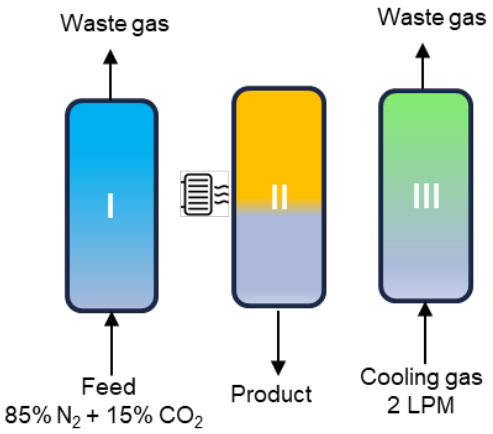

Figure 25. Schematic of a temperature swing adsorption process

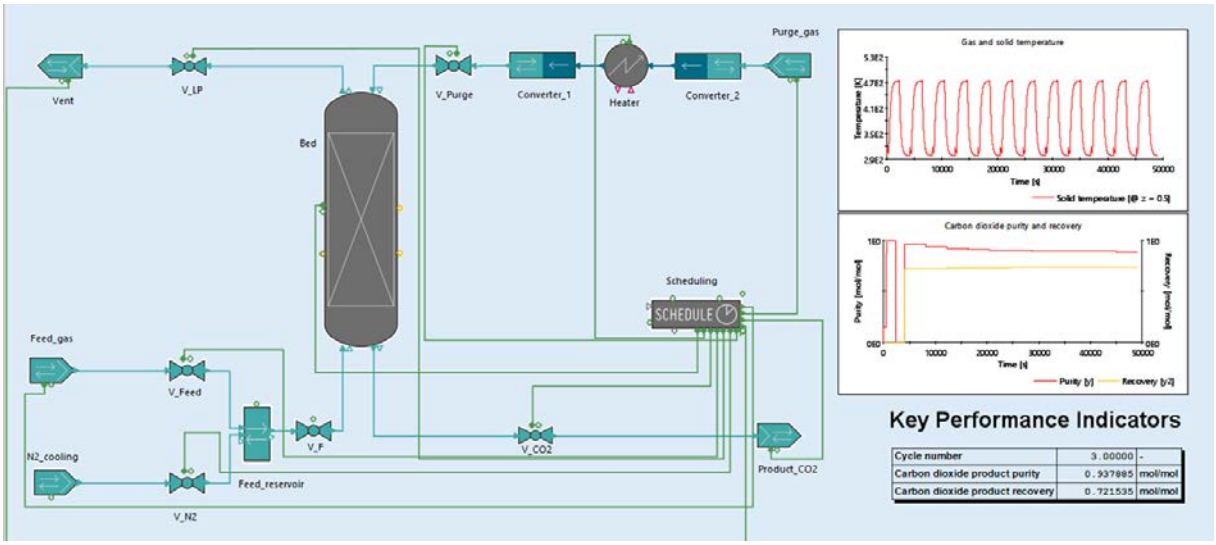

Figure 26. TSA process in gPROMS simulator

For the purpose of validation, the process employed NaUSY (Sodium exchanged Ultra Stable Y type zeolite) as the adsorbent. The rationale behind selecting NaUSY was underpinned by the availability of sufficient literature information. Pertinent data, such as isotherms and heat of adsorption values, were extracted from the literature.[24]

Table 8 shows the comparison between the simulation results (Figure 26) and experimental data from the literature[24]. Observing the deviation values, it's evident that the discrepancies between the simulated and experimental values are minimal. Specifically, the deviations for purity and recovery percentages are consistently low across all temperature points, showcasing the robustness and accuracy of the simulation in replicating real-world experimental results. This signifies that the model is reliable and effectively captures the dynamics of the TSA process.

Furthermore, energy consumption was analyzed at varying regeneration temperatures. A notable observation was made at 150°C (desorption temperature), where the energy consumption for adsorption (2.68 MJ/kg CO_2) (Table 9) was found to be 1.5 times less than that of the state-of-the-art liquid amine-based absorbent (Monoethanolamine - MEA), which is ~4.21 MJ/kg CO_2.[25]

Table 8. Comparison of the purity and recovery from the simulated and reported experimental data

Simulated			Reported (Experimental)		Deviation	
Temp (°C)	Purity (%)	Recovery (%)	Purity (%)	Recovery (%)	Purity (%)	Recovery (%)
150	91.72	54.10	91.21	53.24	0.05	1.21
200	92.23	72.86	91.36	76.60	0.87	3.74
250	93.61	86.18	91.68	88.27	1.93	2.09

Table 9. Productivity and energy consumption of the TSA process at different regeneration temperatures

Temp (°C)	Productivity (kg CO_2/kg adsorbent.h^{-1})	Energy consumption (MJ/kg CO_2)
150	0.40	2.68
200	0.53	2.75
250	0.61	2.92

To conclude, the developed TSA model is accurate and reliable, aligning closely with experimental data. Our findings underscore the potential of solid sorbents, especially when considering their energy efficiency compared to liquid-based absorption processes.

2.3 Activities and results (second year)

2.3.1. WP1. Design of the CO_2 separation demonstrator:

Qualitative and quantitative results achieved in the elapsed year, plus findings and experiences

During the second year, we continued to wait for the completion of the building where the demonstrator pilot plant would be installed. The construction of the building was completed in July 2024, and we were fully prepared for the installation of the pilot plant (Figure 27). However, the installation was delayed due to a workforce shortage at the company doing the installation, which prevented them from proceeding with the installation until November 2024. Despite this, we arranged for the installation of the mass spectrometer detector by a technical expert on May 14-16, 2024. In the meantime, we also organized the installation of additional components, such as gas cabinets for storing various flue gas mixtures, pressure regulators, and an automatic gas cylinder setup. Finally, the pilot plant was installed on November 18-29, 2024. This installation included a comprehensive training of EPFL staff and demonstrated full functionality of the instrument as planned except for humidity control. All team members from EPFL also completed specific safety trainings related to the pilot plant, ensuring that operations were ready to begin in January of 2025.

Figure 27. Image of the installed pilot plant unit.

During the installation and training, various activities were carried out to ensure the successful operation and understanding of the CO_2 separation demonstrator. The selected adsorbent during commissioning was **structured zeolite 13X**, and specific attention was given to the bed preparation process, which included determining the appropriate amount of adsorbent for the adsorbent column. During the installation, **in situ activation** of the adsorbent was also achieved at **300°C for 12 hours under vacuum**, followed by CO_2/N_2 adsorption at **313K**, demonstrating the CO_2 adsorption process. The breakthrough of N_2/CO_2 was also observed using the newly installed mass spectrometer (MS). For regeneration, we to tested two approaches: **TSA (Temperature Swing Adsorption**, Figure 28**)** with desorption at temperatures above **120°C**, using either 100% CO_2 (or N_2) as the carrier gas, and **TVSA (Temperature Vacuum Swing Adsorption)**, which applies vacuum along with heating. We also received training on the pilot plants control panel and software, focusing on how to plan continuous cycles, extracting data from temperature and pressure sensors, and managing the system as efficiently as possible. Throughout the installation and preliminary testing, we documented the process with plots of breakthrough data and relevant information from the control panel, as well as photographs of key operational steps like column filling, gas connections, valve operations, MS detection, and compressor functionality.

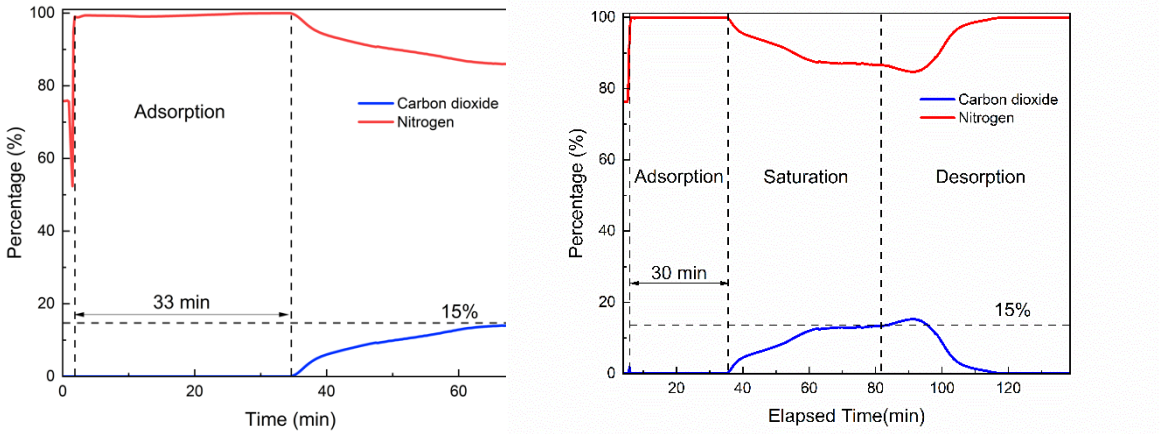

Figure 28.TSA experiment with a dry flue gas mixture consisting of 15% CO2 and 85% N2. Desorption was carried under N_2 at 200 deg C. Flow of N_2 was 3116 ml per min and CO_2 was at 1 g per min. Breakthrough time of 30 minutes was observed (Right). TVSA measurement with a dry flue gas mixture consisting of 15% CO_2 and 85% N_2. Desorption was carried under vacuum followed by heating at 200 ^oC. The flow of N_2 was 3116 ml per min and CO_2 was at 1 g per min. Breakthrough time of 33 minutes was observed (Left).

2.3.2. WP 2 Design, scale-up, and structuring of adsorbents for carbon capture:

Silica-amine composite:

Mesoporous silicas are an appealing class of materials for CO_2 separations. Thus, in this project we aimed to post-synthetically modify a selected silica with amines given the physical and chemical robustness of silica materials and their large pore apertures, which allow amines to readily go inside. As described in the previous report, our lab developed methods to incorporate amines in the pores of porous silicas, such as SBA-15 and KIT-6, while being able to extend their cyclability and lifetime. Notably, the use of silicas with larger pore volumes such as KIT-6 favored higher loadings and the use of larger amine-containing polymers like polyethyleneimine (PEI, Mw 800). So, during the last months, we have reproduced and scaled-up the synthesis of KIT-6[26] judiciously selecting a method that leads to the highest pore volume. It is well described that the use of different temperatures during the hydrothermal synthesis of KIT-6, promotes different nucleation around the templating agents, which directly impacts the pore volume of the sample. Given this, we have used 135 °C for the temperature synthesis, which provides a final pore volume >1 cm^3/g. We have produced 500 g of KIT-6 to date (Figure 29). Below outlines the protocol used for the scaled-up synthesis and the cost versus the commercial material (Table 10-11).

Scale-up synthetic protocol of KIT-6 mesoporous silica:

Pluronic acid polymer (P123, 40.5 g) was melted at 70 °C and weighed in the balance. The melted P123 was added to deionized water (1.46 L), stirred and then placed in a 2 L Teflon reactor. Hydrochloric acid (37 %, 78.3 g) was added dropwise and stirred until complete dissolution. The reactor was heated to 35 °C in an oven. Upon stable temperature, 1-butanol (50 mL) was added, and allowed to stir for 1 h. Tetraethyl orthosilicate (TEOS, 92.6 mL) was quickly added under vigorous stirring (450 rpm) and kept at 35 °C for 24 h. Note: a white precipitate formed in the first few hours of the reaction.

After the 24-hour period, the reactor was cooled and the stirring magnet was removed from the reactor. The reactor was then transferred into a stainless-steel autoclave and placed in a preheated oven at 135 °C for 24 h. After cooling to RT, the obtained product was vacuum-filtered using a Buchner funnel, and the solid left was dried in the oven at 100 °C overnight. The solid was then ground to break down large chunks of material, and the synthesized KIT-6 was calcinated under air using the following procedure: heated in 30 min to 180 °C, held 2 h at 180 °C, heated in 4 h to 550 °C and held 6 h at 550 °C. The material was then cooled down naturally.

Figure 29. Pictures of the KIT-6 synthesis protocol.

This lab-made scale-up protocol leads to a cost of 921.37 CHF/kg, which is at least 10 times lower than purchasing 1 kg of KIT-6 silica on the market (**Fehler! Verweisquelle konnte nicht gefunden werden.** and **Fehler! Verweisquelle konnte nicht gefunden werden.**).

Table 10. Price of reagents for the KIT-6 silica synthesis.

Reagent	Quantity (kg)	Price (CHF/kg)	Price (CHF)

TEOS	4.085	135.66	**554.10**
P123	1.901	118.50	**225.32**
HCl	3.676	18.08	66.46
1-butanol	1.901	39.70	75.49

Table 11. Prices of commercial KIT-6 silica sold by three different companies.

Company	**Price (CHF/kg)**
MSE	9904 CHF/kg
ACS	**8996 CHF/kg**
Matexcel	24120 CHF/kg

Given the large pore apertures of KIT-6 mesoporous silica, small-angle X-ray scattering (SAXS) was used to identify the main peak below 1°, which confirms the proper structure of the silica (Figure 30a). In addition, N_2 adsorption isotherm at 77 K was used to prove the porosity of the sample, which presents a BET surface area of 505 m^2/g and a pore volume of 1.31 cm^3/g, which fall in the range of the reported values for KIT-6 synthesis using the specified conditions (135 °C hydrothermal step) (Figure 30b).

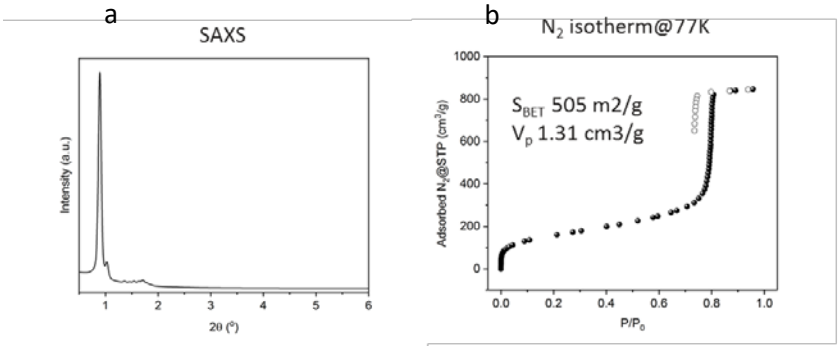

Figure 30. a) Small-angle X-ray scattering and b) N_2 isotherm at 77 K of the bare KIT-6 silica.

The synthesized KIT-6 silica was then grafted with an amine-containing polymer (PEI, Mw 800) in a two-step fashion: the silica was reacted with 3-glycidoxypropyltrimethoxy silane and then with PEI, allowing the PEI to become covalently tethered to the silica support, as shown in Figure 31. Prior to the grafting step, KIT-6 (100 mg) was activated at 150 °C overnight under vacuum and then transferred to a round bottom flask equipped with a stopcock and condenser. Anhydrous toluene (10 mL) and 3-glycidoxypropyltrimethoxy silane (245 µL, 1.13 mmol) were added. The reaction mixture was refluxed under magnetic stirring at 120 °C for 12 h. PEI (Mw 800, 300 mg, 2.91 mmol) was added and allowed to stir for 5 h under a nitrogen flow, heated at 50 °C for 2 h, and then vacuum dried overnight. Figure 32 shows that the grafted silica has a CO_2 capacity of 1.48 mmol/g at 0.15 bar and 40ºC, which is also retained after reactivation and a second CO_2 adsorption cycle (1.44 mmol/g).

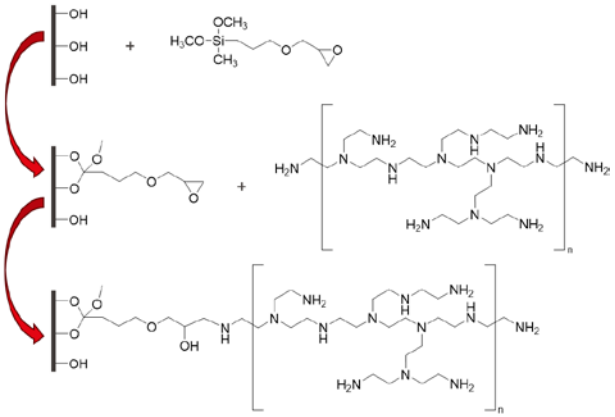

Figure 31. Grafting method of polyethyleneimine onto the pores of KIT-6 silica.

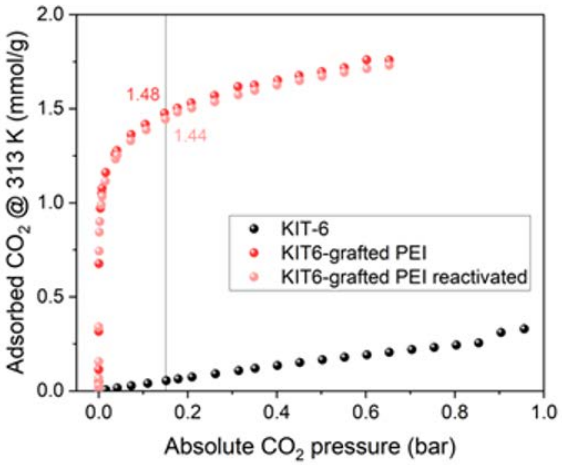

Figure 32. CO_2 adsorption isotherms of PEI-grafted KIT-6 silica collected at 40ºC.

Shaping the KIT-6 composite:

It was hypothesized that the amine grafted into the silica may act as a binder and help structure the material during a subsequent pelletization step. To prove this, about 10 mg of silica adsorbent (with and without amine) was put in the die of an industrial pelletization machine and the upper punch was pushed on the powder with a force varying between 0.1 and 0.5 kN. The upper punch was immediately removed and the pressed powder recovered. To assess the stability of the obtained pellet, the pellet was put inside a rotary friability machine, which was rotated 100 times at 25 rpm. We inspected for visible signs of breakage during the rotations and weighed the largest part of the pellet before and after the rotations allowing us to qualitatively assess pellet robustness. We tested pellets obtained from the bare KIT-6 and the amine impregnated KIT-6. As expected, we found the amine plays a binding role, as shown in Figure 33: in fact, the pellet produced from the pressed silica powder crumbles as soon as it is removed from the die used for pressing. On the other hand, the pellet obtained from the amine-grafted silica is robust and able to sustain 100 rotations in a device used to test friability without breakage or mass loss.

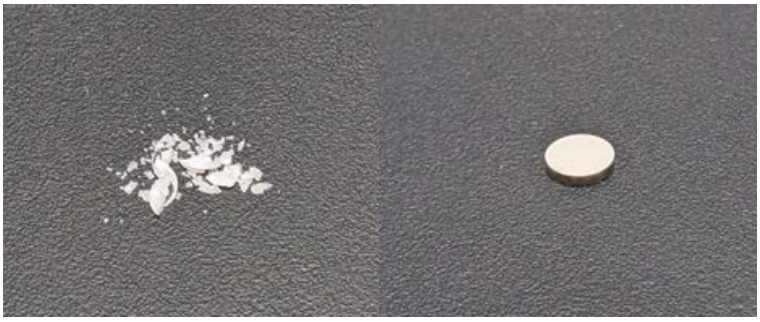

Figure 33. Pellet of bare KIT-6 (left) and PEI-grafted KIT-6 (right).

Other amine composite and structuring:

Other types of supports were also briefly studied as carbon capture materials. These supports were selected because they show remarkable thermal and chemical stabilities, as well as a high thermal conductivity, which could lead to lower energy consumption during a TSA process. Furthermore, unlike MOFs, these support materials often do not possess metals that can catalyze the degradation of amines, the active species responsible for CO_2 adsorption. This support was selected because it is mesoporous; it was hypothesized that large mesoporosity (> 2.5 cm^3/g with a pore size around 12 nm) would allow for a high amine loading. Also, this support is bio-derived. So, a similar amine-impregnation approach was used, aiming at a reduced amine leaching and thus performance loss during repeated usage. The below NMR shows evidence of TEPA-BDE impregnation inside the support and Figure 35 shows an example of TEPA-BDE dimer that forms in the pores.

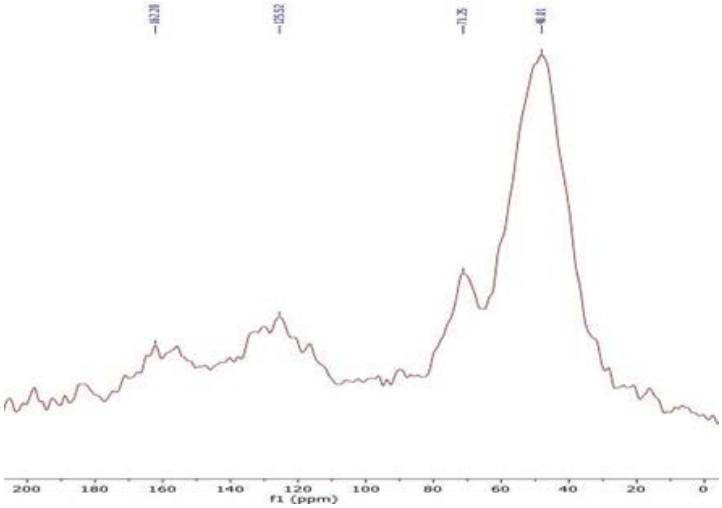

Figure 34. Solid-state ^{13}C NMR spectrum of TEPA-BDE impregnated mesoporous support..

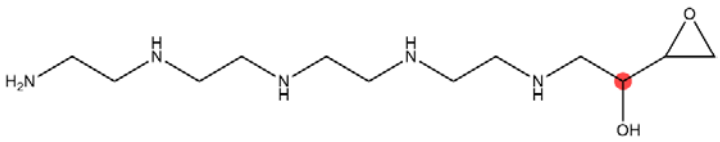

Figure 35. Structure of a TEPA-BDE dimer in side porous support.

ESI-MS (Figure 36 left) shows a clear shift from low m/z for TEPA (in red) to higher m/z for TEPA-BDE (in blue). The plot shows characteristic peaks of TEPA-BDE oligomers, such as a trimer consisting of 2 TEPA and 1 BDE (at 465.1) and a tetramer consisting of 2 TEPA and 2 BDE (at 549.5). This demonstrates the formation of longer polymers from the TEPA and BDE monomers. As expected, the

crosslinking helped to retain the amines inside the porous support, leading to a higher cyclable CO_2 capacity. This can be seen from the repeated temperature swing cycles in Figure 36 right. The mesoporous support containing the crosslinked TEPA-BDE polymers showed less polymer loss during the cycles (flat baseline), while the one impregnated with TEPA monomers only showed a significant weight loss. The amine loss is apparent from the very first few cycles and stems from the small, low-molecular weight TEPA monomers flying out of the support.

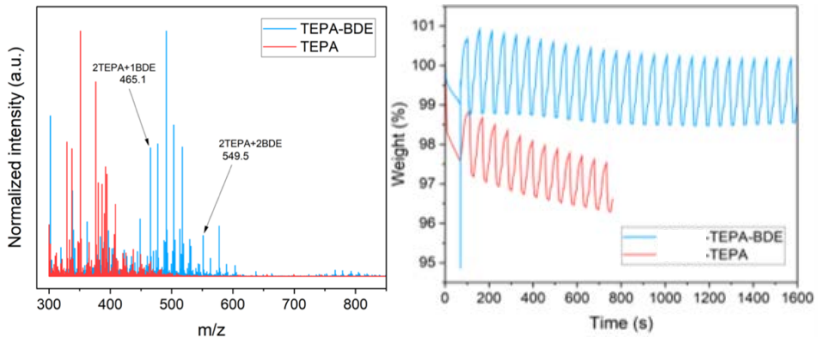

Figure 36. a) ESI-MS spectra and b) temperature swing adsorption cycles under 313 K adsorption and 393 K desorption with pure CO_2, of TEPA and TEPA-BDE impregnated mesoporous support.

The TEPA-BDE impregnated material was subsequently structured using an industrial tableting machine. The stability of the obtained pellets was assessed via friability tests carried out in a device in our lab. The mesoporous pellets impregnated with TEPA-BDE showed good stability during friability tests, as the pellets experienced no weight loss over the course of 100 cycles indicating the pellets are robust (Figure37 left). This was not the case for the pressed support excluding amines and epoxides, which crumbled back into powder as soon as it was removed from the die (Figure37 right).

The pressed mesosupport containing TEPA-BDE had a decreased gravimetric CO_2 capacity (Figure 38) compared to the parent powder (1.8 mmol/g instead of 2.3 mmol/g). This could stem from pore compression, reducing accessibility of CO_2 to the amine groups inside. It could also stem from additional crosslinking that may occur between amines and epoxies, further reducing the number of primary amines inside. However, the reduction of the gravimetric capacity is compensated by the increased density of the powder once pelletized' this leads to a similar volumetric CO_2 capacity before and after pressing (the volumetric capacities of both the powder and the pellet are ~0.4 mmol/mL).

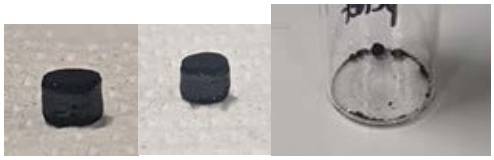

Figure 37. (Left) Pellet of support containing TEPA-BDE before and after friability test and (right) pressed mesoporous powder.

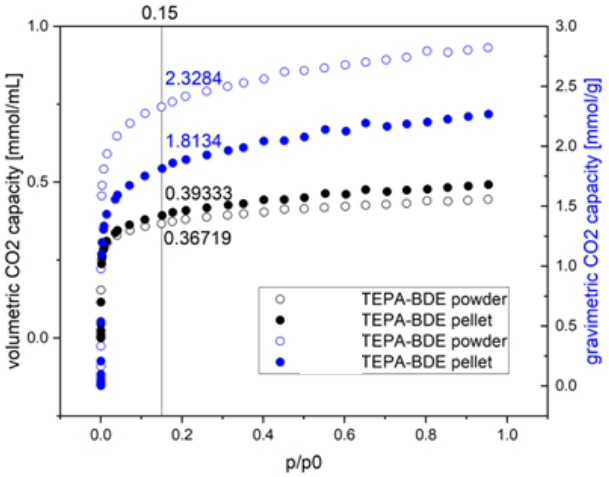

Figure 18. Gravimetric (blue) and volumetric (black) CO_2 adsorption capacity of mesoporous support impregnated with TEPA-BDE at 40ºC.

Design of N-doped carbons:

Given the interesting performance of several previously reported N-doped carbon produced in our laboratory, we continued to explore the advantages that these adsorbents may provide for CO_2 capture. These materials are highly stable (chemically and physically), they offer high thermal conductivities (favoring heat transfer during adsorption-desorption cycles) and their physisorptive interaction with CO_2 molecules could reduce the energy required to fully desorb the gas when compared to chemisorbents containing amines.

In a previous publication (*Adv. Funct. Mater.,* 2023, 33, 2212283), we described the use of 3,8-dibromo-1,10-phenanthroline (2Br-phen) combined with a cobalt salt that upon pyrolysis led to a porous carbon with a remarkable CO_2 capacity of 1.1 mmol/g at 40 °C and 0.15 bar. While the high N content and the density of micropores are hypothesized to be responsible for such performance, one of the main drawbacks of this porous carbon is the cost of the starting monomer 2Br-phen. As such, our aim was to synthesize new carbon-based adsorbents with enhanced performance and reduced cost. To do this, we screened different monomers using a similar synthetic protocol as previously reported.

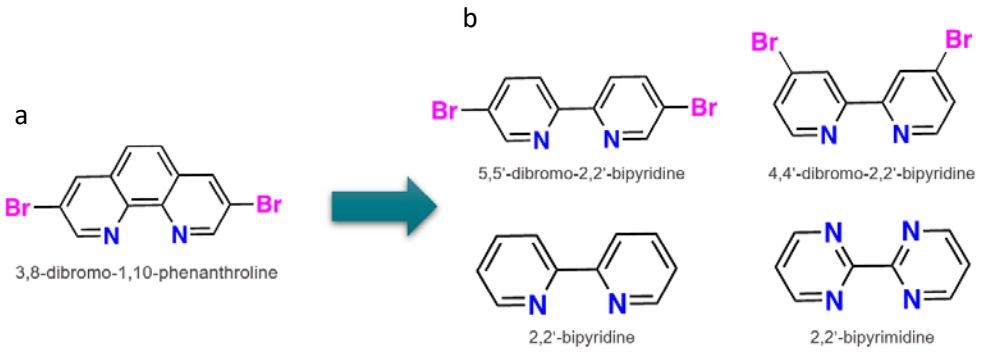

Figure 39. a) 2Br-Phen molecule and b) new monomers employed in carbon synthesis.

First, the phenanthroline core of the molecule was exchanged with a bipyridine core (Figure 39), which reduces the cost of the commercial molecule. In addition, the presence and position of the Br atoms was also considered to determine the effect during the pyrolysis step with the cobalt salt. The monomers without Br moieties combined with cobalt nitrate and carbonized at 600 °C did not exhibit relevant CO_2 adsorption capacity based on the isotherms collected at 40 °C (Figure 40). On the contrary, the

monomers containing Br (4,4''-Dibromo-2,2''-bipyridine and 5,5''-Dibromo-2,2''-bipyridine) led to significantly higher CO_2 capacities. In addition to testing different monomers, we also varied the ratio of Co salt to monomer. It should be noted that when the same molar ratio (3:2 $Co(NO_3)_2 \cdot 6H_2O$: monomer) is kept, the carbon obtained from the pyrolysis of 4,4''-Dibromo-2,2''-bipyridine (black circles Figure 40) present a higher capacity than the 5,5''-Dibromo-2,2''-bipyridine (gray circles Figure 40). On the other hand, when testing a ratio of 2:1 $Co(NO_3)_2 \cdot 6H_2O$: monomer the difference was not as large (red and orange circles Figure 40).

With these results, we exposed the carbonized sample using 4,4''-Dibromo-2,2''-bipyridine (3:2 $Co(NO_3)_2$.$6H_2O$: monomer) to a concentrated acid solution to leach the cobalt out of the material; this led to a CO_2 capacity of 1.2 mmol/g. Not only is this capacity higher than the previously reported carbon using 2Br-phen, but the cost of the starting molecule is 3.5 times less expensive (21.4 CHF/g instead of 70.5 CHF/g). These microporous, N-doped carbons already offer significantly higher CO_2 capacities in the low pressure regime (0.15 bar and 40ºC) when compared to commercially available activated carbons (by over a factor of 2). Despite this, there is still room for further cost and performance optimization by altering the selected monomers; we anticipate that should such carbons offer CO_2 capacities in the range of 1.5-2.0 mmol/g regime (at 0.15 bar and 40ºC), they could be highly promising materials for post-combustion capture applications.

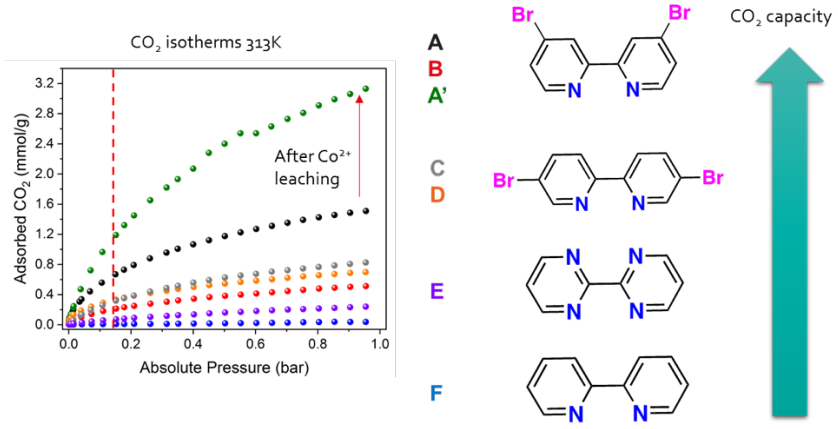

Figure 40. CO_2 adsorption isotherms at 40 °C from various monomers combined with $Co(NO_3)_2$.$6H_2O$ and carbonized at 600 °C.

Chromium-MOF:

Further work on the scale-up of the Cr-MOF was also carried out in our laboratory. We have optimized the synthetic protocol and washing steps. To accumulate more MOF, various batches were made from a protocol carried out in 1 L reactor (yielding 20g-25g per batch). After characterization of each batch, to ensure consistency, they were combined to reduce the time during the washing step comprising several solvent exchanges. Given the large volume of supernatant after combining several batches, we tried to replace the centrifugation step (maximum 1 L in 4 centrifuge bottles) with a filtration step using a vacuum pump, which is a common procedure for the large-scale industrial processes. However, the filtration step brought several difficulties (Figure 41). For example, there were problems related to filter clogging and the process was much slower than centrifugation. Further, handling such large quantities of solvent posed other problems that led to damaged pumps. Given this, after several trials, we reverted back to centrifugation.

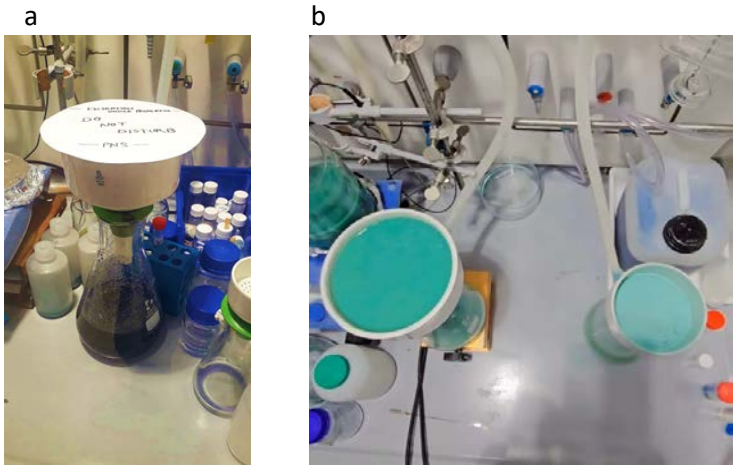

Figure 41. a) Front view of filtration setup. b)Top view of simultaneous filtration in 2L and 1L scale.

Next, the reaction scale was increased to 2 L (yielding 40g-50g per batch). For this, we purchased four 2 L reactors, and further optimized the synthetic protocol. With this, we were able to accumulate 1226 g of solid Cr-MOF in our lab, which is nearly five times of our previous reported quantities (Figure 42). Importantly, the performance of the materials is retained despite doubling the scale. In fact, the solid has a surface area of 2900-3000 m^2/g, which is slightly better than our previously reported data. Figure 43 shows that the sample is highly crystalline and offers a high surface area that is also reproducible.

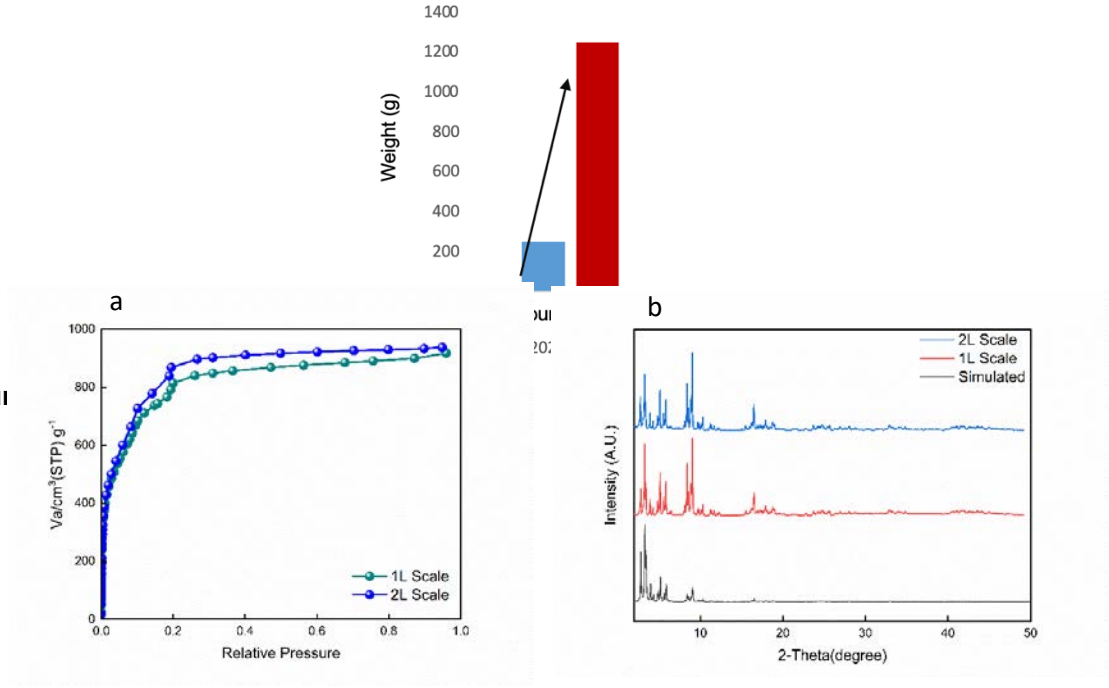

Figure 43. a) Nitrogen isotherm at 77K and b) PXRD patterns of the MOF obtained from the 1L and 2L reaction scales.

Scale-up synthetic protocol of Cr-MOF (2L reaction):

To synthesize MIL-101-Cr on a 2L scale, 105.6 g of $Cr(NO_3)_2 \cdot 9H_2O$ salt and 36 g of BDC ligand are combined with 1320 mL of H_2O as the solvent. Next, 17.12 mL of HNO_3 is added as a modulator. The mixture is placed in a 2L reactor and stirred at room temperature for 30 minutes. Afterward, the reactor is sealed and heated in an oven at 200°C for 16 hours.

After the synthesis is complete, the solution mixture is divided into three 1L bottles and centrifuged at 5000 RPM for 5 minutes. The supernatant is decanted, and 400 mL of DMF is added, evenly distributed among the three bottles. The mixture is stirred in three cycles of 6 hours, 12 hours, and 6 hours, replacing the solvent with fresh DMF after each cycle. The same washing process is repeated using EtOH. After washing, the solid is air-dried for 12 hours, yielding the final product. Each 2L reaction typically yields approximately 40–50 g of the product.

Synthesis of MOF-amine composites and their CO_2 uptake:

Next, amine-impregnation was carried out inside the Cr-MOF using a slightly modified protocol that was previously developed in our laboratory. This protocol involves amine-impregnation and subsequent crosslinking with epoxides to stabilize the amines in the pores. In year 1, we compared and contrasted various amine and epoxide combinations. We found that, of the materials screened, the Cr-MOF containing TAEA (Tris(2-aminoethyl)amine) and BDE (1,3-Butadiendiepoxide) was the best as it offered the highest CO_2 capacity (Figure 44). However, as we approached the scaling step this year, we began looking at the cost and toxicity of the different components (Table 12). Considering the extremely high cost of TAEA and BDE and the also high toxicity of BDE, we decided to eliminate this combination, and selected starting materials that may lead to a more economically and environmentally viable process. Thus, TEPA and TMPTE were instead used. It is noted in Figure 44, that the combination of TEPA and TMPTE had the lowest performance of the amines and epoxides screened in year 1. So, we worked to optimize it further.

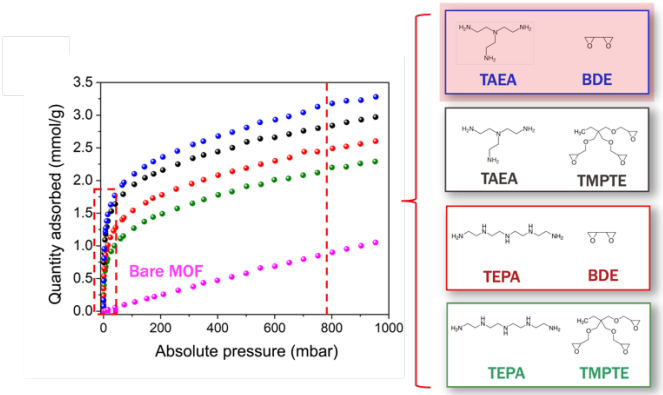

Figure 44. CO_2 adsorption capacity (left) collected from the Cr-MOF impregnated with various amine and epoxide combinations (right).

Table 12. Cost analysis of MOF and its composites.

Name	Full name	Cost (CHF/kg)
Cr-MOF	MIL-101-Cr	925
TEPA	Tetraethylenepentamine	94
TAEA	Tris(2-aminoethyl)amine	2’440
BDE	1,3-Butadiendiepoxide	6’240
TMPTE	Trimethylolpropane triglyciyl ether	227

The CO_2 adsorption and separation performance of the amine-epoxide composites is directly related to the quantity of accessible amines present in the pores. Thus, our intention was to boost the amine (TEPA) loading. However, to do this, we also had to increase the quantity of crosslinking epoxides,

which are responsible for inhibiting amine leaching during the adsorption/desorption cycling. Overall, the amine loading can be impacted by the quantity and ratio of amines and epoxides in the reactions, reaction time, and/or reaction temperature. Hence, we proceeded to further optimize the synthetic protocol varying these parameters during amine impregnation reactions. For example, Table 13 and Figure 45, show examples of protocols screened, where the MOF:amine:epoxide ratios were varied. Importantly, the quantity of CO_2 adsorbed at 0.15 bar and 40ºC (the concentration of CO_2 in post-combustion flue gas) varies greatly depending on the protocol employed.

Table 13. Different synthesis procedures for MOF composites.

Protocol	MOF:TEPA:TMPTE	Leaching	Capacity at 0.15 bar (mmol/g)
P1	59:2:1	No	1.1
P2	59:4:1	Yes	2.6
P3	12:4:1	No	1.7
P4	29:2:1	No	1.9

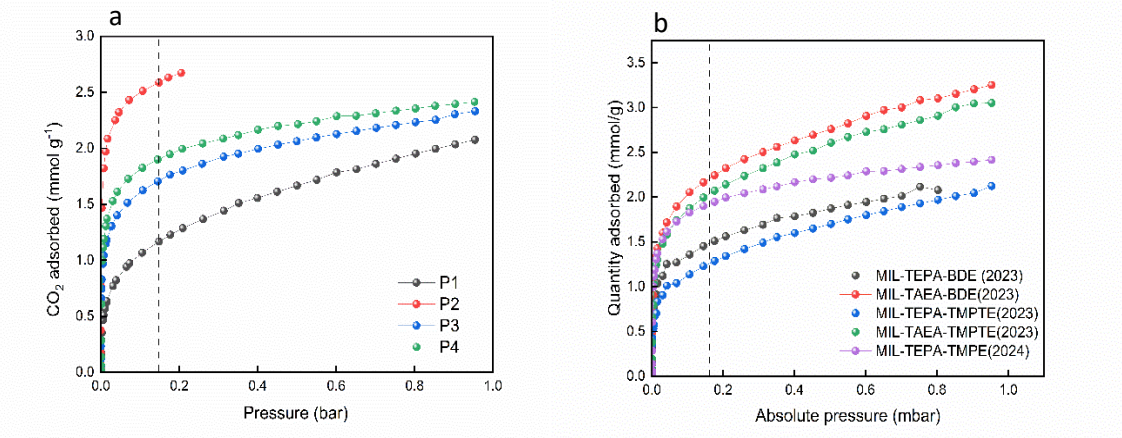

Figure 45. a) CO_2 isotherm at 40ºC for different ration MIL-TEPA-TMPTE. b) CO_2 isotherm at 40ºC for different composites from year 1 (2023) and year 2 (2024)

As shown in Figure 45, four different synthetic protocols were compared; P1 is the protocol reported in 2023 (year 1). After some optimization, the capacities were improved from 1.1 mmol/g (P1) to 1.9 mmol/g (P4). It is worth noting that the protocol referred to as P2 shows the highest sorption isotherm. However, as indicated in Table 13, amine leaching occurs in the sample tube during the activation process required to measure the CO_2 adsorption capacity. As a result, this protocol is deemed unsuitable and was therefore discarded. Furthermore, we acquired cycling data and showed that there was no leaching observed in protocol P4 (Figure 46). P4 was first carried out on a 0.55 mg scale and later, and we also scaled this up from 0.55g to the ~2g scale. MIL-TEPA-TMPTE is the cheapest and more environmentally friendly composite, and with the improved synthesis protocol (P4)l, our capacities were enhanced close to the one of MIL-TAEA-BDE. The adsorption isotherms of the P4 materials at different scales and from several batches are shown in Figure 46, indicating that the process is likely scalable and reproducible. Thus, in year 3, we will continue scaling the amine-epoxide impregnation step.

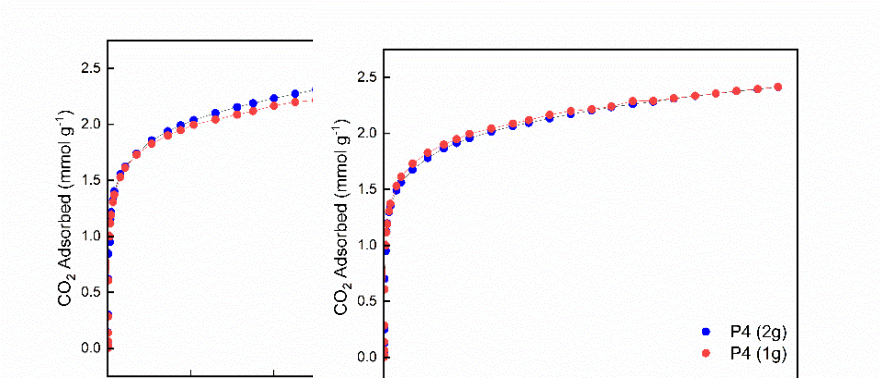

Figure 46. (left) CO2 isotherm at 313K of P4 MIL-TEPA-TMPTE. (right) CO2 isotherm at 313K of P4 at 1g and 2g scale.

Protocol Cr-MOF-TEPA-TMPTE (2g-scale):

To functionalize MIL-101-Cr, 2200 mg of bare MOF is placed in a 500 mL round-bottom flask, followed by the addition of 80 mL of methanol. Next, 42 mL of TEPA is added, and the mixture is stirred for 5 minutes. In a separate flask, 20.5 mL of TMPTE is dissolved in 80 mL of methanol, and the solution is added to the initial mixture. The combined mixture is stirred at 25°C for 3 hours, then centrifuged at 7800 RPM for 7 minutes. The supernatant is decanted, and the solid is vacuum-dried at 60°C for 24 hours.

CO_2 adsorption/desorption cycling studies of amine-impregnated Cr-MOF:

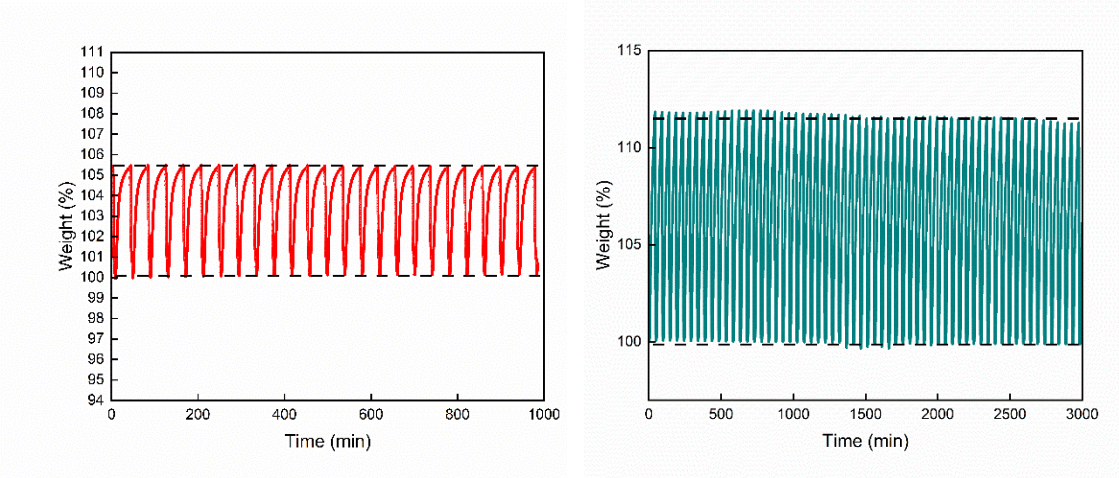

Figure 47. (left) Dry cyclic data of Cr-MOF-TEPA-TMPTE produced via P4 at 313K under 15% N_2 and 85% CO_2. (right) Humid cyclic data of P4 at 313K under 15% N_2, 85% CO_2, and 80%RH.

We have also tested the cyclicality of the best performing material (Cr-MOF-TEPA-TMPTE) and we found that the material's performance is maintained over the course of 60+ cycles. Importantly, we have observed a flat baseline, which suggests that the material retains the amines inside (otherwise indicated by a downward slope) and the amines are not degrading (i.e., irreversible CO_2 adsorption via urea formation would be indicated by an upward slope). However, we have observed fluctuations in the saturation capacity when we cycle for extended periods. The observed fluctuations are attributed to variations in the ambient temperature of the room where the measurements are conducted, which in turn lead to changes in the humidity levels. Please refer to the Figure 47 for the cycling performance. We cycled the material in 15% CO_2 and 85% Nitrogen with Adsorption temperature of 40°C and Desorption temperature of 120°C, in both dry and humid conditions, with relative humidity of 70-80%. Please refer Figure 47 for the cycling data.

Shaping the Cr-MOF-amine composite:

We have also worked on developing structuring methods for the MOF. We are trying to avoid the use of additional binders, such as clays or cellulose, which will decrease the materials CO_2 capacity. As such, we aimed to see if incorporating the amines and epoxides may serve as a binder. Given that our demonstration unit has a column, the MOF pellets must be <4mm, which is the column diameter. Hence, we aimed to optimize the pellets using a 3mm diameter die on an automated tableting machine. The final pellet should be robust, and its pores should remain open and intact. For the course of this year, efforts were focused on optimizing pellets of the bare Cr-MOF. For pellet preparation, we varied certain parameters like pressure, time, pellet height (amount of composite), etc. and compared the CO_2 adsorption performance. Please refer Figure 48 for the pictures of pellets.

Figure 48. Pellets of Cr-MOF

Surface area measurements were performed on pellets produced at varying pressures, Figure 49. The surface areas and pore volumes derived from the N_2 adsorption isotherms are shown in Table 14. For example, for pressure 1, the pores collapse fully; however, lower pressure 3 has minimal to no impact on the surface area, and the Cr-MOF pellets are found to be robust. Preliminary efforts to use the same procedure to structure the amine-containing MOF, have encountered difficulties; the pressed powder of the amine containing MOF adhere to the die surface, leading to pellet breakage when removed from the die. Given this, we will likely try die coatings to reduce surface adhesion or other structuring methods in the future. Once more of the Cr-MOF TEPA-TMPTE is produced, efforts can be better made to optimize the structuring protocol for the composite in the following year.

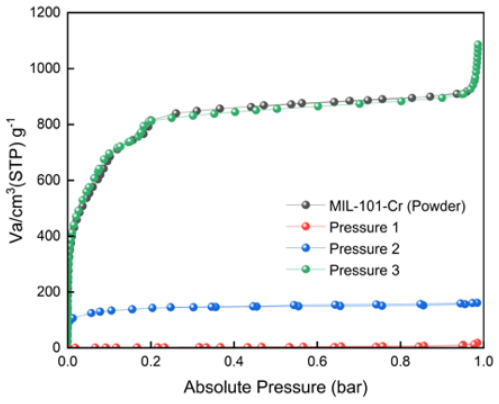

Figure 49. N2 isotherms at 77K of MIL-101-Cr pellets.

Table 14. Surface areas and pore volumes determined from pellets made at varying pressure.

Pressure	Surface Area	Pore Volume
Powder	2800	1.6793
Pressure 1	7	0.0278
Pressure 2	516	0.2493
Pressure 3	2700	1.4194

Protocol for Pellets of the Cr-MOF:

This year, we experimented with a 3mm die in the automatic pellet-making machine in our laboratory. The actual column in the demonstrator pilot plant device requires a pellet diameter within the 2mm–4mm range. To produce pellets, we adjusted the die depth and corresponding pressure to optimized levels on the automatic pellet machine. The die was manually filled to the top with bare MOF powder, and the machine was activated to complete one cycle, during which it automatically ejected the pellet.

2.3.3. WP 3 Techno-economic studies to investigate the viability of the CO_2 capture process:

Building on the previous work where the TSA model was successfully developed and validated using NaUSY zeolites, this year significant progress was made in terms of process modeling. We have developed models for both the TCSA (Temperature Concentration Swing Adsorption) and TVSA (Temperature-Vacuum Swing Adsorption) processes, incorporating a vacuum step for adsorbent bed regeneration. These models were used to simulate data for zeolite 13X as the adsorbent material. The sustainability of these processes were also evaluated through a life cycle assessment (LCA), with the goal of reducing the environmental impact. While the techno-economic assessment (TEA) is an important part of this project, it is planned to be conducted in the future. This is because the demonstrator has yet to be commissioned, and the model must first be validated.

Process description of TCSA and TVSA processes

The TCSA process has been modelled encompassing a four-step cycle, which includes adsorption, desorption through heating, purge, and cooling (Figure 50). The TCSA process model has been developed using the gPROMS modeling tool that solves conservation equations including mass, energy, and heat balances. The relevant equations along with adsorbent properties including its isotherm characteristics, density, specific heat, interparticle and intraparticle voidage were derived from the literature.

There are some important assumptions made for simulating the TCSA process, as follows:

- Ideal gas behavior
- Negligible radial heat and mass transport phenomena
- No axial conductivity along the wall
- Mass transfer resistance is described by the linear driving force model (LDF)

- Temperature-independent mass transfer coefficients, isosteric heats of adsorption and heat capacities of the solid phase and the wall.
- Adsorption equilibrium described by the dual site Langmuir isotherm with temperature dependence
- Non-isothermal with no conduction
- Thermal equilibrium between the fluid and the adsorbent particles

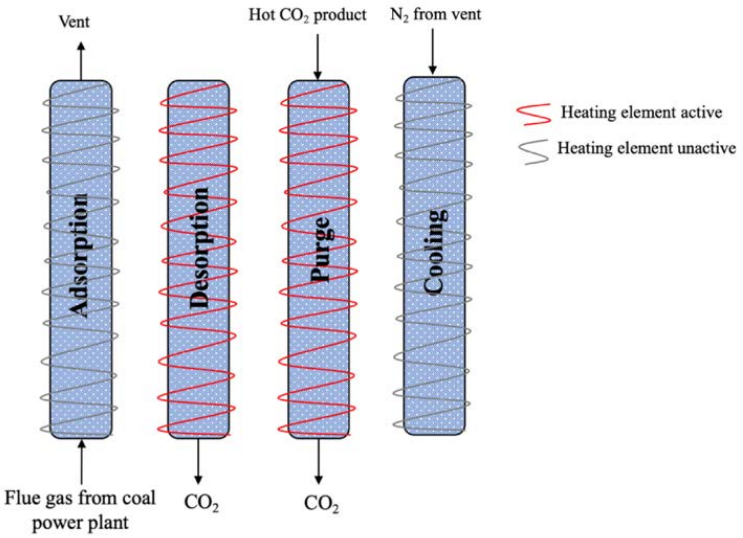

Figure 50. A schematic of four-step TCSA cycle for post-combustion carbon capture

The model uses numerical method of lines to solve the time-dependent partial differential equations (PDEs). PDEs describe the intricate transport phenomena of mass, momentum, and energy between the gas phase and the adsorbent particles during each step of the TSA cycle. The model ensures accuracy in depicting the dynamic behavior of the system by using a 'Smooth' upwinding approach (flow reversibility within the system is captured by considering the gradual variations in the Peclet number), aiding to minimize the numerical dispersion and ensuring a more physical representation of the transport processes.

Furthermore, the model discretization is tuned, employing a finite volume method, which is divided into a specific number of discretization points per layer allowing for a detailed spatial resolution of the bed, enabling the capture of local gradients and ensuring that the simulation accurately reflects the physical behavior of the system. In this setup, the number of discretization points per layer is set to 100. These nodes or points are where the PDEs are solved, providing a detailed profile of the temperature, concentration, and velocity within the adsorption bed at every step of the TCSA cycle. Last, in the TVSA process model developed this year, along with the above steps, a vacuum is provided in the second step along with heating.

Table 15. Isotherm parameters fitted to the extended Langmuir model. Isotherm data for CO_2 and N_2 at different temperatures were taken from[1]

	IP1	**IP2**	**IP3**	**IP4**	**ΔH (kJ/mol)**
CO_2	$2.88e^{-7}$	3574	$6.18e^{-5}$	3603	−37
N_2	$7.18e^{-7}$	1670	$6.21e^{-4}$	1359	−18.5

2.3.4. Sensitivity analysis on different process parameters

A sensitivity analysis was carried out by varying several process parameters, including desorption temperature, purge-to-feed ratio, adsorption time, desorption time and vacuum pressure to evaluate their impact on key performance indicators (KPIs) such as purity and recovery. The objective here is to achieve 95 % purity and 90 % recovery. For this analysis, we used a total cycle time of 3970 seconds as the starting point, with 370 seconds for adsorption, 1800 seconds for desorption, and 1800 seconds for cooling. These initial time parameters were taken from the optimized case for NaUSY-type zeolite (the work done in the first year) and were used as the starting point for optimization in this zeolite 13X study.

(i) Influence of desorption temperature on purity and recovery

Figure 51 shows the effect of desorption temperature on the purity and recovery of the system. As the desorption temperature increases from **140°C to 300°C**, both purity and recovery improve significantly. At 140°C, the system achieves a purity of 82.5% and a recovery of 38.8%. With increasing desorption temperatures, these values rise steadily, reaching a purity of **89.5% and a recovery of 72.8% at 200°C**. Beyond this point, further increases in temperature provide diminishing returns, with only minor improvements observed. At 300°C, the system attains a purity of 91.4% and a recovery of 91.5%, but the energy cost required to achieve these marginal gains becomes significant.

Given these results, a desorption temperature of **200°C** was selected for further optimization. At this temperature, the process offers a good balance between system performance and energy efficiency. Although higher temperatures could yield slightly better recovery and purity, the energy demand for heating becomes a limiting factor. With this temperature chosen, the process parameters were optimized by adjusting the cycle times, including adsorption time, desorption time, and the purge-to-feed ratio.

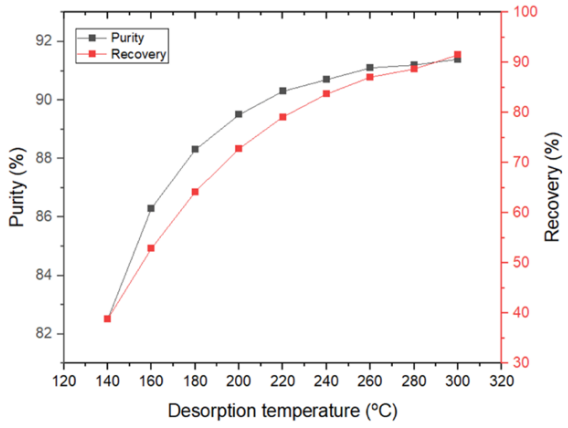

Figure 51. Effect of desorption temperature on CO2 purity and recovery

(ii) Influence of purge to feed ratio on purity and recovery

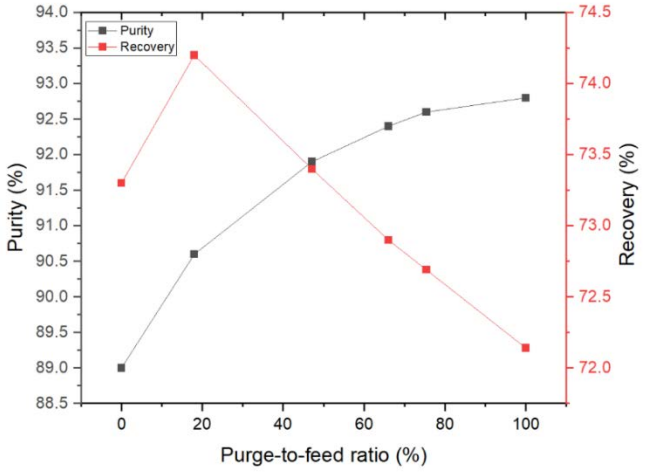

Figure 52. Influence of purge to feed ratio on purity and recovery

Figure 52 presents the effect of the purge-to-feed ratio on CO_2 purity and recovery for a fixed desorption temperature of 200°C. The purge-to-feed ratio varied between 0% to 100%. It depicts that the purity of the captured CO_2 improves with the purge-to-feed ratio, rising from 89% at 0% to 92.8% at 100%. This occurs because the hot CO_2 effectively regenerates the adsorbent, flushing out CO_2 with higher concentration in the captured stream.

On the other hand, CO_2 recovery shows a different pattern. It increases slightly from 73.3% at 0% to 74.2% at 18%, as the hot CO_2 helps regenerate the absorbent, allowing it to capture more CO_2 in the cycle. However, beyond 18%, recovery declines, reaching 72.14% at 100%. While the hot CO_2 purge initially aids desorption, excessive purging introduces too much CO_2, reducing the system's efficiency by diluting the capture process and potentially wasting energy without a corresponding benefit in CO_2 recovery.

(iii) Influence of adsorption time on purity and recovery

The influence of adsorption time on purity and recovery has been studied. From Figure 53, CO_2 purity increases with increase in adsorption time, rising from 66.5% at 150 seconds to 91.8% at 600 seconds, and reaching a maximum of 92.2% at 700 seconds. This steady increase in purity can be explained by the extended contact time between the adsorbent and the feed gas, allowing the adsorbent to selectively capture more CO_2 from the flue gas mixture. However, after 600 seconds, the rate of increase in purity becomes marginal, indicating that the adsorbent is approaching its saturation point. At this point, the system's ability to further increase CO_2 purity is limited, as the adsorbent has already captured most of the CO_2 it can handle. Thus, further increasing the adsorption time only yields slight improvements in purity.

CO_2 recovery shows a different behavior. Recovery increases steadily from 51.9% at 150 seconds to a peak of 73.8% at 390 seconds. The initial increase in recovery corresponds to the longer adsorption time allowing the absorbent to capture more CO_2 from the feed gas before reaching its saturation limit. At these lower adsorption times, the system is more effective in capturing CO_2 while limiting the capture of N_2, which is present in greater quantity in the feed gas.

However, beyond 390 seconds, the recovery begins to decline, dropping to 55.6% at 700 seconds. The decrease in recovery at longer adsorption times can be attributed to the adsorbent becoming saturated with CO_2. Once saturation is reached, the system becomes less efficient at capturing additional CO_2, and the adsorbent may begin adsorbing more of the lighter N_2 gas from the feed mixture, reducing the overall recovery of CO_2. This decline in recovery suggests that an optimal adsorption time exists beyond which the performance of the system diminishes due to saturation and inefficiencies. Based on the

results, an adsorption time of **390 seconds** is identified as the optimal point. Currently, the system achieves a CO_2 purity of **90.4%** and a recovery of **73.8%**.

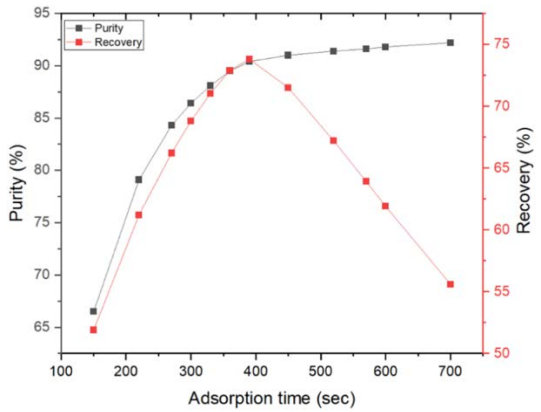

Figure 23. Influence of adsorption time on purity and recovery.

(iv) Influence of desorption time on purity and recovery

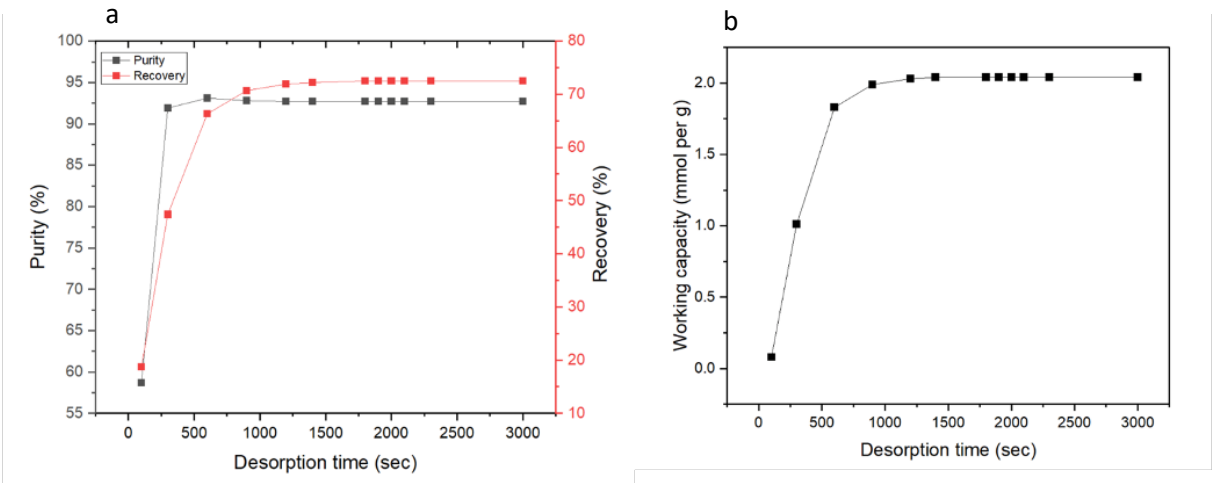

Figure 54. a) Influence of desorption time on purity and recovery b) influence of desorption time on working capacity

Figure 54 shows the effect of desorption time on CO_2 purity and recovery. Both purity and recovery rise in the first 1000 seconds, with CO_2 purity exceeding 90% and recovery reaching 70%, after which they plateau. The working capacity increases rapidly, achieving nearly 2 mmol/g in the same time frame before stabilizing. Beyond 1000 seconds, further increase in desorption time shows minimal impact on these metrics. These results suggest that a desorption time of approximately 1000 seconds is optimal for maximizing CO_2 purity, recovery, and working capacity, making it the most efficient duration for the process. Extending the desorption time beyond this point may not be energy efficient.

(v) Influence of vacuum step on purity and recovery

To evaluate the effect of the vacuum step on the desorption process, the system was tested under varying vacuum pressures, and the corresponding CO_2 purity and recovery were measured. From Figure 55, the effect of vacuum pressure on purity and recovery has been studied. It can be observed that as the vacuum pressure decreases, both the purity and recovery increase. At a vacuum pressure of 0.2 bar, the system achieves a purity of approximately 91.5% and a recovery of around 94%. The deeper vacuum leads to facilitating an increase in the working capacity, thereby improving desorption efficiency, which leads to a higher recovery. Thus, a deeper vacuum proves to be beneficial in enhancing both the purity and recovery of the system.

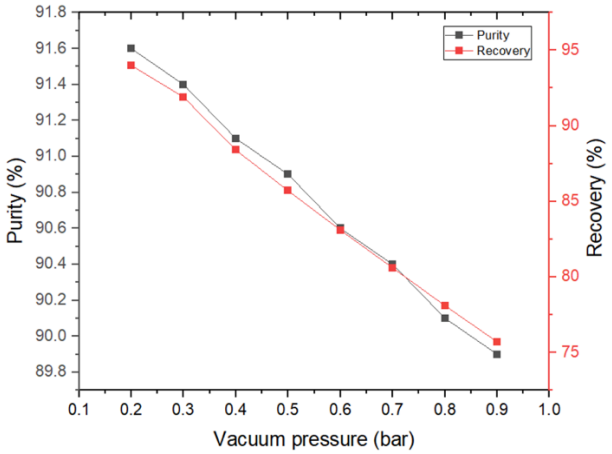

Figure 55. The influence of vacuum pressure on purity and recovery

With an adsorption time of **390 seconds**, desorption time of **1000 seconds**, purge time of **120 seconds**, cooling time of **1800 seconds**, and a vacuum pressure of **0.2 bar**, the system achieves a **purity of 91.5%** and a **recovery of 94%**. These results are in close alignment with the Department of Energy (DOE) standards, indicating that the process is operating efficiently under the specified conditions. The energy consumption and productivity of the process is yet to be evaluated.

2.3.5. Life cycle assessment methodology

LCA was conducted on the TSA, TVSA and Steam Assisted Temperature Concentration Swing Adsorption (SA-TSA) based carbon capture focusing on the environmental emissions associated with capturing CO_2 with a purity greater than 90%. This analysis centered around the functional unit of 1 kg of captured CO_2 to ensure a consistent basis for comparison and evaluation. The LCA adopted a cradle-to-grave approach, encompassing the emissions associated with the technology operation, manufacturing (includes the infrastructure of adsorption columns and zeolite material production), and end-of-life stages. Data for the inventory analysis was sourced from the Ecoinvent database, ensuring a comprehensive and reliable dataset. The Impact World+ methodology was utilized to assess environmental impacts, focusing on endpoint indicators such as carbon footprint, water footprint, ecosystem quality, human health, and resource footprint. These indicators were selected to provide a broad understanding of the environmental performance of the different regeneration processes and its implications for research communities, policymakers, and environmental enthusiasts.

The goal of this LCA study is to assess and compare the environmental impact of CO_2 capture process when zeolite 13X is implemented as the adsorbent material. Temperature Swing Adsorption (TSA), Temperature Vacuum Swing Adsorption (TVSA) and Steam assisted TVSA (SA-TVSA) processes have been compared. The relevant key parameters required for conducting this LCA are taken from the work of Jian et al.[1] and Liu et al [2]. One of the primary reasons for commissioning an LCA is to provide a rigorous and evidence-based evaluation of the environmental performance of different regeneration processes in using zeolite 13X for CO_2 capture. Another reason is to inform decision-making processes in selecting the most environmentally sustainable CO_2 capture technology among the available regeneration techniques. The results of this LCA study perhaps would also assist policymakers and regulatory bodies in establishing guidelines and standards related to carbon capture technologies. Additionally, the impact assessment of LCA was performed, which is aimed to determine the impactful stages of the process life cycle.

Assumptions in modelling

The following assumptions have been made to make the system modeling more accessible.

Location

First and foremost, this study is assumed to take place at EPFL in Sion, Switzerland. Therefore, the electricity mix of Switzerland is used and the corresponding emissions as given in the Ecoinvent Database. Distances for transportation and landfill are considered in accordance.

Process aspects

- The lifetime of the zeolite is assumed to be 20 years, and it is considered that the zeolite is landfilled at the end of its lifetime.
- The lifetime of the plant infrastructure is assumed to be 20 years, and that to be the same lifetime for the pump used in TVSA process as well. The operating days of the plant were assumed to be 330 days per year and 12 hours per day. Some parts of the infrastructure are incinerated, and some parts will be landfilled at the end of their lifetime.
- The amount of adsorbent required to provide the functional unit remains constant over the entire duration of study, as has been done in previous similar LCA studies (i.e no deterioration in zeolite quality over time).
- It is assumed that all energy required for the processes is supplied by electricity. Therefore, the total energy needed per functional unit is directly converted into electricity consumption.
- It is assumed that the cooling step does not require an energy input (as initial adsorption and cooling temperatures are the same), and instead affects the overall process productivity only due to the consequently longer overall cycle time.
- The scope of this study does not assess environmental impact beyond the CO_2 capture stage. i.e. the compression, transportation and storage of the captured CO_2 is not considered as this is equal for both processes.
- It is assumed that the columns are made of steel having a total mass calculated by the dimensions given in the data sources. The mass of the heat exchanger, steam generator and vacuum pump is assumed to be equal to what is given in the Ecoinvent Database. Additional infrastructure items needed for the process are disregarded. These items include possible expansion valves, tubes, thermostats and compressors as well as any other materials present in the columns other than steel.

Function and functional unit

The function of the model is to capture CO_2 in Switzerland in 2023. The functional unit (FU) is 1 kg of CO_2 captured with a purity above 90% in Switzerland in 2023.

Product system boundaries

This LCA includes all the life cycle stages from cradle to grave. Figures 56-58 show the process trees and the system boundaries for TSA, TVSA and SA-TSA processes, respectively. Both technologies have an infrastructure process which consists of production processes for the zeolite, the bed columns and heat exchangers. Additionally, for TVSA there is a separate process for production of the vacuum pump. In the use phase the different technologies consume energy for the process of capturing CO_2. TSA and TVSA processes utilize electricity from the electrical grid. Transportation involves firstly the column from the production site to the CO_2 capture site, and secondly, the transfer of the end-of-life infrastructure from the CO_2 capture site to the waste management facility where it is either landfilled or incinerated. The transport and the storage of the captured CO_2 are excluded as it is assumed to be the same for both the technologies.

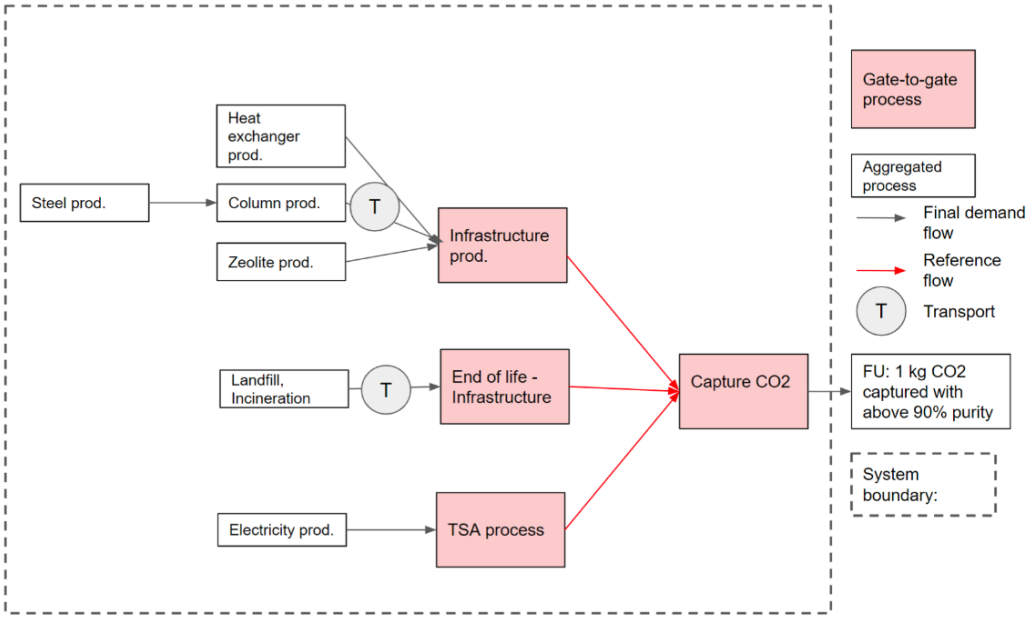

Figure 56. Process tree of TSA process

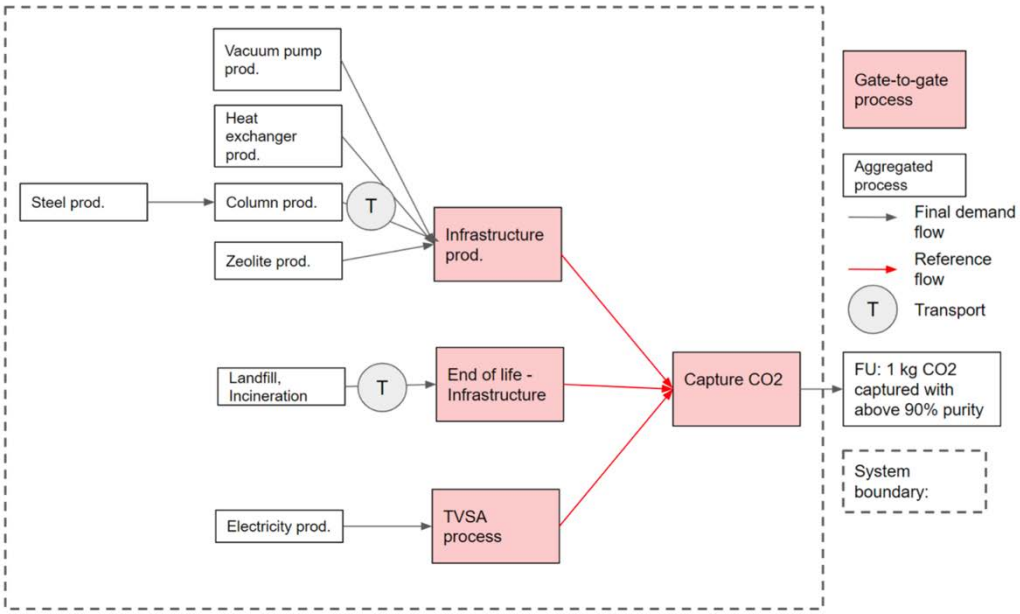

Figure 57. Process tree of TVSA process

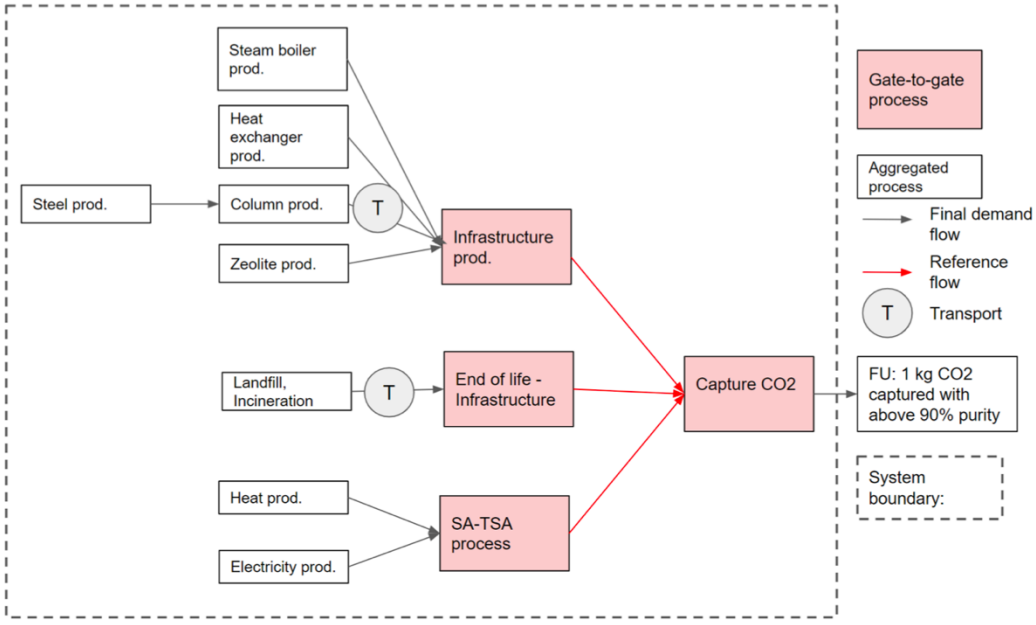

Figure 58. Process tree of SA-TSA process

Reference Flows and Key Parameters

The process tree diagrams in Figures 56-58 illustrate three gate-to-gate unit processes: the technology (TSA, TVSA, or SA-TSA regeneration process), the infrastructure production and the end-of-life (EoL) of the infrastructure. The associated reference flows for these unit processes are the consumed energy

(RF_E [MJ/FU]), the infrastructure (RF_{inf} [p/FU]), and the end-of-life of the infrastructure (RF_{EoL} [p/FU]), respectively. The reference flows and key parameters are presented in Table 16. The equations used to calculate the reference flows are listed below and are common to the TSA, TVSA, and SA-TSA.

Table 16. Reference flows and key parameters.

Reference flows	**Units**	**Key parameters**	Symbols	Units
Infrastructure	p/FU	Number of infrastructure	inf	p
		Lifetime of the infrastructure	Y	years/p
		Number of operating days in a year	D	days/year
		Number of operating hours in a day	H	h/day
		Number of hours required to fulfill the FU	X_i	h
Energy	MJ/FU	Amount of energy consumed to fulfill the FU	E	MJ
		Power consumed in X_i hours	P_i	W
		Number of hours required to fulfill the FU	X_i	h
EoL of infrastructure	p/FU	Number of infrastructure	inf	p
		End of life infrastructure rate	η_{EoL}	%

The index i in the above equations indicates that the corresponding key parameter varies according to the TSA, TVSA, or SA-TSA regeneration method. Table 17 presents the key parameter values based on the assumptions mentioned in the previous section of the report. Table 18 shows the corresponding calculated reference flows.

Table 17. Key parameter values and calculated reference flows for TSA. TVSA. and SA-TSA.

Key parameters		**Technologies**		
Smbols	**Units**	**TSA**	**TVSA**	**SA-TSA**
inf	[p]	1	1	1
Y	[p/years]	20	20	20
D	[days/year]	330	330	330
H	[h/day]	12	12	12
X	[h]	2.18	0.95	1.3
P	[W]	861.4	964.9	2179.5
η_{EoL}	[%]	100	100	100

Table 18. Key parameter values and calculated reference flows for TSA, TVSA, and SA-TSA.

Reference Flows		**Technologies**		
Symbol	**Units**	**TSA**	**TVSA**	**SA-TSA**
RF_{inf}	[p/FU]	$2.7.10^{-5}$	$1.2.10^{-5}$	$1.6.10^{-5}$
RF_E	[MJ/FU]	6.76	3.3	10.2
RF_{EoL}	[p/FU]	$2.7.10^{-5}$	$1.2.10^{-5}$	$1.6.10^{-5}$

Data sources

As shown in the below Table 19, data from Jian et al.[27], and Liu et al.[28] were used for conducting the study. Additional calculations of the presented parameters are given in Appendix. These data were used to calculate the intermediary flows, listed in Tables 20, 21, and 22 in Appendix.

Table 19. Data needed for calculating input parameters for OpenLCA

	Unit	**TSA**	**TVSA**	**SA-TSA**
Reference		Jian et al.[1]	Jian et al.[1]	Liu et al.[2]
Height of Bed	m	1.00	1.00	1.20
Diameter of Bed	m	0.10	0.10	0.10
Wall Thickness of Bed	m	0.01	0.01	0.05
Mass of Steel in Column	kg	13.74	13.74	16.33
Mass of Zeolite/bed	kg	3.68	3.68	4.42
Number of beds	-	4	4	3
Feed CO_2 Composition	$\%CO_2$	15%	15%	15%
Cycle Time	s	4000	4000	9000
Adsorption Temperature	°C	95	89	70
Desorption Temperature	°C	137	135	95
Energy Required	$MJ/kgCO_2$	6.76	3.22	10.20
Purity	%	95.04%	97.27%	90.24%
Recovery	%	90.27%	97.66%	96.00%
Productivity	$mol/kg_{ads}/h$	0.71	1.63	0.86

Impact assessment results and interpretation

Following the ISO 14040/14044 standards, the life cycle impact assessments of the TSA and TVSA technologies were conducted using the footprint version of the IMPACT World+ characterization method. This LCA method covers five environmental impact categories:

1) Carbon footprint: climate change, short term [kg CO_2-eq]
2) Water footprint: water scarcity [m^3 world-eq]
3) Remaining ecosystem quality (EQ): rest of ecosystem quality [PDF. m^2. yr]
4) Remaining human health (HH): rest of human health [DALY]
5) Resource footprint: fossil and nuclear energy use [MJ deprived]

Along with accessing the above impacts, one other important parameter of carbon capture efficiency (CCE) was accessed. CCE is the percentage of captured CO_2 that results in a net reduction of CO_2 emissions after accounting for the CO_2 generated by the capture technology itself (e.g., energy used to run the system from electricity consumption along with any other ancillary emissions). It is defined as:

$$\text{Carbon Capture Efficiency} = \left(1 - \frac{\text{CO}_2 \text{ emissions from technology}}{\text{CO}_2 \text{ captured}}\right) \times 100$$

Impact scores and profiles

Table 20 presents the impact scores of the TSA, TVSA, and SA-TSA related to the impact indicators mentioned above.

Table 20. Impact scores for each TSA, TVSA, SA-TSA technologies.

Metric	Unit	TSA	TVSA	SA-TSA
Carbon footprint	kg CO_2-eq (short)	0.221	0.105	0.886
Water footprint	m^3 world-eq	0.845	0.402	0.359
Ecosystem Quality	PDF.m^2.yr	0.037	0.017	0.081
Human Health	DAILY	$1.52e^{-7}$	$7.17e^{-8}$	$3.45e^{-7}$
Resource footprint	MJ deprived	10.1	4.80	16.9

The functional unit common to all technologies consists of capturing 1 kg of CO_2. Considering the mass of CO_2-equivalent gases emitted during each process, it can be observed that all the technologies capture more CO_2 than they emit since their carbon footprints are less than 1 kg CO_2 eq. Defining carbon capture efficiency (CCE) as the ratio of avoided CO_2 emissions to the captured CO_2, it is evident that SA-TSA demonstrates a notably low CCE at 11.4%, emitting 886 g of CO_2 equivalent to capture 1 kg of CO_2. In contrast, TSA and TVSA release 221 g and 105 g of CO_2 equivalent to achieve the same functional unit. Consequently, TSA and TVSA exhibit significantly higher CCE values compared to SA-TVSA, standing at 77.9% and 89.5%, respectively. The results in Table 20 are graphically represented in Figure 59, illustrating the impact profiles of TSA, TVSA, and SA-TSA through an internal normalization. The normalized profile of the results allows us to directly compare technologies. SA-TSA shows the poor impact profile in the carbon footprint, ecosystem quality, human health, and resource footprint impact categories. The corresponding impact scores are two to ten times higher than those of TSA and TVSA. In contrast, TVSA has the lowest impact score in most categories and appears to be the most environmentally friendly technology.

To better understand and interpret these results, a contribution analysis (which depicts which stage contributes for the emissions associated) is required for each technology. Figure 60 and Figure 61 shows the contribution analysis per process for TSA, TVSA, and SA-TSA, via internal normalization, at the first and second level respectively. Figure 59 shows that the operations are the most contributing to the five impacts for TSA, TVSA, and SA-TSA. Conversely, the impact profiles across the other two categories are minimally influenced, or even negligible, by the unit processes of infrastructure production and EoL. Within the categories of ecosystem quality and human health the infrastructure production has a higher contribution.

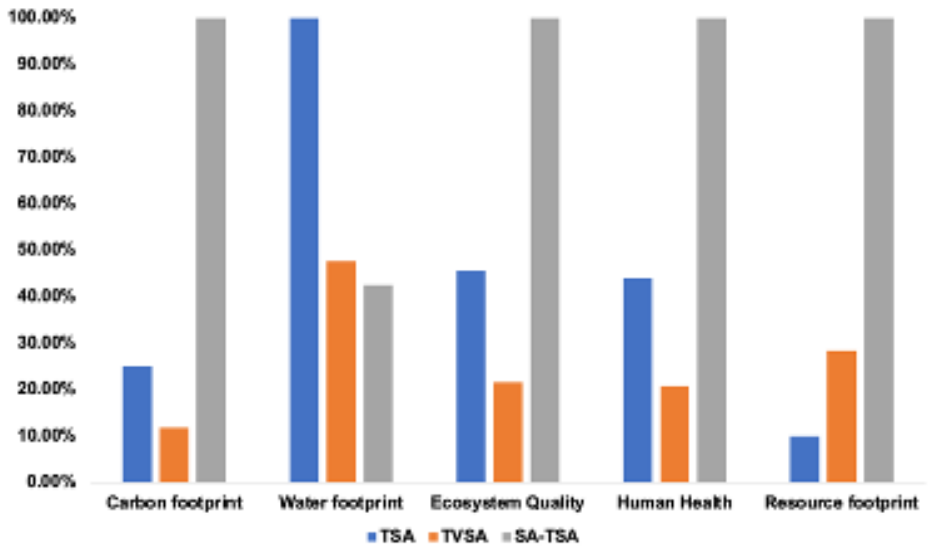

Figure 59. Impact profile of TSA, TVSA, and SA-TSA via an internal normalization.

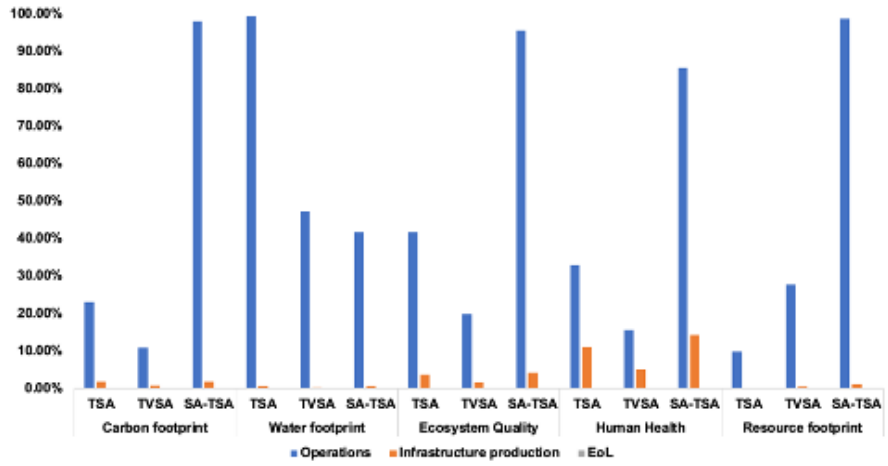

Figure 60. Contribution analysis per process at the first level for TSA, TVSA, and SA-TSA via internal normalization.

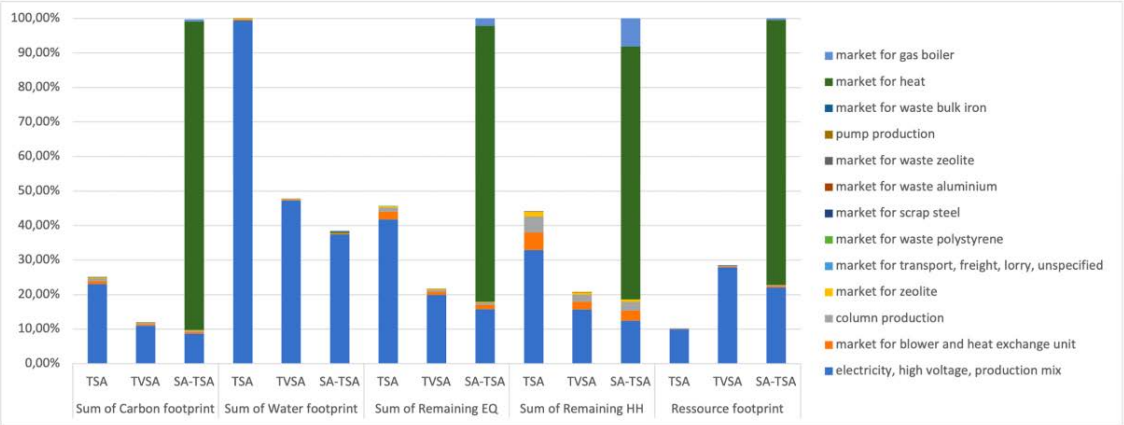

Figure 61. Contribution analysis per process at the second level for TSA, TVSA, and SA-TSA via internal normalization.

From Figure 61, it can be observed that the market for heat is the primary aggregated process contributing significantly to the higher SA-TSA impact profile in four out of the five impact categories. This can be explained by the energy mix in the SA-TSA technology. As indicated in Table 21 (see Appendix), 75% of the total energy consumption in SA-TSA is derived from heat, while the remaining 25% is sourced from electricity. This amount of electricity is about 2.55 MJ, which is less than the electricity consumption of TVSA and TSA, standing at 3.3 MJ and 6.76 MJ, respectively (see Table 22 in the Appendix , assuming 100% of the energy from electricity). Considering the predominant use of hydropower in Switzerland's electricity mix (see Figure 62 found in Appendix), these numbers elucidate the TSA's more substantial impact profile in the water footprint impact category.

Overall, based on the results obtained, **TVSA** emerges as the most sustainable process, contributing the least emissions and achieving a **net carbon capture efficiency of 89.5%**. This makes TVSA the most environmentally favorable option among the evaluated processes.

3 Conclusions and outlook

3.1 Evaluation of first year results

Pilot plant design and assembly

We have successfully completed this task in collaboration with the company PID Eng & Tech and we have carried out the FAT at their facilities. The delivery of the unit at our site has also been completed; however, we are currently waiting for the construction of the building at the Energypolis campus (Sion) to finalize the installation. It was supposed to be finalized by Fall 2023, but after the latest estimations it was postponed to late 2023/early 2024 due to issues with planning and construction due to delays with the funding transfer from the funding source among other issues. We have also received the gas analyzer from Hiden, which will be installed together with the main unit at the same time.

Adsorbent scale-up

We have demonstrated a large cost reduction by optimizing the washing step of the MOF adsorbent, which will be critical when further increasing the scale of reaction. We could synthesize a large amount

of the parent Cr-MOF (250 grams) with our current 1 L reactor upon running multiple reactions. However, we are working on acquiring a larger reactor of 10 L, which will resemble a more realistic scale-up synthetic approach. We expect to receive this reactor in the following months and proceed in further optimizing not only the larger scale reaction, but also the subsequent filtration and washing steps.

We have demonstrated that we can obtain up to 8 g of modified MOF amines in the pores in a single reaction batch. However, we are aware that larger amounts should be obtained in one batch, and we will work towards a larger synthesis with 100-200 g of starting MOF to produce the final amine-modified adsorbent.

Process modelling

We have successfully developed a process model for temperature swing adsorption and it has been validated from experimental data. This model will further support in identifying the right process conditions for the state-of-the-art zeolite material and the Cr-MOF-amine and silica-amine composites for their implementation in the CO_2 demonstrator.

3.2 Evaluation of second year results

Provisional evaluation of the results obtained to date and the activities that have been carried out

Pilot plant design and assembly

During the second year, the construction of the building for the pilot plant was completed, in July 2024. We also arranged for the installation of a mass spectrometer detector completed in May 2024 and installed additional components such as gas cabinets and pressure regulators as required for the pilot plant operation. Despite the building being ready for installation, staff shortages caused a delay, pushing the pilot plant installation back to November 2024. A two-week installation and training were successfully completed at EPFL on November 29th. The pilot plant commissioning included various experimental activities using structured zeolite 13X as the adsorbent. The planned procedures included in situ activation at 320°C, CO_2/N_2 adsorption at 313K, and regeneration using the TVSA approach. Tests were conducted under both dry and humid conditions to assess water and CO_2 competition during adsorption. We also conducted compression tests and receive training on control panel operations. All team members have also completed the necessary safety training and are ready to begin pilot plant operations in January of 2025. Last, we also had a new TGA/DSC combo installed in the facility for cycling measurements under vacuum and temperature swing conditions in October 2024.

Adsorbent scale-up

During the second year, we were not able to purchase the 10 L reactor as originally planned for the scale-up synthesis of the Cr-MOF and KIT-6 silica. We found during the study that the MOF synthesis corrodes standard stainless-steel reactors; thus, the 10 L reactor would require a special alloy that is acid resistant, increasing cost by a factor of 10. This inhibited our ability to make the reactor purchase due to budget limitations. Thus, we instead proceeded with the purchase of multiple 2 L autoclaves, and the reaction was increased from the 1L to the 2L scale, yielding 40-50 g batches of MOF. Importantly, the MOF scaling process has been linear allowing us to simply scale the reaction directly with reactor size. Further, to accumulate more material, we simply increased the frequency of syntheses. In fact, using the 2 L reactions, we were able to reach a total of 1.23 kg of high-quality Cr-MOF (2900 m2/g). Next, we successfully elucidated methods to structure the bare MOF into pellets using an industrial tableting machine, which can produce thousands of pellets per day.

We also worked on amine impregnation inside the Cr-MOF. This year we focused on optimizing the performance of Cr-MOF-TEPA-TMPTE composite achieving a capacity of ~1.9 mmol/gram CO_2 at 0.15 bar and 40^{o}C; our focus on this composite was not originally planned. The change in project direction stems from the fact that this amine (TEPA) and epoxide (TMPTE) have much lower cost and are more environmentally friendly relative to the amine (TAEA) and epoxide (BDE) we originally planned to employ

in the scale-up synthesis of the composite. After optimization of Cr-MOF-TEPA-TMPTE performance with production at the 0.5 gram scale we successfully carried out the synthesis on the 2 g with no changes in material quality as reflected by the high CO_2 capacity at 0.15 bar and 40ºC, which is comparable to the material produced on the 0.5 g scale.

Last, we started the scale-up synthesis of KIT-6 silica on a 2 L scale, which is again the maximum scale achievable in our laboratory at the moment. The material can be made in 20 gram scale per 2L reaction and to date we have accumulated about 500 g of bare material in the lab. The scaling process has been linear up to this point, and we are not intending to increase the scale further. Thus, we will continue making the material on the 2L scale to increase the quantity to the desired 2 kg scale. The grafting of KIT-6 silica with an amine-rich polymer (PEI) was also successful, leading to an adsorbent with a CO_2 capacity of ~1.4 mmol/g. The amine-containing materials was also shown to retain its capacity after reactivation showing the amines are immobilized inside. Efforts to structure the amine-impregnated silica was also shown to be successful with the production of robust tablets that readily withstand friability tests with no visible signs of pellet breakage.

Process modelling

This year, TSA and TVSA models have been successfully developed for zeolite 13X. The TVSA model showed promising results, achieving both purity and recovery levels close to the Department of Energy (DOE) targets. Specifically, for a temperature of **200°C** and a vacuum pressure of **0.1 bar**, a **purity of 92%** and a **recovery of 94%** were achieved. Additionally, a Life Cycle Assessment (LCA) was conducted to compare the environmental impacts of the TSA, TVSA, and SA-TSA processes. The TVSA process demonstrated the lowest environmental emissions and a **carbon capture efficiency of 89.5%**, making it the most sustainable option among the three processes evaluated. The life cycle impact results of the TVSA process will be compared to the benchmark process for CO_2 capture, which is the conventional amine-based scrubbing method.

3.3 Next steps

Discussion of the steps to be taken in the following year, for example planned activities and (where applicable) required measures

Cr-MOF-TEPA-TMPTE

The main tasks we aim to achieved within the next year for Cr-MOF-TEPA-TMPTE include:

- ***Scale the Cr-MOF using 2L batch reactions.*** We will continue to synthesize the MOF using 2L reactors. Our aim is to accumulate >2 kg in the lab using previously established procedures.
- ***Scale the amine impregnation using TEPA and TMPTE to the 40-50 g.*** While MOF synthesis has remained relatively linear while scaling up to a 2L reaction volume (40-50 gram yield), we must proceed now with scaling the amine impregnation. We note that while the amine-impregnation part of the work is rather simple, it does require reagents to diffuse into the MOF pore and subsequent cross-linking inside. For this, the MOF-powder must be immersed in a solution and the reaction proceeds rather rapidly at room temperature. While the process has remained linear from the 0.5 to 2-gram scale, we would like to get to the 40-50gram scale to match the current scale of the MOF synthesis. However, given the high reactivity of the starting materials, we run the risk that the polymerization occurs outside the MOF pores with scaling the reaction size, reducing the materials performance; thus, our aim is to go stepwise from 2 g to the 10, 20, and then 40-50 g scale to see if the process remains linear (determined by maintained performance) or if the process becomes non-linear (due to a decrease in performance). If so, we expect we may need to optimize several parameters during the amine impregnation process, including the ratios of starting materials (MOF, amines, and epoxide) and their concentrations,

reaction temperature and time, stirring rate, and the amount of solvent used. Numerous experiments will thus likely be needed to fine-tune the amine impregnation process. For Cr-MIL-TEPA-TMPTE and all other amine-containing materials, the goal is to get to cyclable CO_2 capacities, using vacuum and/or temperature swing desorption processes are > 1.0 to 2 mmol CO_2/g adsorbent. Should we find that we are unable to fine tune the reaction parameters as needed using batch reactions, we may also resort to trying continuous flow methods. This method will allow us to more intimately mix the MOF and reactants relative to large scale batch reactions.

- ***Develop a structuring protocol to make tablets of the Cr-MIL-TEPA-TMPTE composite.*** Once we obtain large quantities of a high performing Cr-MIL-TEPA-TMPTE, we will continue working to develop strategies to structure the materials using tableting or other methods. Given our difficulty with the amine-impregnated materials sticking to the die used to make the tablets, we first aim to explore the use of a spray coatings, which may decrease tablet adhesion to the die surface. Such coatings will be employed before proceeding with any potential other potential tableting methods. Should the spray coatings not work, we will explore other methods, for example, the tableting by curing the samples rather than using pressure.

Amine-appended KIT-6

The main tasks we aim to achieved within the next year for the amine-appended KIT-6 include:

- ***Scaling KIT-6 silica using 2L batch reactions to accumulate 1.0-2 kg of material.*** As in the case of the Cr-MOF, we have demonstrated a scale up of the silica, KIT-6, using the 2L reactors, which yield ~20 grams of silica per batch. While we do not plan to use larger reactors in the future, we will continue to accumulate the silica to increase our stock from 500 g up to the 1-2 kg scale using multiple reactions.
- ***Scale the amine impregnation step to the 40-50 g scale using batch reactions or continuous flow methods.*** As in the case of the Cr-MOF, we have demonstrated a scale up of the silica, KIT-6, using the 2L reactors, which yield ~20 grams of silica per batch. While we do not plan to use larger reactors in the future, we will continue to accumulate the silica to increase our stock from 500 g up to the 1-2 kg scale using multiple reactions.

We will also increase the scale of the amine impregnation process. Currently we are producing ~1 gram per batch and would like to go to the 10 gram scale; however, like the MOF, we expect that the amine-impregnation could become non-linear at some point in the scaling process. Thus, we will vary reaction conditions, similarly described for the MOF. The goal will be to scale an amine-appended material up to the 40-50 g scale having a cyclable CO_2 capacity (via vacuum and/or temperature swing desorption processes) > 1.0 to 2 mmol CO_2/g adsorbent.

We are also testing the amine-grafting under continuous flow conditions, to see if it is possible to significantly increase the space-time yield of the reaction as well as accelerate and ease the scale-up process. The parameters of the flowthrough reaction include: residence temperature, residence time, concentration of reagents in the solvent, and ratio of reagents to silica. Such parameters will need to be altered to optimize performance towards the desired CO_2 capacity. Last, preliminary tests on the amine-appended material have already shown good potential for pelletization.

- ***Demonstrate the tablet making process under continuous flow.*** So, after producing large quantities of the amine-containing composite, our next goal will be to begin accumulating pelletized amine-appended KIT-6 via continuous flow pellet production in our industrial tableting machine. Given the robustness of the tablets already prepared in the project, we do not expect this process to pose any significant problems.

Process modelling and including techno-economic assessments

From the process modeling perspective, the following tasks are planned for completion in 2025:

- ***Validation of TVSA model***. Experiments will be conducted in the pilot plant where the demonstrator will be packed with zeolite 13X. The purity and recovery of the process will be evaluated and validated against the TVSA model, ensuring alignment between simulation and real-world performance.
- ***Techno-Economic Analysis.*** A techno-economic analysis (TEA) will be performed for the validated TVSA process to estimate the CO_2 capture cost, providing critical insights into its economic viability.
- ***Life Cycle Assessment with waste heat integration.*** Building on the LCA performed last year comparing TSA, TVSA, and steam-assisted TSA processes, this year's focus will include evaluating the steam-assisted TSA process with the incorporation of waste heat. The impact of waste heat integration on emission reduction during adsorbent regeneration will be analyzed to highlight its potential sustainability benefits.

Comparative LCA with amine scrubbing process. Carbon capture is tested using various techniques, including polymeric membranes (TRL 6), oxy-combustion in power plants (TRL 7), chemical looping combustion (TRL 7), and the use of ionic liquids, among others. Among these, amine scrubbing remains the only commercialized process (TRL 9) and is the implemented method in power plants. The focus of this project is to compare the sustainability of adsorbent-based processes with amine scrubbing. This comparison will leverage data available in the literature, and where such data are lacking, efforts will be undertaken to develop a life cycle assessment (LCA) model for the amine scrubbing process.

- ***Process modelling of amine incorporated materials.*** If time allows process modeling for MOFs impregnated with amines or amine impregnated silica will be established. The operating conditions necessary to achieve a purity of over 90% will be investigated, including regeneration temperature, cycle times (adsorption/desorption), and other parameters. These estimations will be tailored to pilot plant-scale dimensions, providing a pathway for future scale-up.

Technology Roadmap

To address the contractual clause about the technology roadmap, we will focus on defining a clear strategy for transitioning the CO_2 capture technology into the market. The roadmap will prioritize collaboration with industrial partners, particularly Casale SA, which will play a role in validating the results of techno-economic analysis (TEA) and life cycle assessment (LCA). Additional applications in high-emission sectors, such as waste incineration plants, steel, and chemical manufacturing, would be interesting for people working in these domains. Waste incineration plants typically have a CO_2 composition ranging between 10-15%, making this approach more compatible with our current work on post-combustion flue gas mixtures from power plants.

The roadmap will also detail intellectual property (IP) protection and licensing strategies to safeguard the innovations developed in this project. The remaining technical challenges, such as material scalability, energy efficiency optimization in TSA and TVSA cycles, and ensuring the long-term durability of adsorbents, will be critical, and the same will be addressed in the roadmap. Additionally, targeted research and development activities will further be outlined.

4 National and international cooperation

None.

5 Publications and other communications

- Now that the pilot plant is up and running we aim to put project results on a tab on the LFIM website for all stakeholders to see project results now that the pilot plant is up and running.

  Here is the link to the project tab on LFIM website.

- We have already engaged in Scientistic events (open-door events to the public) held at EPFL-Valais, allowing us to communicate the results of the project to the public on our carbon capture project.
- We have shown the demonstrator and highlighted the results of our projects at multiple informal meetings held at EPFL, that has engaged industry, the public, and other academics.
- Several research papers were already submitted to peer-reviewed journals communicating results to the scientific community. There is already an additional report under peer review at the moment, and we expect to have several more before and/or after the project end.
- Presentations/seminars were given at academic institutions, conferences, company visits, and at EPFL events to politicians, industry, high school students and teachers, and/or the general public. For example, in the past two years, Prof. Queen has presented the title project in a host of invited or keynote seminars given at:
    a. *The Out of the Blue Conference* in Crete, Greece (2024),
    b. *The 9th EuChemS Meeting* in Dublin Ireland (2024),
    c. *The UK PorMat Meeting* at Liverpool, England (2024),
    d. Frühjahrssymposium 2024, titled “Rethinking Chemistry: Towards A Greener Future” in Ulm, Germany,
    e. *The Swiss Snow Symposium 2024* in Saal-Allmagell, Switzerland,
    f. *EuroMOF 2023* in Grenada, Spain,
    g. A *GRC* titled “Nanoporous Materials and their Applications” in New Hamshire, USA,
    h. A *GRC* titled “Atomically Precise Nanochemistry” (2024) in Galveston Texas (USA)
    i. A Telluride Conference on Porous Materials in Telluride Colorado, USA,
    j. Japanese Decarbonization Delegation Meeting Sion, Swtizerland
    k. The 1st Mediteranean Conference on porous materials (MEDPore 23) in Crete, Greece,
    l. A CCUS workshop in 2024, which had many players from the cement industry, Lausanne, Switzerland
    m. An event for high school teachers (2024) held at EPFL in Sion Switzerland
    n. *Sustainability Week* for High School Students (2023 & 2024) held at EPFL Lausanne, Switzerland
    o. The University of Zurich, Switzerland
    p. The University of Basel, Switzerland
    q. The University of California Berkeley, USA
    r. Clemson University, South Carolina, USA
- We have also discussed the results with various industries throughout Switzerland, including incineration and cement plants. Normally, we interact with multiple industries per year during their visits to EPFL (like Total, ExxonMobil, and OCP). Last, we also have yearly project meetings with Gaznat, which will also be very interested to see the results.

- We aim to have a workshop next year on CCUS, in partnership with the EPFL energy center next year in 2025.

List of published material

- Post-synthetic Covalent Grafting of Amines to NH_2-MOF for Post-Combustion Carbon Capture" A. Justin, J. Espín, M. J. Pougin, D. Stoian, T.Schertenleib, M. Mensi, I. Kochetygov, A. Ortega-Guerrero, W. L. Queen*, *Adv. Funct. Mater.* **2023**, published online.
- N-containing carbons derived from microporous coordination polymers for use in post-combustion flue gas capture" V. V. Karve, J. Espín, M. Asgari, S. Van Gele, E. Oveisi, W. L. Queen*, *Adv. Funct. Mater.*, **2023**, 33, 2212283.
- Densification and shaping of pure Cu-BTC powders using a solid-state chemical transformation" V. V Karve, A. Mabillard, J. Espin, M. Asgari, W. L. Queen, M. Soutrenon, *Mater. Res. Express* **2024**.
- We have also filed on patent application in 2023.

6 References

1. Adil, A. & Chohan, U. Climate change as socioeconomic threat: International Perspectives. (2020).

2. Winski, D. *et al.* A 400-Year Ice Core Melt Layer Record of Summertime Warming in the Alaska Range. *J. Geophys. Res. Atmos.* 123, 3594–3611 (2018).

3. Melet, A., Meyssignac, B., Almar, R. *et al.* Under-estimated wave contribution to coastal sea-level rise. *Nature Clim Change* 8, 234–239 (2018).

4. Sun, D. T. & Queen, W. L. Mystical Material Might Help Solve Global Energy Problems. *ACS CentSci.* 5, 1307–1309 (2019).

5. Quadrelli, R., et al., The energy–climate challenge: Recent trends in CO_2 emissions from fuel combustion. *Elsevier* (2007).

6. Kohl, A. & Nielsen, R. *Gas purification*. (1997).

7. Analysis, A. R. J.-E. L. R. N. & & 2011. Federal control of carbon capture and storage.

8. Asgari, M., Streb, A., Van Der Spek, M., Queen, W. & Mazzotti, M. Synergistic material and process development: Application of a metal-organic framework, Cu-TDPAT, in single-cycle hydrogen purification and CO 2 capture from synthesis gas. *Chem. Eng. J.* 414, 128778 (2021).

9. Siemens, gPROMS modelling tool. https://www.psenterprise.com/products/gproms.

10. May-Yin (Ashlyn) Low et al., Analytical review of the current state of knowledge of adsorption materials and processes for direct air capture, Chemical Engineering Research and Design , 189,745-767 (2023).

11. Seider, W. D,et al., Product and Process Design 435 Principles - Synthesis, Analysis and Evaluation, 3rd ed.; John Wiley & Sons, Inc.(2009), 436.

12. James R. Couper et al., Chemical Process Equipment: Selection and Design,3, Elsevier (2012)

13. Turton, R. et al., Analysis, synthesis, and design of chemical processes (3rd ed.). Prentice Hall (2009).

14. M. M. Faruque Hasan, et al. Modeling, Simulation, and Optimization of Postcombustion CO2 Capture for Variable Feed Concentration and Flow Rate. 1. Chemical Absorption and Membrane Processes. Industrial & Engineering Chemistry Research 2012, 51 (48) , 15642-15664.

15. Stefano E. Zanco et al. Post- combustion CO2 Capture: A Comparative Techno-Economic Assessment of Three Technologies Using a Solvent, an Adsorbent, and a Membrane, ACS Engineering Au (2021), 1 (1), 50-72

16. M. M. Faruque Hasan, et al. Modeling, Simulation, and Optimization of Postcombustion CO2 Capture for Variable Feed Concentration and Flow Rate. 2. Pressure Swing Adsorption and Vacuum Swing Adsorption Processes, Industrial & Engineering Chemistry Research 2012 51 (48), 15665-15682.

17. Garrett, D. E. Chemical Engineering Economics (1989)

18. Zhao, T. *et al.* High-yield, fluoride-free and large-scale synthesis of MIL-101(Cr). *Dalt. Trans.* 44, 16791–16801 (2015).

19. Milner, P. et al. Overcoming double-step CO_2 adsorption and minimizing water co-adsorption in bulky diamine-appended variants of Mg_2(dobpdc), *Chem. Sci*., 2018,9, 160-174

20. Whiting, G. T. et al. Multiscale mechanistic insights of shaped catalyst body formulations and their impact on catalytic properties. *ACS Catal*. 9, 4792–4803 (2019).

21. Cavenati, S.; Grande, C. A.; Rodrigues, A. E., Removal of carbon dioxide from natural gas by vacuum pressure swing adsorption. *Energy & Fuels* (2006), 20 (6), 2648-2659.

22. Min, K., Choi, W., Kim, C. et al. Oxidation-stable amine-containing adsorbents for carbon dioxide capture. *Nat Commun* 9, 726 (2018).

23. Young, J. et al. The impact of binary water–CO2 isotherm models on the optimal performance of sorbent-based direct air capture processes. *Energy Environ. Sci.* 14, 5377–53942 (2021).

24. Ntiamoah, A., Ling, J., Xiao, P., Webley, P. A. & Zhai, Y. CO2 Capture by Temperature Swing Adsorption: Use of Hot CO2-Rich Gas for Regeneration. *ACS Publ.* 55, 703–713 (2015).

25. Sharma, S. & Maréchal, F. Carbon Dioxide Capture From Internal Combustion Engine Exhaust Using Temperature Swing Adsorption. *Front. Energy Res.* 7, 465010 (2019).

26. Deng, X., Chen, K., & Tüysüz, H. Protocol for the nanocasting method: Preparation of ordered mesoporous metal oxides. *Chemistry of Materials*, 29(1), 40–52 (2016).

27. Jiang, N. et al. CO2 capture from dry flue gas by means of VPSA, TSA and TVSA. Journal of CO2 Utilization 35, 153–168 (2020).

28. Liu, W. *et al.* Steam-assisted temperature swing adsorption for carbon capture integrated with heat pump. *Case Studies in Thermal Engineering* **49**, 103233 (2023).

7 Appendix

Reference flow equations used in LCA assessment

In the following equations, mCO_2 is the amount of captured CO_2, expressed in the functional unit: FU = 1 [kg] mCO_2

Equation for the energy reference flow:

$$RF_E = \frac{X_i \cdot P_i}{m_{CO_2}} \cdot \frac{1\ kW}{1000\ W} \cdot 3.6\ \frac{MJ}{1\ kWh} = \frac{E}{m_{CO_2}}$$
$$RF_E = \frac{[h] \cdot [W]}{FU} \cdot \frac{[kW]}{[W]} \cdot \frac{[MJ]}{[kWh]} = \frac{[MJ]}{FU}$$

Equation for the infrastructure reference flow:

$$RF_{inf} = \frac{X_i}{m_{CO_2}} \cdot \frac{1\ day}{H} \cdot \frac{1\ year}{D} \cdot \frac{1\ inf}{Y} = \frac{inf}{m_{CO_2}}$$
$$RF_{inf} = \frac{[h]}{FU} \cdot \frac{[day]}{[h]} \cdot \frac{[year]}{[days]} \cdot \frac{[p]}{[years]} = \frac{[p]}{FU}$$

Equation for the end-of-life reference flow:

$$RF_{EoL} = \frac{inf}{m_{CO_2}} \cdot \eta_{EoL}$$
$$RF_{EoL} = \frac{[p]}{FU} \cdot [-] = \frac{[p]}{FU}$$

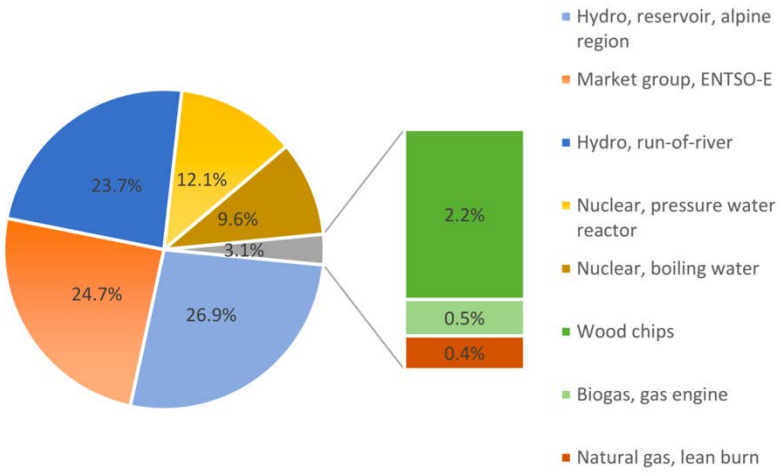

Figure 62. Switzerland electricity mix

Table 21. SA-TSA process flows for the specific unit processes and their respective values and ecoinvent 3.6 process used.

Unit processes	Flow type	Flow	Quantity	Unit	Ecoinvent 3.6 process or created process	Comment
Captured CO2	Final demand flow - Output	Captured CO2	1.00	kg	Captured CO2, SA-TSA | Cutoff, U, MABOR	
	Reference flows - Inputs	Energy	10.20	MJ	Energy, SA-TSA | Cutoff, U, MABOR	Energy consumption from [20]
		Infrastructure	1.60E-05	Item(s)	Infrastructure production, SA-TSA - CH | Cutoff, U, MABOR	Calculated with an infrastructure operating for 330 days per year, 12 hours a day and with a lifetime of 20 years.
		EoL - Infrastructure	1.60E-05	Item(s)	EoL of infrastructure, SA-TSA - CH | Cutoff, U, MABOR	The infrastructure is assumed to be 100% landfilled or incinerated at the end of its lifetime.
Infrastructure production	Reference flow - Output	Infrastructure	1.00	Item(s)	Infrastructure production, SA-TSA - CH | Cutoff, U, MABOR	
	Intermediary flows - Inputs	Zeolite	13.30	kg	market for zeolite, powder | zeolite, powder | Cutoff, U - GLO	This ecoinvent process is assumed to be similar as the NaX composition from the studies used.
		Heat exchanger	1.00	Item(s)	market for blower and heat exchange unit, decentralized, 180-250 m3/h | blower and heat exchange unit, decentralized, 180-250 m3/h | Cutoff, U - GLO	A substitute for the heat exchanger needed for the technology.
		Column production	3.00	Item(s)	Column production, SA-TSA | Cutoff, U, MABOR	The technology is assumed to need 3 columns.
		Steam boiler prod.	1.00	Item(s)	market for gas boiler | gas boiler | Cutoff, U - GLO	The steam boiler is assumed to consist of the same material as this gas boiler ecoinvent process.
		Column transport	5.44E+03	kgkm	market for transport, freight, lorry, unspecified | transport, freight, lorry, unspecified | Cutoff, U - RER	Estimated 111 km transport from producer in Sierre to the facility in Lausanne. The unspecified transport process is used because of lack of data about the specific vehicle.
SA-TSA technology	Reference flow - Output	Energy	1.00	MJ	Energy, SA-TSA | Cutoff, U, MABOR	
	Intermediary flows - Inputs	Electricity	0.25	MJ	electricity, high voltage, production mix | electricity, high voltage | Cutoff, U - CH	The technology is assumed to consist of this ecoinvent average energy mix.
		Heat	0.75	MJ	market for heat, from steam, in chemical industry | heat, from steam, in chemical industry | Cutoff, U - RER	This ecoinvent market for heat process from steam is a substitute for the steam needed for the technology.
EoL of Infrastructure	Reference flow - Output	EoL infrastructure	1.00	Item(s)	EoL of infrastructure, SA-TSA - CH | Cutoff, U, MABOR	
	Intermediary flows - Outputs	Waste zeolite	13.30	kg	market for waste zeolite | waste zeolite | Cutoff, U - CH	The zeolite is assumed to be 100% landfilled.
		Scrap steel	73.00	kg	market for scrap steel | scrap steel | Cutoff, U - CH	A sum of steel inputs with the highest share of the different processes in the Infrastructure process
		Waste aluminium	15.40	kg	market for waste aluminium | waste aluminium | Cutoff, U - GLO	A sum of aluminium inputs with the highest share of the different processes in the Infrastructure process.
		Waste polystyrene	7.20	kg	market for waste polystyrene | waste polystyrene | Cutoff, U - CH	A sum of polystyrene inputs with the highest share of the different processes in the Infrastructure process.
	Intermediary flows - Inputs	Waste transport	4.35E+03	kgkm	market for transport, freight, lorry, unspecified | transport, freight, lorry, unspecified | Cutoff, U - RER	Estimated 40 km transport of waste from the facility in Lausanne to a recycling facility in Montreux. The unspecified transport process is used because of lack of data about the specific vehicle.
Column production	Intermediary flow - Output	Column	1.00	Item(s)	Column production, SA-TSA | Cutoff, U, MABOR	
	Intermediary flows - Inputs	Steel production	16.30	kg	market for steel, chromium steel 18/8 | steel, chromium steel 18/8 | Cutoff, U - GLO	Substitute for the column material.

Table 22. TVSA flows for the specific unit processes and their respective values and ecoinvent 3.6 process used

Unit processes	Flow type	Flow	Quantity	Unit	Ecoinvent 3.6 process or created process	Comment
Captured CO2	Final demand flow - Output	Captured CO2	1.00	kg	Captured CO2, TVSA | Cutoff, U, MABOR	
	Reference flows - Inputs	Energy	3.22	MJ	Energy, TVSA | Cutoff, U, MABOR	Energy consumption from [19]
		Infrastructure	1.20E-05	Item(s)	Infrastructure production, TVSA - CH | Cutoff, U, MABOR	Calculated with an infrastructure operating for 330 days per year, 12 hours a day and with a lifetime of 20 years.
		EoL - Infrastructure	1.20E-05	Item(s)	EoL of infrastructure, TVSA - CH | Cutoff, U, MABOR	The infrastructure is assumed to be 100% landfilled or incinerated at the end of its lifetime.
Infrastructure production	Reference flow - Output	Infrastructure	1.00	Item(s)	Infrastructure production, TVSA - CH | Cutoff, U, MABOR	
	Intermediary flows - Inputs	Zeolite	14.70	kg	market for zeolite, powder | zeolite, powder | Cutoff, U - GLO	This ecoinvent process is assumed to be similar as the NaX composition from the studies used.
		Heat exchanger	1.00	Item(s)	market for blower and heat exchange unit, decentralized, 180-250 m3/h | blower and heat exchange unit, decentralized, 180-250 m3/h | Cutoff, U - GLO	A substitute for the heat exchanger needed for the technology.
		Column production	4.00	Item(s)	Column production, TVSA | Cutoff, U, MABOR	The technology is assumed to need 4 columns.
		Vacuum pump prod.	1.00	Item(s)	pump production, 40W | pump, 40W | Cutoff, U - CH	Substitute for the vacuum pump
		Column transport	6.01E+03	kgkm	market for transport, freight, lorry, unspecified | transport, freight, lorry, unspecified | Cutoff, U - RER	Estimated 111 km transport from producer in Sierre to the facility in Lausanne. The unspecified transport process is used because of lack of data about the specific vehicle.
TVSA technology	Reference flow - Output	Energy	1.00	MJ	Energy, TVSA | Cutoff, U, MABOR	
	Intermediary flows - Inputs	Electricity	1.00	MJ	electricity, high voltage, production mix | electricity, high voltage | Cutoff, U - CH	The technology is assumed to consist of this ecoinvent average energy mix.
EoL of Infrastructure	Reference flow - Output	EoL infrastructure	1.00	Item(s)	EoL of infrastructure, TVSA - CH | Cutoff, U, MABOR	
	Intermediary flows - Outputs	Waste zeolite	14.70	kg	market for waste zeolite | waste zeolite | Cutoff, U - CH	The zeolite is assumed to be 100% landfilled.
		Scrap steel	267.00	kg	market for scrap steel | scrap steel | Cutoff, U - CH	A sum of steel inputs with the highest share of the different processes in the Infrastructure process
		Waste aluminium	15.40	kg	market for waste aluminium | waste aluminium | Cutoff, U - GLO	A sum of aluminium inputs with the highest share of the different processes in the Infrastructure process.
		Waste polystyrene	7.20	kg	market for waste polystyrene | waste polystyrene | Cutoff, U - CH	A sum of polystyrene inputs with the highest share of the different processes in the Infrastructure process.
		Waste bulk iron	1.20	kg	market for waste bulk iron, excluding reinforcement | waste bulk iron, excluding reinforcement | Cutoff, U - CH	A sum of bulk iron inputs with the highest share of the different processes in the Infrastructure process.
	Intermediary flows - Inputs	Waste transport	1.22E+04	kgkm	market for transport, freight, lorry, unspecified | transport, freight, lorry, unspecified | Cutoff, U - RER	Estimated 40 km transport of waste from the facility in Lausanne to a recycling facility in Montreux. The unspecified transport process is used because of lack of data about the specific vehicle.
Column production	Intermediary flow - Output	Column	1.00	Item(s)	Column production, TVSA | Cutoff, U, MABOR	
	Intermediary flows - Inputs	Steel production	13.50	kg	market for steel, chromium steel 18/8 | steel, chromium steel 18/8 | Cutoff, U - GLO	Substitute for the column material.